

Liquid Crystal Phases of Colloidal
Platelets and their Use as
Nanocomposite Templates



Universiteit Utrecht

Cover: Polarization micrograph of the isotropic-nematic interface in an aqueous gibbsite suspension (200 g/L, 1 mM NaCl), 1.5 years after preparation

Cover design: Jesse Hoosemans

ISBN 978-90-393-5153-6

Subject Headings: Colloids/Platelets/Phase Separation/Liquid Crystals/
Nanocomposites/Gel/Glass/Clay.

Liquid Crystal Phases of Colloidal Platelets and their Use as Nanocomposite Templates

Vloeibaar kristallijne fasen van colloïdale plaatjes
en hun toepassing als modelvorm voor nanocomposieten

(met een samenvatting in het Nederlands)

Proefschrift

ter verkrijging van de graad van doctor aan de
Universiteit Utrecht op gezag van de rector magnificus,
prof. dr. J. C. Stoof, ingevolge het besluit van het
college voor promoties in het openbaar te verdedigen
op woensdag 30 september 2009 des middags te 4.15 uur

door

Maurice Christian Danho Mourad

geboren op 9 februari 1982 te Leiden

Promotor: Prof. dr. H. N. W. Lekkerkerker

Co-promotoren: Dr. A. V. Petukhov

Dr. G. J. Vroege

Het in dit proefschrift beschreven onderzoek werd gefinancierd door het gebied Chemische Wetenschappen (CW) van de Nederlandse Organisatie voor Wetenschappelijk Onderzoek (NWO).

Contents

Chapter 1. General Introduction	1
Bibliography	5
Part 1. AQUEOUS GIBBSITE SUSPENSIONS	7
Chapter 2. Sol-Gel Transitions and Liquid Crystal Phase Transitions in Concentrated Aqueous Suspensions of Colloidal Gibbsite Platelets	7
Bibliography	30
Chapter 3. Columnar Liquid Crystals of Gibbsite Platelets as Templates for the Generation of Ordered Silica Structures	32
Bibliography	45
Part 2. STERICALLY STABILIZED GIBBSITE	48
Chapter 4. Lyotropic Hexagonal Columnar Liquid Crystals of Large Colloidal Gibbsite Platelets	48
Bibliography	60
Chapter 5. The Nematic Phase of Sterically Stabilized Gibbsite Platelets as Template for Ordered Polymer Nanocomposites	62
Bibliography	73
Part 3. OTHER STERICALLY STABILIZED PLATELETS	74
Chapter 6. Formation of Nematic Liquid Crystals of Sterically Stabilized Layered Double Hydroxide Platelets	74
Bibliography	96
Chapter 7. Isotropic-to-Nematic Phase Transition of Sterically Stabilized Hectorite Platelets and Hectorite-Polymer Nanocomposites	98
Bibliography	104
Summary	109

Samenvatting voor iedereen	111
List of publications	119
Curriculum Vitae	120
Acknowledgement	121

1

General Introduction

1.1. COLLOIDS

Dispersions of colloids are ubiquitous in nature. Colloidal particles, or *colloids*, can be defined as particles that have at least one dimension in the size range between 1 nm and 1 μm and are dispersed in a continuous phase, or *dispersion medium*. They may be regarded as an intermediate state of matter in between molecules and bulk matter. The dispersion of colloids in liquids such as water makes that the dynamical and statical properties of the liquid may change significantly in comparison to the pure liquid.

The importance of colloids to the natural sciences in general, however, was recognized relatively late. In 1915, Wo. Ostwald published his textbook on colloid science, that referred to this disregard in science (“*Die Welt der vernachlässigten Dimensionen*”). In this book he stated that the study objects of colloid chemistry can not be regarded as a specific group of matter, but rather as a physical-chemical state that in principle all matter may reach [1].

Notably, in a seminal theoretical paper Einstein pointed out that -according to molecular kinetic heat theory- dispersed colloids should move so much that their random displacement can be observed in microscopy [2, 3]. Later, Perrin investigated the sedimentation behavior of colloidal spheres in microscopy and found great similarities between the behavior of these colloids and dilute molecular gases [4, 5]. Key to the work of Einstein and Perrin is the fact that colloids are subject to thermal or *Brownian* motion. Both colloids and atoms obey the same laws of statistical physics. Combined with the fact that they are observable in microscopy, colloids make up practical systems to study fundamental physical phenomena. Ever since Perrin, model systems of colloids

have been studied with great interest for their analogy to atoms. Colloidal systems display for instance *phase transitions*, transformation of matter of one state to another, such as gas, liquid and crystal phases, liquid crystal phases, glasses and gels.

Another feature of colloids is that their interaction potential can be tuned. Charges on the colloids are responsible for long-range repulsive and attractive interactions. Shielding of these charges can be implemented by addition of ions to the dispersion medium (as applied in Chapters 2, 6). The adhesion of polymers to the surface can turn the colloids into sterically stabilized particles. These do not interact when they are separated from each other, but do behave strongly repulsive as soon as they start to touch (as applied in Chapters 4 - 7).

1.2. LIQUID CRYSTALS

Spherical colloids already display an enormous variety of physical processes, such as crystallization, melting and glass formation [6]. Anisometric particles can have an even richer phase behavior, which makes them particularly interesting systems with which phase transitions can be studied. Since Reinitzer and Lehmann it is known that anisometric molecules have more phase transitions than crystal-to-liquid and liquid-to-gas. In their pioneering work [7, 8] the existence of mesomorphic, liquid crystal phases was demonstrated. These liquid crystals are partly ordered materials: their building blocks are often shaped as rods or plates, such that they have additional *orientational* degrees of freedom and can have collective alignment, which accounts for the extra phase transitions. In the case of anisometric molecules the phase transitions occur at distinct temperatures of the system. For anisometric particles, however, the concentration of the colloids determines the state of the system, which is therefore called *lyotropic*.

In the 1920s the first liquid crystal phases of anisometric colloids were reported by Zocher, who studied Vanadium pentoxide ribbons [9]. Other early work was performed by Langmuir, who reported on rodlike tobacco mosaic virus and lathlike natural hectorite clay particles, which he knew as *California bentonite* [10]. At the same time theoretical work was done by Onsager, who first treated the effect of the ellipsoidal shape on the viscosity of suspensions [11] and later treated the effect of the rod and plate shape on the phase transitions [12, 13]. Based on statistical mechanics Onsager described the transition from the isotropic to the nematic phase as a minimization of the free energy. In particular, the insight that the entropy alone can favor (nematic) alignment of the colloids at relatively low concentrations in a system is due to Onsager's work. While orientational ordering is usually connected to a decrease of the entropy, he showed that it is the increase of the total entropy as a result of the loss of orientational entropy in combination with the (larger) increase in excluded volume entropy in such systems that stabilizes the nematic state.

1.3. LIQUID CRYSTALS OF PLATELIKE PARTICLES

Starting with the first report on liquid crystal phase separating suspensions of plate-like particles by Langmuir, researchers have been confronted with gelation and glass formation in such suspensions. Attempts to reproduce Langmuir's results failed, because of gelation and glass formation. Nowadays, gelation in suspensions of natural platelike clay particles has been investigated [14] and even has widespread application in industry. However, little is known about the forces responsible for the gelation behavior. Furthermore it is unclear why so little known examples of liquid crystal phase separating platelike particles appeared in literature.

1.4. PLATELIKE MODEL COLLOIDS IN THIS THESIS

The work described in this thesis is connected to the liquid crystal phase separation, gelation and glass formation of platelike colloidal particles. As the main model system for colloidal platelike particles in this thesis we use gibbsite (γ -Al(OH)₃) platelets, in charged form (Chapter 2), in mineral coated form (Chapter 3) and in sterically stabilized form (Chapter 5, 6). Starting from aluminium alkoxides in aqueous solution, these particles can be synthesized in the laboratory. The advantages of the use of charged gibbsite over clays in general are that it has a uniform charge behavior of the edges and faces at working conditions (low pH), it has great stability, it does not gel easily (only at concentrations of tens of weight percents or at 10⁻¹M NaCl and higher), is relatively monodisperse in comparison to clays or synthetic clays [15] and displays liquid crystal phase transitions. Silica coated gibbsite forms hexagonal columnar phases in water and ethanol (Chapter 3). Polyisobutylene stabilized gibbsite forms interesting hexagonal columnar phases in tetralin (Chapter 4).

As a second model system of anisotropic particles we investigated hydrotalcite, a layered double hydroxide, in which divalent cations are substituted by trivalent cations to yield a positive charge. Although in water the formation of a nematic phase of these hydrotalcite particles takes years, we show that polyisobutylene grafting enables the particles to form tactoids and nematic phases in toluene within days. The third model system we investigate in this work is natural hectorite clay, which consists of lathlike colloidal particles. For hectorite we show that again grafting with polyisobutylene is helpful to circumvent gelation and form a nematic phase in toluene.

1.5. NANOCOMPOSITE TEMPLATES

In this work several routes are presented to obtain nematic and hexagonal columnar liquid crystal phases of charged and sterically stabilized systems of platelike colloids. In materials science, ordering on nanometer scale of one specimen in a continuous phase is of particular interest because of the outstanding optical [16] and mechanical [17] properties of such hybrid, or *nanocomposite*, materials. Peculiar natural examples of ordered nanocomposites include opals, nacre, bone and enamel. We exploit liquid crystal forming platelike colloids to use these as nanocomposite templates. The hexagonal columnar phase of silica coated gibbsite platelets is used to achieve gibbsite-silica nanocomposites with hexagonal columnar order (Chapter 3). Furthermore, the nematic liquid crystal phase of sterically stabilized gibbsite platelets is used as a template for gibbsite-polymer nanocomposites with nematic order (Chapter 5).

1.6. OUTLINE OF THIS THESIS

In this thesis the gelation and liquid crystal phase behavior of colloidal dispersions of platelike particles as well as the use of such dispersions for nanocomposite generation are explored. In part I of this thesis we study suspensions of charged gibbsite platelets. In Chapter 2, the liquid crystal phase transitions and sol-gel transitions are investigated. In Chapter 3, the generation of hexagonal columnar ordered nanocomposite materials of gibbsite in silica from such charged suspensions is discussed. In Part II we study systems of sterically stabilized gibbsite platelets. The structure of columnar hexagonal samples of these gibbsite platelets is investigated in Chapter 4. The use of these systems for the generation of polymer-gibbsite nanocomposite materials is described in Chapter 5. Part III of this thesis contains work on other platelike particles. Chapter 6 is about hydrotalcite, a layered double hydroxide with magnesium and aluminium ions. Both the liquid crystal phase behavior of charged platelets and platelets that are grafted with steric stabilizer are discussed. Finally, in Chapter 7 suspensions of sterically stabilized colloidal hectorite plates are explored.

Bibliography

- [1] Wo. Ostwald. *Die Welt der vernachlässigten Dimensionen*. Steinkopf, Dresden, 1915.
- [2] A. Einstein. Über die von der Molekularkinetischen Theorie der Wärme geforderte Bewegung von in ruhenden Flüssigkeiten suspendierten Teilchen. *Annalen der Physik*, 322(8):549–560, 1905.
- [3] A. Einstein. *Investigations on the Theory of the Brownian Movement*. Dover, New York, 1956.
- [4] J. Perrin. Mouvement brownien et réalité moléculaire. *Annales de Chimie et de Physique*, 18:5–114, 1909.
- [5] J. Perrin. *Les Atomes*. Libr. Felix Alcan, Paris, 1920.
- [6] P. N. Pusey and W. van Megen. Phase behaviour of concentrated suspensions of nearly hard spheres. *Nature*, 320:340–342, 1986.
- [7] F. Reinitzer. Beiträge zur Kenntniss des Cholesterins. *Monatshefte für Chemie / Chemical Monthly*, 9(1):421–441, 1888.
- [8] O. Lehmann. Über fließende Krystalle. *Zeitschrift für Physikalische Chemie*, 4:462–472, 1889.
- [9] H. Zocher. Über freiwillige Strukturbildung in Solen. (eine neue Art anisotrop flüssiger Medien.). *Zeitschrift für Anorganische und Allgemeine Chemie*, 147(1):91–110, 1925.
- [10] I. Langmuir. The role of attractive and repulsive forces in the formation of tactoids, thixotropic gels, protein crystals and coacervates. *Journal of Chemical Physics*, 6:873–896, 1938.
- [11] L. Onsager. Viscosity and particle shape in colloid solutions. *Physical Review*, 40:1028, 1932.
- [12] L. Onsager. Anisotropic solutions of colloids. *Physical Review*, 62:558, 1942.
- [13] L. Onsager. The effects of shape on the interaction of colloidal particles. *Annals of the New York Academy of Sciences*, 51:627–659, 1949.
- [14] S. Abend and G. Lagaly. Sol-gel transitions of sodium montmorillonite dispersions. *Applied Clay Science*, 16(3-4):201, 2000.
- [15] D. W. Thompson and J. T. Butterworth. The nature of laponite and its aqueous dispersions. *Journal of Colloid and Interface Science*, 151(1):236–243, 1992.
- [16] J. Sanders. Diffraction of light by opals. *Acta Crystallographica Section A*, 24(4):427–434, 1968.
- [17] H. Gao, B. Ji, I. L. Jäger, E. Arzt, and P. Fratzl. Materials become insensitive to flaws at nanoscale: Lessons from nature. *Proceedings of the National Academy of Sciences of the United States of America*, 100(10):5597–5600, 2003.

2

Sol-Gel Transitions and Liquid Crystal Phase Transitions in Concentrated Aqueous Suspensions of Colloidal Gibbsite Platelets

ABSTRACT

In this chapter we present a comprehensive study of the sol-gel transitions and liquid crystal phase transitions in aqueous suspensions of positively charged colloidal gibbsite platelets at pH 4-5 over a wide range of particle concentrations (50 g/L - 600 g/L) and salt concentrations (10^{-4} M - 10^{-1} M NaCl). A detailed sol-gel diagram was established by oscillatory rheological experiments. These demonstrate the presence of kinetically-arrested states both at high and at low salt concentrations, enclosing a sol region. Birefringence and iridescence show that in the sol state nematic and hexagonal columnar liquid crystal phases are formed. The gel and liquid crystal structures are studied in further detail using small angle x-ray scattering (SAXS) and cryo-focused ion beam/scanning electron microscopy (cryo-FIB-SEM). The gel formed at high salt concentration shows signatures of a sponge-like structure and does not display birefringence. In the sol region -by lowering the salt concentration and/or increasing the gibbsite concentration- the nematic phase gradually transforms from the discotic nematic (N_D) into the columnar nematic (N_C) with much stronger side-to-side interparticle correlations. Subsequently, this N_C structure can be either transformed into the hexagonal columnar phase or arrested into a birefringent gel state with N_C structure.

Reproduced in part with permission from M.C.D. Mourad, D.V. Byelov, A.V. Petukhov, D.A.M. de Winter, A.J. Verkleij, and H.N.W. Lekkerkerker, J.

Phys. Chem. B 113 (2009) 11604. Copyright 2009 American Chemical Society.

Reproduced in part with permission from M.C.D. Mourad, D.V. Byelov, A.V. Petukhov, H.N.W. Lekkerkerker *J. Phys.: Condens. Matter* 20 (2008) 494201. Copyright 2008 by IOP Publishing Ltd.

2.1. INTRODUCTION

Sol-gel transitions and liquid crystal phase transitions in aqueous suspensions of charged colloidal platelets, ranging from natural [1, 2, 3, 4, 5, 6] and synthetic clays [1, 7, 8, 9, 10, 11, 12] to hydroxides (nickel hydroxide [13] and aluminium hydroxide [14, 15]) and layered double hydroxides (takovite [16] and hydrotalcite [17]), have attracted significant attention during the last 15 years.

A particularly well studied class of charged colloidal particles is that of clay platelets. The propensity of suspensions of clay platelets to form gels is well known, widely studied and exploited extensively in industry [18]. While rheological measurements in the early 1950s indicated a minimum in the yield stress as a function of salt concentration in clay sols [19], it is only in the last ten years clearly recognized that clays are in a gel state both at high and at low concentrations of salt, while at intermediate salt concentrations for the same clay content a sol state is found [2].

This sequence of repulsive gel-sol-attractive gel states upon increase of the salt concentration has also been reported for aqueous suspensions of gibbsite [20] and hydrotalcite platelets [17]. An account of this gelation behavior has been put forward in terms of the domination of either attractive or repulsive interactions [21, 22, 23]. At low salt, the interaction is strongly repulsive and the dispersion appears as a repulsive gel. With increasing salt concentration the repulsion is weakened and the dispersion appears a sol. A further increase of the salt concentration leads to a second gel state (attractive gel) governed by attractive interactions between the platelets.

Another characteristic feature of suspensions of anisometric colloidal particles is their ability to form liquid crystals. In the 1940s Onsager [24] showed that for such systems entropy is responsible for the phase separation into an isotropic (I) and nematic (N) phase. The balance between orientational entropy (favoring the isotropic phase) and excluded volume entropy (favoring the nematic phase), gives rise to a stable nematic phase at higher particle concentrations. Until very recently, reports on the isotropic-nematic (I - N) transition in systems of plate-like particles were particularly rare in literature. In fact, the I - N transition in clay platelets -which was reported initially by Langmuir [25] and inspired Onsager to extend his theory to platelets- is generally obscured by the interference of gelation. Starting in the 1990s emphasis was placed on Laponite [26], a synthetic Hectorite, in an attempt to circumvent the poorly understood behavior of natural clays. However, the main result from persevering investigations on the phase behavior of these suspensions is that gelation is again ubiquitous [7, 1, 9, 12]. Meanwhile, it turned out that more valuable model systems for charged platelets, displaying both liquid crystal transitions and sol-gel transitions, are Na fluorohectorite [11], gibbsite [14, 15] and mixed-metal hydroxides [17]. A breakthrough came with the recent work of Michot et al., who observed I - N phase separation and the sol-gel transition

in suspensions of the *natural* clays nontronite [4, 6] and beidellite [27], dioctahedral smectite clays with ionic substitutions in the tetrahedral layer.

However the relation between the I - N transition (or more generally: liquid crystal phase transitions) and the sol-gel transition remains an unresolved issue. To address this issue we present a multi-technique study of the sol-gel and liquid crystal phase transitions of aqueous suspensions of colloidal gibbsite platelets, over a wide range of particle concentrations and salt concentrations. To elucidate the nature of the liquid crystal and kinetically arrested states of gibbsite platelets we have used polarized light techniques, oscillatory rheological measurements, Small Angle X-ray Scattering (SAXS) measurements and Focused Ion Beam/Scanning Electron Microscopy under cryogenic conditions (cryo-FIB-SEM). From cryo-FIB-SEM and SAXS measurements we obtain a structure of the attractive gel that has great similarity to that in clay systems, although for gibbsite it is observed at a higher salt concentration. In the sol region we observe Isotropic-to-Nematic (I - N) and Nematic-to-Columnar (N - C) liquid crystal transitions. From SAXS measurements it follows that nematic phases of both the discotic nematic (N_D) and the columnar nematic (N_C) type occur. While in the sol region equilibria between N_C and C occur, the repulsive gel at large particle concentrations has the signature of a N_C phase. Apparently, the transition to the columnar phase is preempted by a transition to a repulsive gel state with a kinetically-arrested, glassy nature and the structural features of the N_C phase. Further indication that this glassy state is metastable is provided by the fact that devitrification occurs. In years, a slow transition to hexagonal columnar structure occurs in small grains with a domain size of approximately 20 μm as evidenced by iridescence. This indicates that locally, the kinetically-arrested nematic columnar arrangement develops into a hexagonal columnar arrangement.

2.2. EXPERIMENTAL

Colloidal gibbsite platelets were grown in acidic aqueous solution [28]. First hydrochloric acid (HCl 0.09 M, 37%, Merck), aluminium sec-butoxide (0.08 M, 95 %, Fluka Chemika) and 0.08 M aluminium isopropoxide (98+ %, Acros Organics) were dissolved in demineralized water (15 L, equally divided over three Erlenmeyer flasks). The mixtures were mechanically stirred for 10 days and then heated in borosilicate reaction vessels that were immersed in a thermostatted water bath (85° C for 72h). Next, the colloidal dispersions were centrifuged (1200 g, 15-20 h). The smallest gibbsite particles were then removed from the batch with the supernatant. The size of the gibbsite particles was then analyzed by transmission electron microscopy (TEM). The two systems with smaller gibbsite particles were redispersed in aqueous solution (1.5L) of hydrochloric acid, aluminium sec-butoxide and aluminium isopropoxide (concentrations equal to those described above) and heated at 85° C for 72h in order to perform a seeded growth

of the particles. The mixture was cooled down to room temperature and centrifuged again (1200 g, 15-20 h). Finally the dispersions were added together and dialyzed against demineralized water in tubes of regenerated cellulose (Visking, MWCO 12,000-14,000) until the conductivity dropped to 20 $\mu\text{S}/\text{cm}$. Finally, aluminum chlorohydrate (0.6 g per gram gibbsite particles, Locron P, Hoechst AG, Germany) was added to the suspension to hydrolyze and form Al_{13} Keggin ions ($[\text{Al}_{13}\text{O}_4(\text{OH})_{24}(\text{H}_2\text{O})_{12}]^{7+}$) and thereby increase the stability of the gibbsite platelets in water [29].

2.2.1. Particle characterization

The resulting suspension was analyzed for solid content and inspected with TEM (Figure 2.1). From the micrographs the surface area of over 200 individual hexagonal particles was measured. An average equivalent circular diameter (ECD) was calculated as:

$$ECD = \sqrt{\frac{4A}{\pi}} \quad (2.1)$$

where A is the measured surface area. Furthermore, the particle size distribution (Figure 2.1B) and the standard deviation (σ_{ECD}) were determined. The yield of the entire synthesis was determined to be 58 g (dry particle weight) with $ECD = 205 \text{ nm}$ ($\sigma_{ECD} = 47 \text{ nm}$).

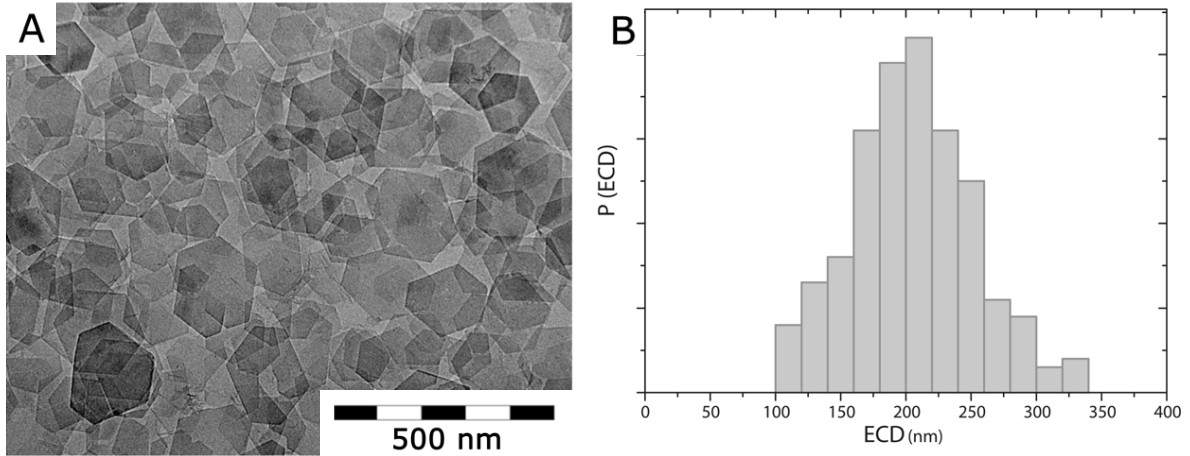


FIGURE 2.1. (A) Transmission electron micrograph of colloidal gibbsite platelets. (B) Histogram of the Equivalent Circular Diameter (ECD) of the platelet surface as determined from transmission micrographs.

2.2.2. Sample preparation and optical observations

Concentrated gibbsite dispersions were prepared and set at fixed ionic strength by centrifugation and redispersion in water with NaCl added. Samples for visual observation were put in large capillaries ($1.0 \times 10.0 \text{ mm}$ cross-section, Vitrotubes, VitroCom Inc.) that were flame sealed. Visual inspection was performed on a regular basis. For this, a

home-built polarization setup was used, consisting of two crossed polarizing filters that could be illuminated by a 150 Watt lamp in combination with a condenser lens and a ground glass diffuser for homogeneous illumination. For X-ray experiments, samples were transferred into round Mark tubes (Quartz, 2 mm diameter and about 10 μm wall thickness, W. Müller, Berlin, Germany).

2.2.3. Rheological measurements

Oscillatory experiments in the frequency range of 0.01 - 100 Hz were performed on gibbsite suspensions using a Physica Anton Paar (MCR-300) controlled stress rheometer operating at a strain amplitude of 0.01. It was verified that at this strain amplitude the system was in the linear viscoelastic regime at all frequencies. A Cone-plate measuring geometry was used having a diameter of 50 mm and a cone angle of 1° . The plate was kept at 20°C by a connection with a thermostatic water bath. All measurements were initiated by a preshear (100 s at a shear rate of 500 s^{-1}). From the measurements the frequency dependent storage (G') and loss modulus (G'') components of complex shear modulus $G^* = G' + iG''$ were determined [30].

2.2.4. Small-angle X-ray scattering

X-ray studies were performed at the Dutch-Belgian beam line BM-26 DUBBLE of the European synchrotron radiation facility (ESRF) in Grenoble, France, 1 month after preparation. We used a microradian X-ray diffraction setup, similar to the one described in literature [31]. The X-ray beam was focused by a set of compound refractive lenses [32] (CRL) at a phosphor screen of the CCD (charge-coupled device) X-ray detector (Photonic Science, 4008×2671 pixels of 22 micron square). Any focusing of the beam before the experimental hutch was avoided to achieve maximum transverse coherence length of the beam. The capillaries were placed just after the CRLs at a distance of about 8 metre from the detector. This setup allows achieving the angular resolution of the order of 5-7 microradians. X-ray photon energies of 13 keV (wavelength = 0.095 nm) and 15 keV (0.0825 nm) were used in 2006 and 2008, respectively. The beam diameter in the sample was about 0.5 mm.

2.2.5. Cryo-Focused Ion Beam/Scanning Electron Microscopy

Droplets of aqueous gibbsite suspensions were put in between two small copper rivets (dimensions 4.5×3 mm, BAL-TEC AG, Liechtenstein). The suspensions were then cryo-immobilized by plunge-freezing of the copper hats in N_2 slush. Samples are transferred under vacuum to the cryostatic preparation chamber (Quorum Technologies, PP2000T, United Kingdom) that is attached to the Focused Ion Beam/Scanning Electron Microscope (FIB-SEM), where one of the copper parts is mechanically removed in order to expose the surface of the frozen suspension. The sample was then passed through on the cryostatic microscope chamber of the cryo-FIB-SEM (Nova Nanolab

600, FEI, the Netherlands) that was operated at 30 kV for the ions and 3 kV for the electrons. Here, the sample can be inspected with both focused ion beam and electron beam imaging. *In situ* sectioning of the sample can be performed by milling with the focused ion beam, which is able to precisely cut through the frozen dispersion and its constituents and thereby create a cross-section that is imaged by (high resolution) SEM [33]. It is important to inspect the structure of the suspension within the droplet rather than on the outer surface, as platelets (or in general: anisometric particles) behave and order differently on interfaces, which may therefore not be regarded as representative for the structure. In order to achieve this, cross-sections that went micrometers deep into the specimen were obtained by ion milling in a two step process. First rough sectioning was performed by high current milling (5.0 nA). This step was followed by a low-current polishing step (0.3 nA), which results in cross-sections with a smooth surface. The structure of the gibbsite platelets as observed in cryo-FIB-SEM is compared with SAXS results, to exclude effects of the freezing and sectioning procedure on the samples from which micrographs were made.

2.3. RESULTS

2.3.1. Rheological measurements

The frequency dependence of the dynamic moduli G' and G'' for aqueous gibbsite dispersions at ionic strength of 10^{-1} , $3 \cdot 10^{-2}$, 10^{-2} , 10^{-3} and 10^{-4} M NaCl and gibbsite particle concentrations ranging from 50 g/L to 600 g/L are presented in Figure 2.2. At salt concentrations of 10^{-1} M and $3 \cdot 10^{-2}$ M NaCl the dynamic moduli are almost independent of frequency for all solid contents measured. For the lower salt concentrations G' and G'' depend on frequency for the lower particle concentrations (100, 200 g/L). These suspensions are only moderately viscous and there are no large differences between the values for G' and G'' . At higher particle concentrations the dynamic moduli are independent of frequency and eventually G' exceeds G'' , sometimes even by an order of magnitude.

In case the value of G' exceeds G'' and G' is of the order of 1 Pa or larger this is a typical signature for the behavior of gels [3, 34, 35]. With help of these criteria sols and gels can be distinguished and the rheological state diagram can be constructed. This rheological state diagram is presented in Figure 2.3. We note that the shape of the rheological state diagram has the same shape as the rheological state diagrams experimentally determined for dispersions of natural clay [2, 3, 5], synthetic clay [9] and MgAl layered double hydroxides [17], all of which are charged, plate-like particles. Hence it appears that this kind of rheological state diagram is generic for dispersions of charged platelets.

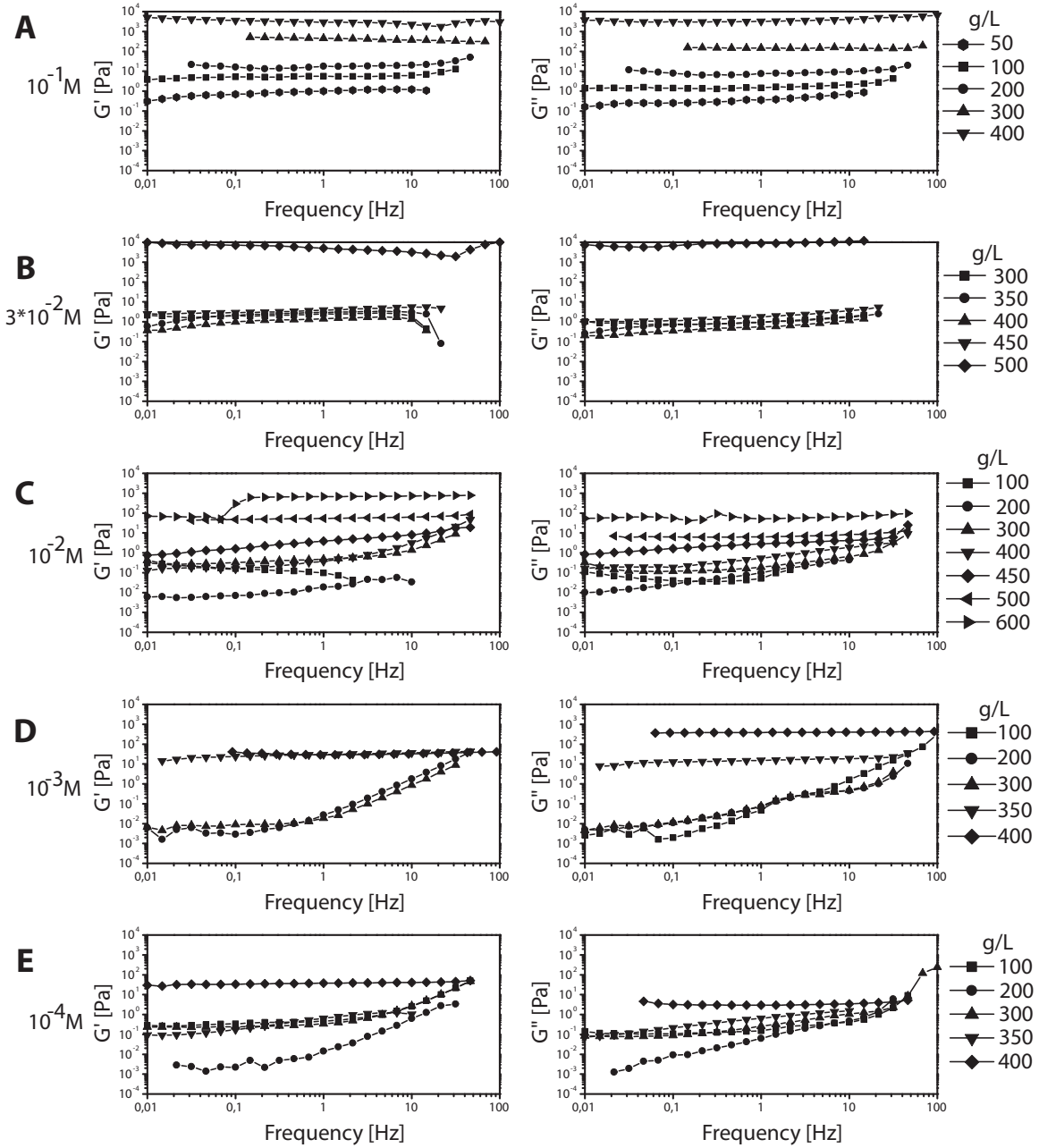


FIGURE 2.2. Rheological measurements on aqueous gibbsite suspensions. Evolution of G' (left Panels) and G'' (right Panels) with the oscillatory frequency for particle concentration series at salt concentration of (A) 10^{-1}M , (B) $3 \cdot 10^{-2}\text{M}$, (C) 10^{-2}M (D) 10^{-3}M and (E) 10^{-4}M .

2.3.2. Optical observations

All samples with salt concentrations $3 \cdot 10^{-2}\text{M}$ NaCl or smaller that were classified by the rheological criteria above as sols showed the first signs of the formation of birefringent phases within one day after preparation. The same behavior was observed

for two samples at the border between the sol and the gel region ($3 \cdot 10^{-2} \text{M}$ 450 g/l and 10^{-3}M 350 g/L) that were rheologically classified as gels. The other samples with salt concentrations $3 \cdot 10^{-2} \text{M}$ NaCl or smaller that were classified as gels, while birefringent, show a somewhat different texture and no signs of phase separation. The gel character of these samples is demonstrated by the trapping of air bubbles in the dispersions. The samples with a salt concentration of 10^{-1}M NaCl show different behavior. They remain isotropic and particularly at the lowest particle concentration expulsion of pure solvent from the gel (syneresis) started within one day after preparation.

All samples were inspected on a regular basis for a period of two years in order to observe changes in the suspensions. To exhibit the course of events photographs of the flat sample cells between crossed polarizers, taken 1 month and 15 months after mixing, are presented in Figure 2.4. The observations presented in Figure 2.4 provide the location of the phase equilibria as a function of the overall gibbsite concentration and the salt concentration. After one month in the phase separating samples a progression of liquid crystal phases ranging from I+N via N to N+C appeared. Due to the action of gravity the volume of the individual phases and even the appearance of the hexagonal columnar phase as such depends on time as is evidenced by the right hand panels in Figure 2.4. Indeed, after 15 months we observed liquid crystal phases ranging from I+N via I+N+C to N+C reflecting the influence of gravity leading to sedimentation equilibria displaying multiple phases. Moreover below the interfaces the birefringent phases of phase separated samples lost turbidity and became more homogeneous. We did not measure the gibbsite concentrations in the individual phases which are -again due to gravity- height dependent. The outward appearance of the non-phase separating samples with salt concentrations $3 \cdot 10^{-2} \text{M}$ NaCl or smaller that were classified as gels did not seem to change.

In the samples with a salt concentration of 10^{-1}M NaCl syneresis continued for the samples at 50, 100 and 200 g/L, whilst the sample at 300 g/L apparently had a gel strength so high that no visible syneresis occurred.

2.3.3. Small Angle X-ray Scattering and Cryo Scanning Electron Microscopy

The dispersions were examined by SAXS in order to obtain more information on the structure. These measurements were performed on one month old samples. While all samples contained in Figure 2.4 were measured by SAXS, here, we highlight the results on three representative series of samples. In the first series of samples, the scattering patterns from the sol region are discussed for a fixed gibbsite concentration of 300 g/L and salt concentrations that vary from $3 \cdot 10^{-2} \text{M}$ down to 10^{-4}M . This series covers the isotropic, nematic and hexagonal columnar liquid crystal phases, (see Figure 2.4). Secondly, the influence of an increase of the gibbsite concentration on the phase behavior is demonstrated by a series at a fixed salt concentration of 10^{-2}M . Finally, in order to

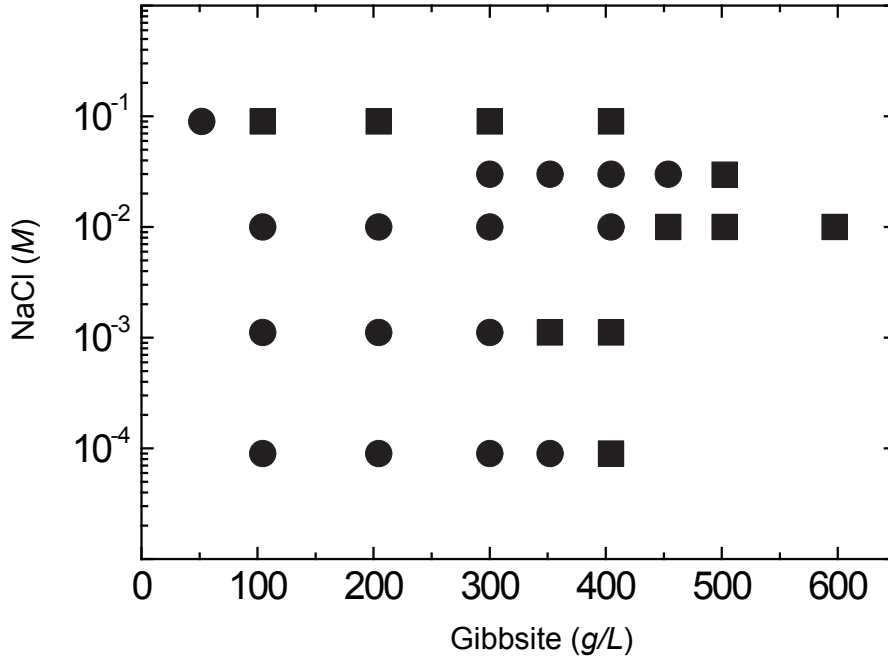


FIGURE 2.3. Sol-Gel diagram of aqueous gibbsite dispersions, based on rheological measurements. The sol states are indicated by (•), while the gel states are indicated by (■).

illustrate the structure of the system in the gel phase at high salt concentration (10^{-1}M), we present the results obtained for the samples with particle concentrations of 100 and 200 g/L.

The scattering patterns of the first series of samples at the fixed gibbsite concentration of 300 g/L are shown in Figure 2.5 and in the form of azimuthally integrated profiles in Figure 2.6. The sample at a salt concentration of $3 \cdot 10^{-2}\text{M}$ displays phase separation in an isotropic (top) and a nematic (bottom) phase. Figure 2.5A displays the scattering pattern from the isotropic phase. We can not detect any sign of anisotropy and the scattering intensity decays monotonically.

For the nematic phase, lower in the capillary, the scattering pattern possesses anisotropy (see Figure 2.5B). This effect originates from the orientational ordering of the gibbsite platelets. The scattering intensity does not display any maximum, which indicates the absence of any pronounced positional correlations between the platelets. The pattern can be identified as discotic nematic (N_D) [36]. For the sample with ionic strength of 10^{-2}M the scattering pattern is given in Figure 2.5C. The pattern possesses clear anisotropy and a pronounced broad peak is observed at $q = 0.118\text{ nm}^{-1}$. This implies the presence of N_D structure in the sample with face-to-face correlation distances between the platelets of 53 nm. An even richer scattering pattern can be seen in the sample upon decreasing the ionic strength to 10^{-3}M . In Figure 2.5D one can again see clear anisotropy in the pattern and a pronounced broad peak at $q = 0.125\text{ nm}^{-1}$,

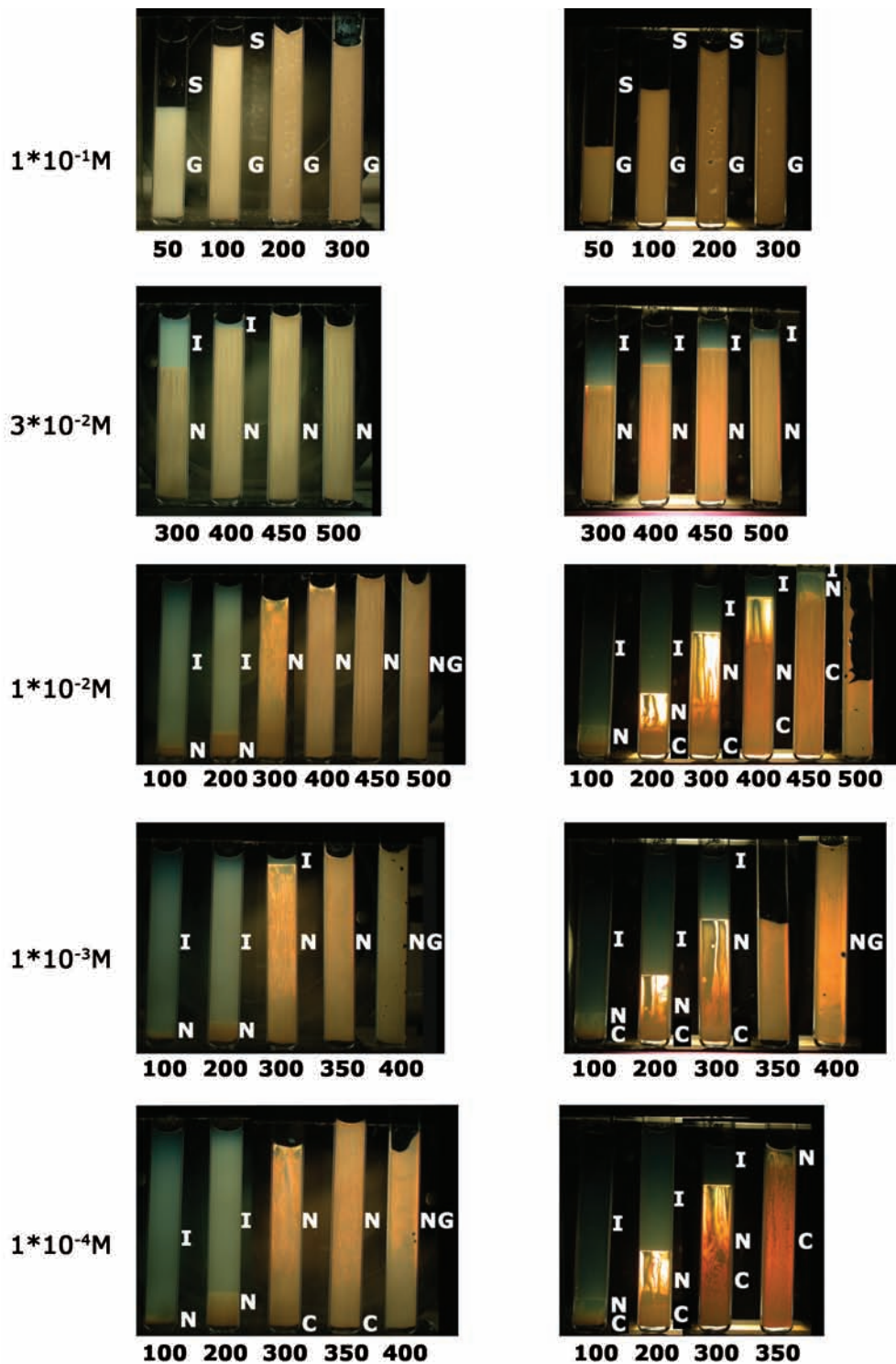


FIGURE 2.4. Aqueous gibbsite suspensions observed in crossed polarizers with back illumination. The panels at the left hand side display the gibbsite concentration series at decreasing salt strengths, one month after preparation, while the panels at the right hand side display the same series 15 months after preparation. At the left hand side the salt concentrations are indicated, while particle concentrations are displayed below each sample (in g/L). Phases are labeled S for solvent, G for (attractive) gel, I for isotropic, N for nematic, C for hexagonal columnar and NG for nematic, repulsive gel.

which indicates a face-to-face distance between the platelets of 50 nm. Moreover, one can now observe an additional broad and weak peak at a q -value of about 0.025 nm^{-1} . This peak indicates that there are pronounced side-to-side positional correlations (251 nm) between the particles on a scale comparable to the particle diameter. For an N_D structure the side-to-side positional correlations can be expected to be very much weaker than the face-to-face correlations due to the high aspect ratio of the particles. The pattern presented therefore fits better the nematic columnar (N_C) structure, in which platelets are piled up in stacks and the stacks themselves form a nematic structure [36, 37, 38].

Upon further decrease of the ionic strength to 10^{-4}M , the sample at 300 g/L separates into two liquid crystal phases. The scattering pattern of the upper phase (Figure 2.5E) shows similarity to that of the sample at 10^{-3}M , having anisotropy and two broad peaks at q -values of about 0.026 nm^{-1} and $q = 0.143 \text{ nm}^{-1}$ (Figure 2.6 curves E) corresponding to 239 nm and 44 nm, respectively. In contrast to the 10^{-3}M sample, however, the peaks are more pronounced, especially for the side-to-side correlations.

In the bottom part of the sample at 10^{-4}M (Figure 2.5F) we observe strong, sharp and ring-like reflections at $q = 0.026$ and 0.045 nm^{-1} . Closer inspection of the data reveals also weaker but sharp rings at $q = 0.052$ and 0.068 nm^{-1} (Figure 2.6 curves F). These q -values are related to each other as $1:\sqrt{3}:\sqrt{4}:\sqrt{7}$, unambiguously confirming that they originate from the (100), (110), (200) and (210) Bragg reflections of the hexagonal columnar structure [36]. In addition, broader reflections at $q = 0.143 \text{ nm}^{-1}$ and $q = 0.287 \text{ nm}^{-1}$ correspond to the (001) and (002) intracolumnar scattering and arise from the (liquid-like) ordering of the platelets within the columns. For the second series, we present diffractograms for 450 and 500 g/L at a fixed salt concentration of 10^{-2}M in Figure 2.7, in addition to the scattering pattern of the sample at 300 g/L, presented in Figure 2.5c. Upon increase of concentration the pattern yields a peak that refers to side-to-side positional correlations ($q = 0.0292 \text{ nm}^{-1}$ for 450 g/L and $q = 0.0296 \text{ nm}^{-1}$ for 500 g/L, respectively) and is most pronounced at largest particle concentration. Furthermore pronounced broad peaks related to face-to-face correlation distances are visible ($q = 0.180 \text{ nm}^{-1}$ for 450 g/L and $q = 0.191 \text{ nm}^{-1}$ for 500 g/L, respectively). Although the SAXS patterns and positional ordering for these two samples are rather similar, rheologically they are characterized as sol and gel, respectively.

In order to obtain a real space image of the gel structure at 10^{-2}M salt cryo-FIB-SEM experiments were performed on cryogenically immobilized dispersion. For this, a sample that was at even further distance from the sol-gel transition boundary, at 600 g/L was used. A focused ion beam was used to create a cross-section through the frozen droplet that allowed for inspection of the new interface by SEM. Figure 2.7C displays a SEM image of such a clean cross-section created by focused ion beam milling. The platelets are light against a dark background and their edges are seen; in other words,

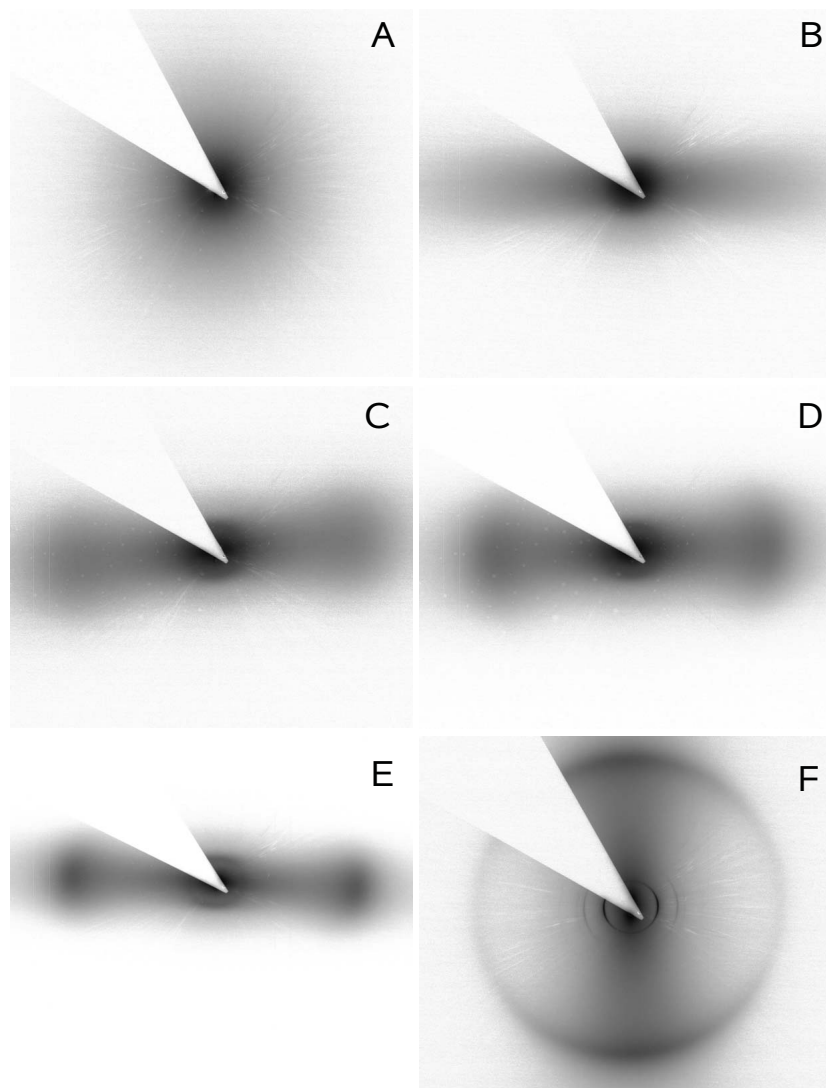


FIGURE 2.5. SAXS patterns of gibbsite dispersions at 300 g/L. Displayed are scattering patterns at salt concentration of $3 \cdot 10^{-2} \text{M}$ (Panel A - *isotropic* upper phase and Panel B - *discotic nematic* lower phase), 10^{-2}M (Panel C), 10^{-3}M (Panel D), and 10^{-4}M (Panel E - *columnar nematic* upper phase and Panel F - *hexagonal columnar* lower phase).

the platelets are aligned perpendicular to the plane of the image. The structure appears to be more ordered than a nematic phase i.e. there is a distinct tendency of the platelets to form stacks. These stacks show capricious meandering that destroys any long range periodical or orientational ordering within the area that is displayed in the SEM image. However, the spatial resolution of the images is too low to extract accurate positions and orientations of individual platelets.

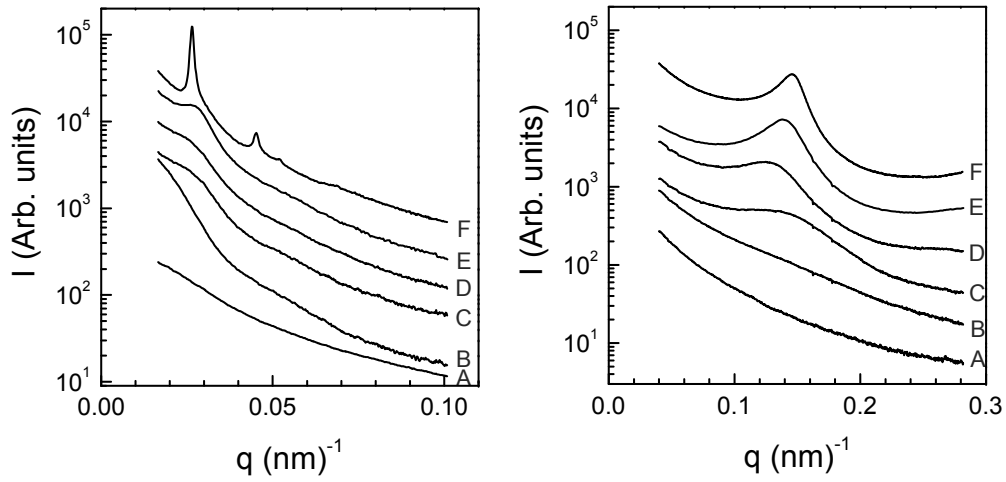


FIGURE 2.6. Azimuthally integrated profiles of the 2D scattering patterns represented in Figure 2.5A-F. On the left hand panel the sector of integration was along the orientations of the 100 peaks. For the right hand panel the sector of integration was selected along the orientations of the 001 peaks. The q -range of both graphs was selected to clearly visualize the peaks in the low q -range (left hand panel) and high q -range (right hand panel), respectively. The index letters in the graphs refer to the panels in Figure 2.5.

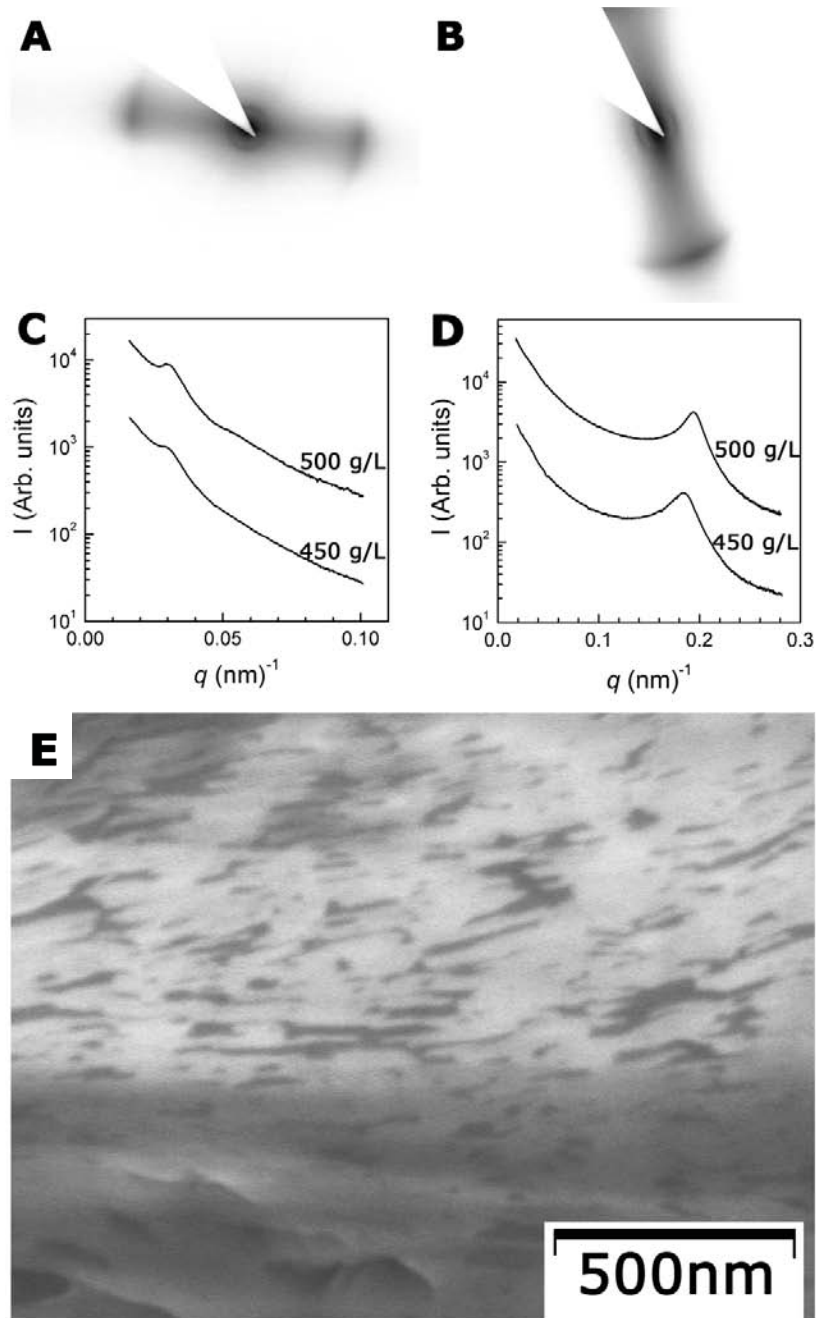


FIGURE 2.7. SAXS patterns of salt concentration 10^{-2}M , 450 g/L (Panel A) and 500 g/L (Panel C). Azimuthally integrated profiles of the scattering patterns in Panels A and B are presented in Panel C (with the sector of integration selected along the orientation of the 100 peaks) and in Panel D (with the sector of integration selected along the orientation of the 001 peaks). In Panel E, a scanning electron micrograph of a cryogenically immobilized dispersion of salt concentration 10^{-2}M and gibbsite concentration of 600 g/L is displayed.

Finally, the scattering patterns for the gel samples at high salt concentration (10^{-1}M) and particle concentration of 100 and 200 g/L are displayed in Figure 2.8A and B. These show a qualitatively different structure in comparison with the scattering patterns of the other samples. In particular, a broad peak is found at very low q -values ($q = 0.0098 \text{ nm}^{-1}$ for 100 g/L and $q = 0.0102 \text{ nm}^{-1}$ for 200 g/L, respectively) that indicates the presence of a characteristic periodicity of 650nm in the sample.

In order to obtain further information on the morphology of the attractive gel-state, again cryo-FIB-SEM experiments were performed on a cryogenically immobilized dispersion. Again, electron micrographs could be taken of a cross-section through the frozen droplet that was created by the focused ion beam (see Figure 2.8C). The micrographs display large structures composed of many gibbsite platelets that are touching each other and that are separated by large water-rich regions of typical size varying from 100 till 800 nanometers.

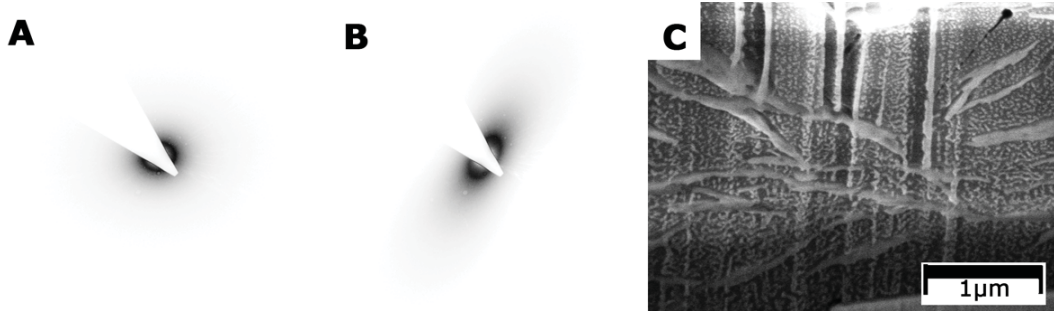


FIGURE 2.8. SAXS patterns of 10^{-1}M , 100 g/L (Panel a) and 200 g/L (Panel b). In Panel c, an scanning electron micrograph of a cryogenically immobilized dispersion of salt concentration 10^{-1}M and particle concentration of 200 g/L is displayed.

Quantitative results from the SAXS experiments within both the sol and repulsive gel region are presented as the variation of the typical interparticle distance with the overall gibbsite concentration (Figure 2.9). The face-to-face distance is estimated as $2\pi/q_{001}$, where q_{001} is the position of the peak at larger q -values. The estimate of the side-to-side distance, $4\pi/(\sqrt{3}q_{100})$, was only possible for those structures possessing a sufficiently pronounced peak at a low q -value. The peak positions were determined whenever possible at the bottom of the capillaries, 1 month after their preparation.

In Figure 2.10 we combine the phase behavior as observed from birefringence, iridescence and SAXS measurements to form a phase diagram.

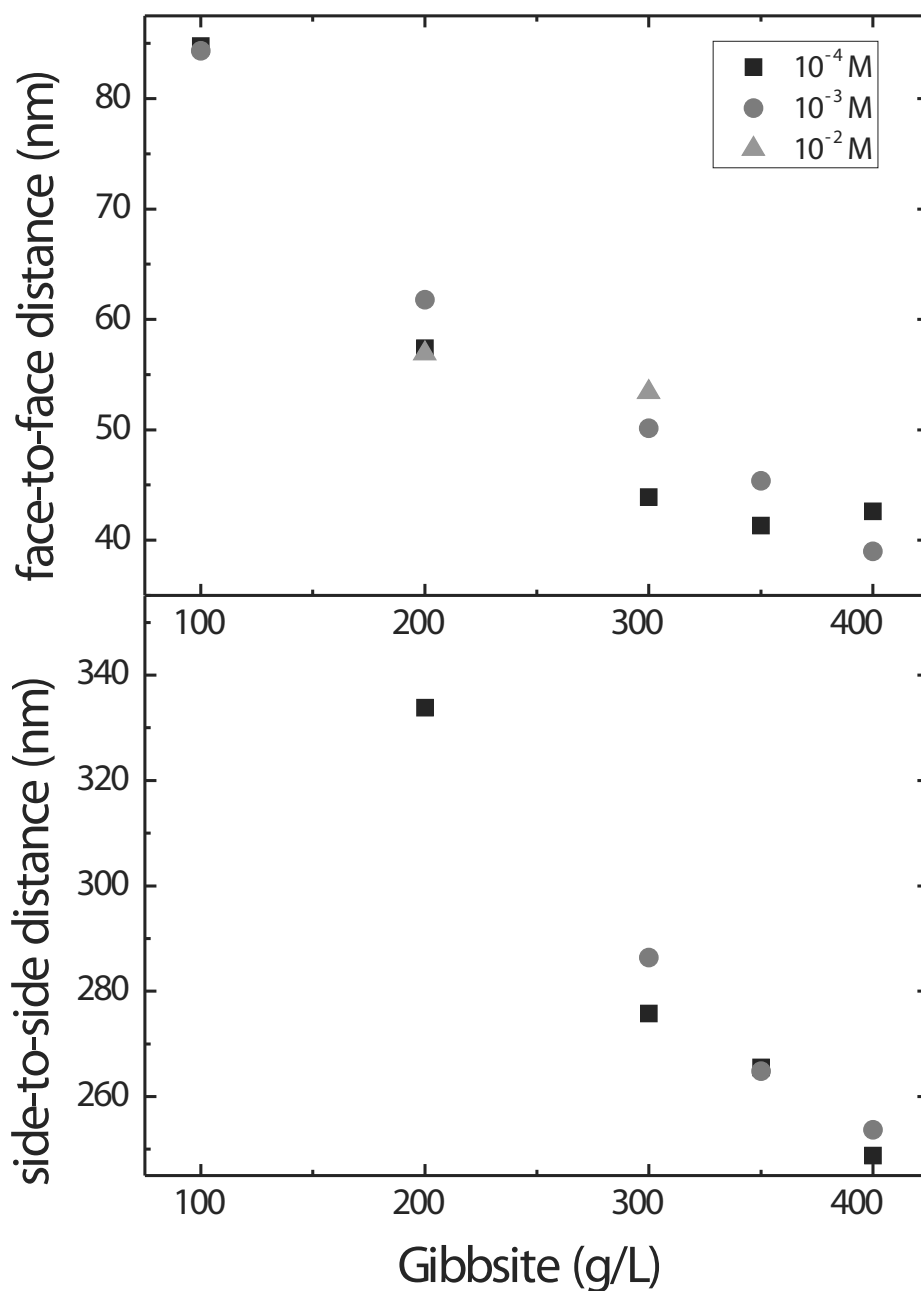


FIGURE 2.9. Variation of the typical face-to-face and side-to-side interparticle distances as a function of the overall gibbsite concentration. The typical distances are determined from the X-ray patterns as described in the text.

2.4. DISCUSSION

From the rheological experiments it follows that there is a sol region that is wedged between two gel regions: one at high salt concentration and one at low salt concentrations and high particle concentrations. This kind of sol-gel state diagram is typically found in rheological experiments on charged platelets [2, 17, 9, 6]. The shape of the

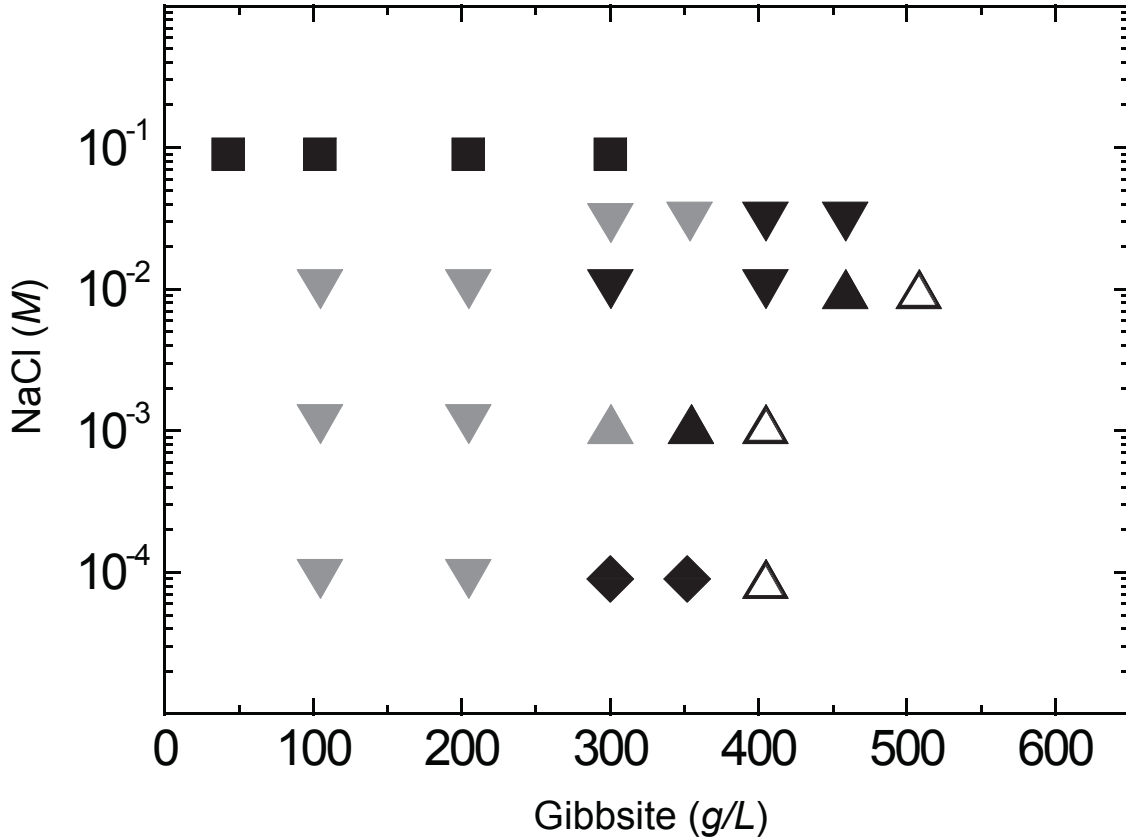


FIGURE 2.10. Phase diagram of aqueous gibbsite dispersions. Non-birefringent gel states are indicated by (■), N_D phases are indicated by (▼), N_C phases are indicated by (▲) and C-phases in coexistence with an N_C upper phase are indicated by (◆). Liquid crystal phases that are in coexistence with an isotropic phase are colored grey, while open symbols refer to repulsive gel states.

diagram suggest that in the high salt case attractions between the particles dominate, while in the low salt case the system is jammed in a repulsive gel.

For dispersions of gibbsite at low pH, as studied in this work, the faces and the edges of the particles have the same charge sign (positive) [39]. In this case the origin of the attraction is the Van der Waals interaction which tends to dominate the electric double layer repulsion at a salt concentration of 10^{-1} M or higher [41, 42]. In the case of clays the difference in face (negative) charge and edge (positive) charge (for a recent direct experimental confirmation of this phenomenon see [40]) leads to an additional source of attraction [23]. There, a minimum in the interaction curve already appears at 10^{-2} M salt. This may explain why the turnover from repulsion dominated to attraction dominated interaction occurs at higher salt concentrations in the case of gibbsite than in the case of clays. Our results show that the formation of liquid crystal phases is

essentially limited to the sol region of the rheological state diagram. This implies that while thermodynamically liquid crystal formation may be favored in parts of the gel region, the system is kinetically arrested. This is in agreement with recent observations in liquid crystal formation on nontronite suspensions [6].

A more detailed view on the structure of the dispersions was obtained by X-ray scattering and electron microscopy. One can see that the typical interparticle distances are mostly governed by the overall gibbsite concentration (Figure 2.9). This is understandable since this concentration determines the amount of space available in the system. In principle, the ionic strength, which affects the details of the interparticle interaction, can influence the proportion of the free space between the faces of the particles compared to the free space between their sides. Our data, however, is not conclusive enough to resolve these effects of the salt concentration.

The SAXS measurements do indicate that the structure of the liquid crystal phases in the sol region strongly depends on the salt concentration: the lower the salt concentration, the more structure was found (Figure 2.5). At high salt concentrations the nematic samples have anisotropic scattering patterns and decay monotonically from the center, as expected for a discotic nematic phase (N_D). On lowering the salt concentration first the face-to-face interparticle correlations appeared. On further lowering the salt concentration, apart from the face-to-face correlations, a gradual transformation of the structure from N_D to N_C can be seen. These two structures differ in the strength of the side-to-side positional correlation between the particles. In N_D the positional correlations mainly exist between the faces of single platelets. The N_C structure consists of (short) stacks of platelets, which strengthen the side-to-side interparticle correlations as is illustrated in Figure 2.11. Since we do not see any clear boundary between N_D and N_C , we choose the presence of both the face-to-face and the side-to-side correlation peaks in the scattering domain to assign the N_C structure. At the lowest ionic strength studied (10^{-4} M) and at sufficiently high particle concentration a hexagonal columnar phase (C) is found that is in coexistence with a nematic phase having an N_C structure. The N_C structure also occurs at a salt concentration of 10^{-2} M be it at higher particle concentration (450 g/L). Guided by the analogy with lowering the salt concentration one would expect that upon further increase of the particle concentration a hexagonal columnar phase (C), possibly in coexistence with N_C , would appear. At 500 g/L however, the structure remains N_C , but we have now entered the repulsive gel. This implies that the repulsive gel state has the signature of a metastable, kinetically-arrested N_C state.

It is interesting to compare at what conditions the dynamical arrest occurs. From Figure 2.10 it appears that the location of the sol-attractive gel transition occurs at a salt concentration between $3 \cdot 10^{-2}$ and 10^{-1} M regardless of the overall colloidal gibbsite concentration. On the other hand, the location of the sol-repulsive gel transition which

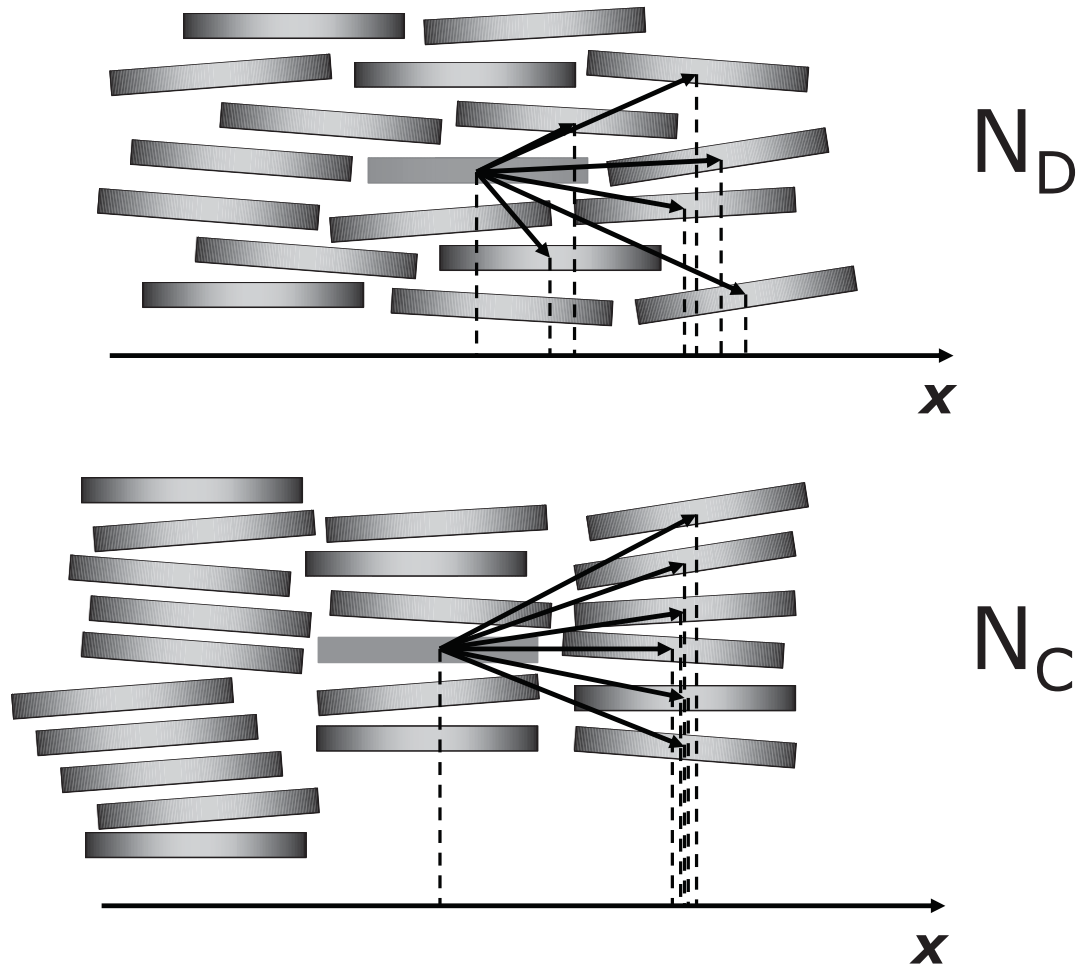


FIGURE 2.11. Schematic illustration of the N_D - and N_C -type structures which differ in the strength of the side-to-side positional correlations between the particles. While in the N_D -type structure there are few pairs of particles separated in the x -direction by the distance of approximately one particle diameter, for the N_C -type structure this occurs for many more pairs of particles.

occurs at salt concentrations of 10^{-2} M and below depends on the overall colloidal gibbsite concentration. The lower the salt concentration the lower the gibbsite concentration at which the sol-repulsive gel transition occurs. In the vicinity of the sol-repulsive gel transition both the side-to-side correlation distances can be determined, since the structure is either hexagonal columnar or has a pronounced nematic columnar signature. In Table 2.1 the average distances for side-to-side correlations in the N_C phases are displayed for the samples at the the sol-gel transition boundary. For the correlation distances, local hexagonal ordering is assumed and the distance that follows

TABLE 2.1. Correlation peaks and distances obtained by small angle X-ray scattering for samples around the sol-gel transition.

salt M	gibbsite g/L	state	q_{100} nm^{-1}	side-to-side
				correlation distance nm
10^{-2}	450	N_C	0.0292	249
	500	repulsive gel	0.0296	245
10^{-3}	350	N_C	0.0274	265
	400	repulsive-gel	0.0286	254
10^{-4}	350	N_C	0.0273	265
	400	repulsive -gel	0.0294	247

from the peak for the side-to-side correlation is multiplied by a factor of $\frac{2}{\sqrt{3}}$. These distances indicate that the structure is jammed when the columns of platelets are separated by approximately 250 nm, still considerably larger the platelet size (ECD , 205 nm). Therefore we conclude that stack formation by the platelets is favored in dense dispersions and is even present in cases where the platelets are jammed due to a lack of space.

Experimental support for the metastability of this glassy N_C state is provided by the observation that after two years, SAXS measurements (Figure 2.12A) on the upper part of two year old gel samples at $10^{-2}M$ salt, 500 g/L displayed two sharp peaks, at $q = 0.052$ and 0.068 nm^{-1} . The ratio of the q -values is close to the $1:\sqrt{3}$ ratio, indicative of a hexagonal columnar arrangement. Therefore, we conclude that in years, the repulsive gel devitrified as the structure transforms locally from N_C to C. While we do not see, by naked eye, the accompanying optical iridescence, the two year old repulsive gel sample at $10^{-3}M$ salt and 400 g/L displayed many small iridescent domains, mainly in the upper half of the sample cell (Figure 2.12B). It is conceivable that nucleation of these crystallites is facilitated by the local columnar order in the preceding arrested state[20]. An interpretation may be that in this repulsive gel state there are dynamical heterogeneities present as observed for colloidal suspensions of hard spheres[43, 44]. Furthermore it may concern a nucleation phenomenon with a low nucleation barrier, which gives rise to many nuclei [45]. In turn, the low nucleation barrier may be related to the columnar nature of the kinetically arrested state.

More than 50 years ago Frank [46] suggested for spheres the possibility of long-lived locally-favored structures, the geometry of which may prevent the system from relaxing to equilibrium (crystal) state. Recently, Royall [47] provided direct experimental evidence of such a local structural mechanism for dynamical arrest. From this perspective, the hard-sphere fluid-to-crystal-transition may be considered as a locally-favored

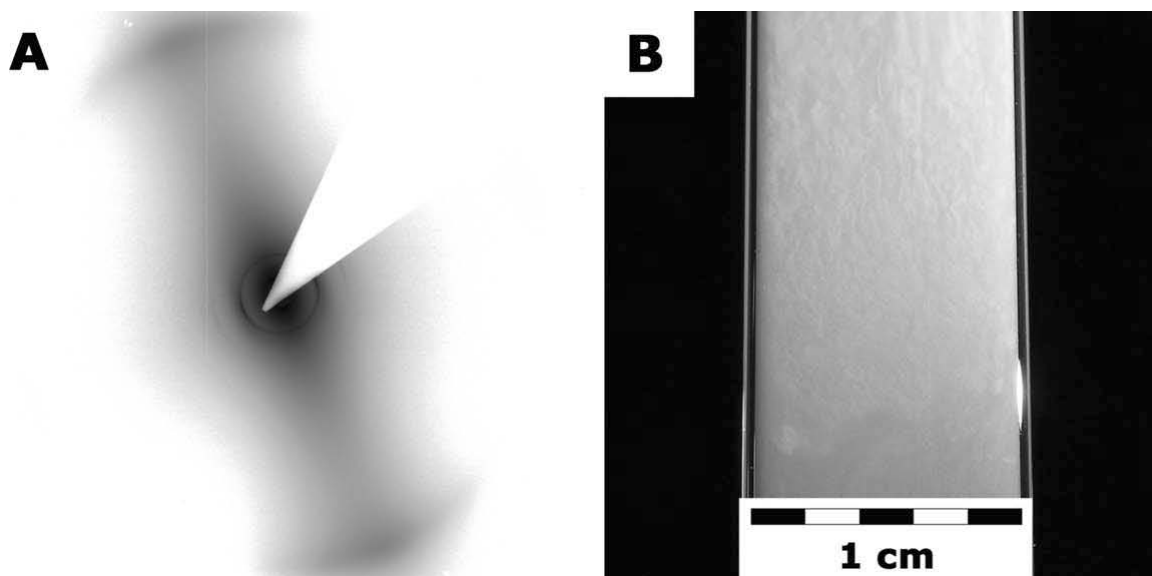


FIGURE 2.12. Devitrification of kinetically-arrested gibbsite dispersions. Panel (A) The upper part of the sample at 10^{-3}M salt and 400 g/L gibbsite displays iridescent spots, two years after preparation. Panel (B) shows the SAXS pattern of the sample at 10^{-2}M salt and 500 g/L gibbsite, recorded two years after preparation of the sample.

structure-avoiding transition.

In the case of platelets there is a strong tendency to form columns of platelets upon increase of the volume fraction [48]. As the volume fraction is increased, these columns grow in length. The columns themselves are flexible and hence there is appreciable interaction between different columns. This interaction among the columns eventually becomes so severe that the columns try to order in such a way that the packing problems are minimized. This then leads to a N_C phase and upon further increase of the volume fraction to the hexagonal columnar phase. Clearly then, the locally-favored structures in the case of platelets do not as such prevent the formation of liquid crystal phases. However, above a limiting concentration the columns may become kinetically arrested, leading to a glassy state. The eventual observation of small crystallites in this case appears to be enabled, rather than obstructed, by locally-favored structures. This is the opposite of the behavior observed in the canonical hard-sphere system [46, 47]. For platelets, the key structural element involved in the arrest transition is a stack of platelets, rather than an individual platelet. Such stacks are already present in the columnar nematic state, as well as in the arrested state itself. It may be that such (flexible) stacks can locally pack better in the arrested state than in the hexagonal columnar phase.

At high salt concentrations highly viscous gels are formed already at low gibbsite concentration. Even from their visual appearance (Figure 2.4), it is clear that these gels are

different from the repulsive gels. The enhanced turbidity suggests that a larger-scale structuring must be involved. Moreover, the absence of birefringence reveals that no orientational ordering is present. Earlier, the formation of clusters larger than the particle size was reported for dispersions of laponite [10] and cloisite [5]. X-ray scattering experiments on gibbsite samples reveal a broad but pronounced peak corresponding to a correlation distance significantly larger than the particle size. This points towards a sponge-like structure of the *attractive* gel. Electron micrographs substantiate the existence of such clusters of gibbsite particles and water regions with a mesh size of hundreds of nanometers.

2.5. CONCLUSIONS

Positively charged aqueous colloidal gibbsite particles show sol-gel behavior similar to clays as they enter kinetically arrested states at both high and low salt concentrations. At intermediate salt concentrations sols are formed up to particle concentrations as high as 500 g/L gibbsite. In this extended sol region I-N and N-C liquid crystal phase equilibria are present, as can be distinguished by observation of birefringence and iridescence. SAXS experiments reveal that the nematic phases at high salt concentrations or low platelet concentrations are of the discotic nematic (N_D) kind, while the nematic phases at low salt/high platelet concentrations are of the columnar nematic (N_C) kind. SAXS and cryo-FIB-SEM measurements show that the repulsive gel also has the signature of a columnar nematic phase. At high salt concentrations (10^{-1} M) a gel is formed, due to domination of attractive interactions. SAXS measurements and Cryo-FIB-SEM indicated a sponge-like structure of the attractive gel that is in agreement with that in clay systems, be it at higher salt concentrations.

2.6. ACKNOWLEDGEMENT

Dmytro Byelov, Matthijs de Winter and Arie Verkleij are acknowledged for their contributions. Chantal Vonk, Annemieke ten Brinke and Hans Meeldijk are thanked for their help in preparing the experiments. Esther van den Pol, Nicolas Vilayphiou, Dirk Detollenaere, Anatoly Snigirev and Wim Bras are thanked for their assistance in the SAXS experiments. Chris Schneijdenberg, Mike Hayles and Jeroen van Duijneveldt are acknowledged for discussions.

Bibliography

- [1] Gabriel, J. C. P.; Sanchez, C.; Davidson, P. *J. Phys. Chem.* **1996**, *100*, 11139–11143
- [2] Abend, S.; Lagaly, G. *Applied Clay Science* **2000**, *16*, 201
- [3] Michot, L.; Bihannic, I.; Porsch, K.; Maddi, S.; Baravian, C.; Mougel, J.; Levitz, P. *Langmuir* **2004**, *20*, 10829–10837
- [4] Michot, L. J.; Bihannic, I.; Maddi, S.; Funari, S. S.; Baravian, C.; Levitz, P.; Davidson, P. *PNAS* **2006**, *103*, 16101–16104
- [5] Shalkevich, A.; Stradner, A.; Bhat, S. K.; Muller, F.; Schurtenberger, P. *Langmuir* **2007**, *23*, 3570–3580
- [6] Michot, L. J.; Baravian, C.; Bihannic, I.; Maddi, S.; Moyne, C.; Duval, J. e. F. L.; Levitz, P.; Davidson, P. *Langmuir* **2009**, *25*, 127–139
- [7] Mourchid, A.; Delville, A.; Lambard, J.; Lécolier, E.; Levitz, P. *Langmuir* **1995**, *11*, 1942–1950
- [8] Kroon, M.; Wegdam, G.; Sprik, R. *Physical Review E* **1996**, *54*, 6541–6550
- [9] Mourchid, A.; Lécolier, E.; Van Damme, H.; Levitz, P. *Langmuir* **1998**, *14*, 4718–4723
- [10] Levitz, P.; Lécolier, E.; Mourchid, A.; Delville, A.; Lyonard, S. *Europhysics Letters* **2000**, *49*, 672–677
- [11] Fossum, J. O.; Gudding, E.; Fonseca, D. d. M.; Meheust, Y.; DiMasi, E.; Gog, T.; Venkataraman, C. *Energy* **2005**, *30*, 873–883
- [12] Ruzicka, B.; Zulian, L.; Ruocco, G. *Langmuir* **2006**, *22*, 1106–1111
- [13] Brown, A.; Clarke, S.; Rennie, A. *Langmuir* **1998**, *14*, 3129–3132
- [14] van der Beek, D.; Lekkerkerker, H. N. *Langmuir* **2004**, *20*, 8582–8586
- [15] Mourad, M. C. D.; Wijnhoven, J. E. G. J.; Van 't Zand, D. D.; Van der Beek, D.; Lekkerkerker, H. N. W. *Philosophical Transactions of the Royal Society a-Mathematical Physical and Engineering Sciences* **2006**, *364*, 2807–2816
- [16] Michot, L. J.; Ghanbaja, J.; Tirtaatmadja, V.; Scales, P. J. *Langmuir* **2001**, *17*, 2100–2105
- [17] Zhang, J.; Luan, L. Y.; Zhu, W. X.; Liu, S. Y.; Sun, D. J. *Langmuir* **2007**, *23*, 5331–5337
- [18] Darley, H.; Gray, G. R. *Compostion and Properties of Drilling and Completion Fluids*, 5th ed.; Gulf Publishing Company: Houston, 1988
- [19] van Olphen, H. *Discussions of the Faraday Society* **1951**, *11*, 82–84
- [20] Mourad, M. C. D.; Byelov, D. V.; Petukhov, A. V.; Lekkerkerker, H. N. W. *Journal of Physics: Condensed Matter* **2008**, *20*, 494201, 0953-8984
- [21] Norrish, K. *Discussions of the Faraday Society* **1954**, *18*, 120–134
- [22] Schofield, R. K.; Samson, H. R. *Discuss. Faraday Soc.* **1954**, *18*, 135
- [23] Jönsson, B.; Labbez, C.; Cabane, B. *Langmuir* **2008**, *24*, 11406–11413
- [24] Onsager, L. *Annals of the New York Academy of Sciences* **1949**, *51*, 627–659
- [25] Langmuir, I. *Journal of Chemical Physics* **1938**, *6*, 873–896
- [26] Thompson, D. W.; Butterworth, J. T. *Journal of Colloid and Interface Science* **1992**, *151*, 236–243, 0021-9797
- [27] Michot, L. J. *private communication*, 2008

- [28] Wijnhoven, J. E. G. J.; van 't Zand, D. D.; van der Beek, D.; Lekkerkerker, H. N. W. *Langmuir* **2005**, *21*, 10422–10427
- [29] Hernandez, J. Ph.D. thesis, Université Pierre et Marie Curie, 1998
- [30] Goodwin, J. W.; Hughes, R. W. *Rheology for Chemists. An Introduction*; Royal Society of Chemistry: Cambridge, 2000
- [31] Petukhov, A. V.; Thijssen, J. H. J.; 't Hart, D. C.; Imhof, A.; van Blaaderen, A.; Dolbnya, I. P.; Snigirev, A.; Moussaid, A.; Snigireva, I. *Journal of Applied Crystallography* **2006**, *39*, 137–144
- [32] Snigirev, A.; Kohn, V.; Snigireva, I.; Lengeler, B. *Nature* **1996**, *384*, 49
- [33] Hayles, M. F.; Stokes, D. J.; Phifer, D.; Findlay, K. C. *Journal of Microscopy* **2007**, *226*, 263–269
- [34] Winter, H.; Morganelli, P.; F., C. *Macromolecules* **1988**, *21*, 532–535
- [35] Almdal, K.; Dyre, J.; Hvidt, S.; Kramer, O. *Polymer Gels and Networks* **1993**, *1*, 5–17
- [36] Laschat, S.; Baro, A.; Steinke, N.; Giesselmann, F.; Hägele, C.; Scalia, G.; Judele, R.; Kapatsina, E.; Sauer, S.; Schreivogel, A.; Tosoni, M. *Angewandte Chemie International Edition* **2007**, *46*, 4832–4887
- [37] Praefcke, K.; Singer, D.; Kohne, B.; Ebert, M.; Liebmann, A.; Wendorff, J. H. *Liquid Crystals* **1991**, *10*, 147 – 159
- [38] Bengs, H.; Karthaus, O.; Ringsdorf, H.; Baehr, C.; Ebert, M.; Wendorff, J. H. *Liquid Crystals* **1991**, *10*, 161 – 168
- [39] Wierenga, A. M.; Lenstra, T. A. J.; Philipse, A. P. *Colloids and Surfaces A* **1998**, *134*, 359–371
- [40] Zhao, H.; Bhattacharjee, S.; Chow, R.; Wallace, D.; Masliyah, J. H.; Xu, Z. *Langmuir* **2008**, *24*, 12899–12910
- [41] Verwey, E. J. W.; Overbeek, J. Th. G. *Theory of the Stability of Lyophobic Colloids* Elsevier Amsterdam **1948**
- [42] Israelachvili, J. N. *Intermolecular and Surface Forces* Academic Press New York **1991**
- [43] Kegel, W. K.; van Blaaderen, A. *Science*, 2000, **287**(5451), 290–293.
- [44] Weeks, E. R.; Crocker, J. C.; Levitt, A. C.; Schofield, A.; Weitz, D. A. *Science*, 2000, **287**(5453), 627–631.
- [45] Shi, F. G.; Tong, H. Y.; Ayers, J. D. *Applied Physics Letters*, 1995, **67**(3), 350–352.
- [46] Frank, F. C. *Proceedings of the Royal Society of London. Series A, Mathematical and Physical Sciences*, 1952, **215**(1120), 43–46.
- [47] Royall, C. P.; Williams, S. R.; Ohtsuka, T.; Tanaka, H. *Nature Materials*, 2008, **7**(7), 556–561.
- [48] Veerman, J.; Frenkel, D. *Physical Review A*, 1992, **45**(8), 5632–5648.

3

Columnar Liquid Crystals of Gibbsite Platelets as Templates for the Generation of Ordered Silica Structures

ABSTRACT

We describe the use of columnar liquid crystals of silica coated colloidal gibbsite platelets as templates for the generation of ordered silica structures. The colloidal liquid crystal phases can be formed in a few hours by modest centrifugation forces (100-200g). Base catalysed hydrolysis of tetra-ethoxysilane (TEOS) is used to deposit silica in the space between the silica coated gibbsite particles. The size of the gibbsite platelets is varied between 200-500 nm and the thickness of the silica coating between 5-15 nm making the system a very versatile templating material. Acid leaching is used to selectively remove the gibbsite material.

Reproduced by permission of The Royal Society of Chemistry. M.C.D. Mourad, E. Groeneveld, P.J. de Lange, C. Vonk, D. van der Beek, and H.N.W. Lekkerkerker, J. Mater. Chem. 18 (2008) 3004

3.1. INTRODUCTION

The use of surfactant liquid crystals for templated synthesis in the early 1990s led to the formation of ordered mesoporous silica structures [1, 2, 3, 4]. This new class of materials has boosted research in the application of catalytically active phases inside the mesopores of these materials [5, 6, 7, 8]. In the first reports on ordered mesoporous silica materials, cationic surfactants were used as structure-directing agent. Due to the very thin porous walls these materials display a rather large instability towards a number of aqueous catalyst precursor solutions, which hamper their application as support material. In 1995 Bagshaw, Prouzet and Pinnavaia [9] and later a group in Santa Barbara reported on the formation of mesoporous silica structures formed using block copolymers as templating materials [10] (for a recent review see [11]). Compared to the materials templated by cationic surfactants these mesoporous materials have the attractive properties of larger pore diameters, thicker walls and higher stability. This makes them attractive candidates as support materials [12]. While interesting and versatile from a structural point of view, porous materials based on supra-molecular organic liquid crystal materials are limited in pore size (to 10 nm or less) by the size of the surfactant aggregates. The breakthrough to the macroporous range (50-1000 nm) came with the use of colloidal crystals as templating materials [13, 14, 15]. In this method first a colloidal crystal of monodisperse spherical colloidal particles is produced. Subsequently sol-gel processing is used to deposit an inorganic material at the exterior of the colloidal particles. When the sol-gel process mixture has polymerised, the colloidal template is removed by calcination or etching. This method leads to macroporous materials with spherical pores up to 1000nm in diameter with fascinating photonic properties [15, 16, 18]. Here we demonstrate that the colloidal crystal templating method can be taken one step further, towards the formation of materials with ordered uniform pores of arbitrary size and shape and adjustable thickness of the pore walls by colloidal liquid crystals as templates. For a colloidal liquid crystal to act as a template for the preparation of an ordered macroporous material it must satisfy three conditions:

- easy and fast formation of the colloidal liquid crystal
- allowing adjustable thickness of the pore wall
- possibility to remove the colloidal liquid crystal template

We will show in this work that colloidal liquid crystals of gibbsite particles do fulfill these three conditions. Over the last few years we have explored the liquid crystal phase behaviour of colloidal gibbsite platelets. In particular, we have observed that suspensions of both sterically [17] and charge-stabilized gibbsite platelets [19, 20, 21] at sufficiently high concentrations display beautiful iridescence. From high-resolution small-angle X-ray scattering [22, 23] measurements we have obtained unambiguous evidence that

these iridescent phases have columnar structure with hexagonal inter-columnar ordering, which is quite remarkable as the platelets have a significant polydispersity of 19% (27%) in diameter (thickness). Under normal gravity, the gibbsite suspensions develop sediments on a timescale of years. These sediments show iridescence, due to Bragg reflections by the columnar arrangement. The slow growth rate of the sediment (1 Å per second) as well as its striking iridescence reminds one of the formation of natural opal. We have shown [24] that the formation process of the opal-like material can be sped up by three orders of magnitude (i.e., 1 day instead of 3 years) by centrifugation. To prepare the system for silica polymerization we coat the gibbsite particles with a silica layer. These silica coated gibbsite particles also form a columnar sediment under centrifugation. This then forms the starting structure for fixation with silica through polymerisation starting from a Stöber mixture [25]. The gibbsite template inside the polymerised silica structure can be removed by acid leaching.

3.2. HEXAGONAL COLUMNAR LIQUID CRYSTAL PHASES OF COLLOIDAL GIBBSITE PLATELETS AT 1 G

Colloidal gibbsite platelets were synthesized by crystallisation from an acidified aluminium-alkoxide solution at 85C, following a procedure developed earlier at our laboratory [26]. The resulting suspension contained 6 g/L gibbsite particles with a well-defined hexagonal shape, which can be observed on Transmission Electron Micrographs (TEM), see Fig. 3.1. From such micrographs, the average particle diameter $\langle d \rangle$, defined as the average of the average corner-to-corner distances, and polydispersity d defined as the standard deviation in the average, were obtained using image analysis software. The average thickness $\langle l \rangle$ of the platelets and the associated polydispersity l were determined to within 0.1 nm using Atomic Force Microscopy (AFM). The sample to be studied was prepared by filling a glass container with the gibbsite suspension. It was left undisturbed in a thermostatted dark room and inspected occasionally. From time to time, photographs were taken, of which three are shown in Fig. 3.2. During 6 years the sample developed a sediment with strong Bragg reflections in the visible light range that are due to the columnar liquid crystalline order. In earlier papers [27, 22, 24], we have employed small-angle X-ray scattering to confirm the existence of a columnar phase of these disk-like particles. From the photographs, two layers can be identified. The lower one has formed very quickly in the early stages of the experiment, i.e., within a few months, and is composed of small columnar crystallites. The top layer grows much more slowly (about 1 Å/s) and as a result, the columnar colloidal crystal formed consists of much larger single domains up to 5 mm. Still, the growth is not finished. Apparently, it is relatively easy to grow large single domains of a columnar colloidal

crystal of polydisperse gibbsite platelets, given enough patience. However, our observations invoke the question as to whether the formation of such a ‘synthetic columnar opal’ can be sped up. Indeed, this appears to be possible using centrifugation.

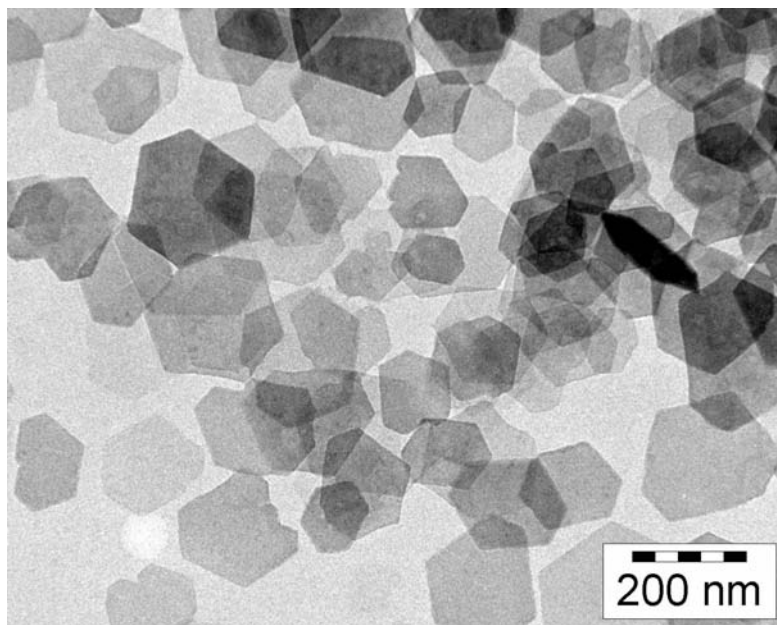


FIGURE 3.1. Transmission electron micrograph of bare gibbsite platelets used in this study. The regular hexagonal gibbsite crystals have an average diameter ($\langle d \rangle = 202$ nm, 19%) and average thickness ($\langle l \rangle = 13.2$ nm, 27%). Reprinted with permission from D. van der Beek, P. B. Radstake, A. V. Petukhov, and H. N. W. Lekkerkerker, *Langmuir* 23, 11343 (2007). Copyright 2007 American Chemical Society.

3.3. HEXAGONAL COLUMNAR LIQUID CRYSTAL PHASES OF COLLOIDAL GIBBSITE PLATELETS AT 900 G

From previous studies, it follows that the presence of Al_{13} -ions has a stabilizing effect on colloidal boehmite ($\text{AlO}(\text{OH})$) and gibbsite particles [28, 29, 30]. In order to enhance the colloidal stability of our gibbsite particles, we have treated them in the same fashion before starting the centrifugation experiments. To the gibbsite dispersion aluminium chlorohydrate was added, which hydrolyses to form Al_{13} -Keggin ions ($[\text{Al}_{13}\text{O}_4(\text{OH})_{24}(\text{H}_2\text{O})_{12}]^{7+}$). The treated batch of the suspension was contained in a glass flask of height 10 cm and centrifuged at 900 g. After one day, all particles were sedimented and formed a viscous layer on the bottom of the flask. The supernatant liquid was removed and the sediment photographed, see Fig. 3.3. The sediment displays bright violet and green iridescent colours and consists of numerous small crystallites, which we attribute to the fast formation like in the early stage of the first sample (Fig.

3.2). Thus, it is clear that the 'synthetic columnar opal production' can be accelerated by orders of magnitude using centrifugation at as much as 900 g without arresting the system in a disordered glassy phase. It was found that samples in smaller tubes (diameter 1 mm) also developed these bright Bragg reflections, which remained present even after 4 years. Despite this stability, in order to obtain a hard opal-like material based on these colloidal liquid crystals, our next step is to prepare gibbsite particles with a discrete layer of silica.

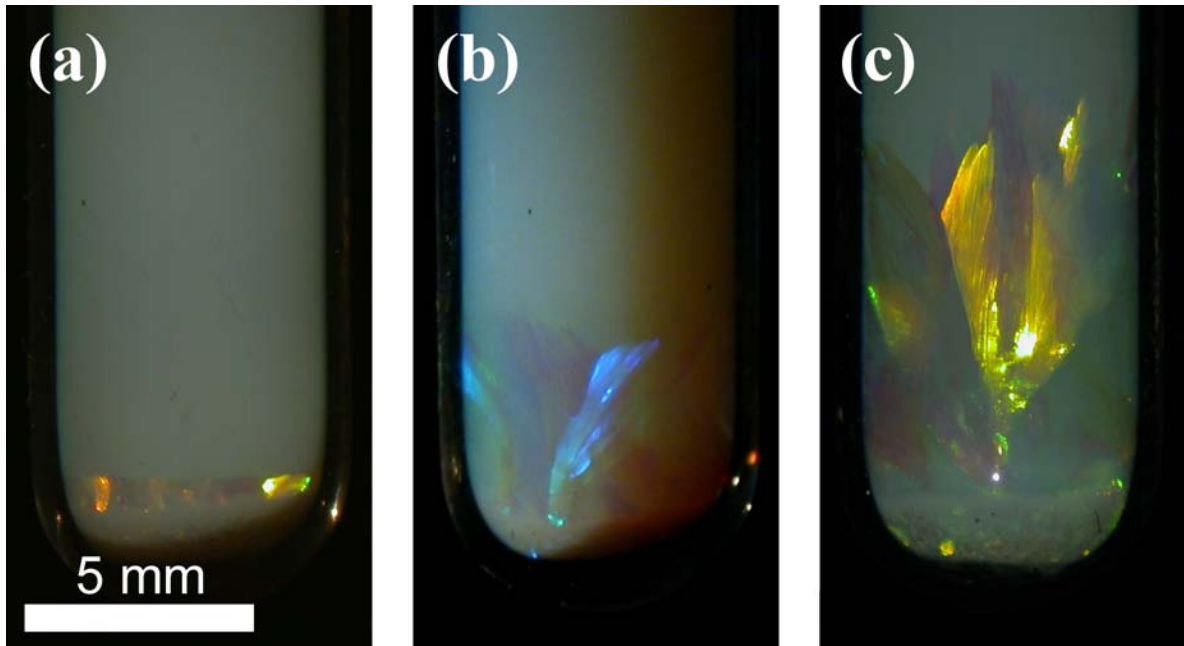


FIGURE 3.2. Iridescent columnar phase of the colloidal gibbsite platelets, grown in the earth's gravitational field (1 g). The sample has been standing for (a) 2 years, (b) 3.5 years, and (c) 6 years, and the columnar phase continues to grow. Figure (a) was reprinted with permission from D. van der Beek, P. B. Radstake, A. V. Petukhov, and H. N. W. Lekkerkerker, *Langmuir* 23, 11343 (2007). Copyright 2007 American Chemical Society.

3.4. SILICA COATED GIBBSITE

As mentioned in the introduction we wish to obtain a templating colloidal liquid crystal that allows an adjustable thickness of the pore wall. In order to achieve this goal we first coat the gibbsite particles with layers of silica of different thickness. Then we produce a hexagonal columnar liquid crystal of these particles in a mixture of TEOS and ethanol, which is subsequently polymerised. This strategy is schematically illustrated in Fig. 3.4. A batch of bare gibbsite particles with $\langle d \rangle = 210\text{nm}$, i.e. very similar in size to the particles described above, was coated with silica using the method described by Wijnhoven [31]. For this purpose a dilute aqueous dispersion containing 0.5 g gibbsite

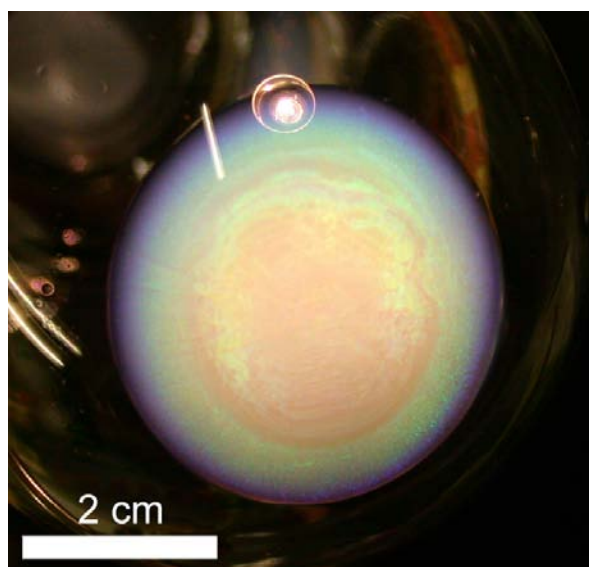


FIGURE 3.3. Iridescent columnar phase of ACH-treated gibbsite particle, formed by centrifugation at 900 g for one day. The columnar layer contains numerous small crystallites that show bright green and purple Bragg reflections due to the hexagonal lattice. Reprinted with permission from D. van der Beek, P. B. Radstake, A. V. Petukhov, and H. N. W. Lekkerkerker, *Langmuir* 23, 11343 (2007). Copyright 2007 American Chemical Society.

particles was centrifuged (2 hours, 1000g). Then, an aqueous solution of PVP (polyvinylpyrrolidone, 100g/L, MW 40000, Sigma) was used to replace the supernatant of the gibbsite. After 24 hours of gentle stirring the excess of poly-vinylpyrrolidone is removed by centrifugation and redispersion in 0.5 L of a mixture of ethanol (Merck, p.a.) and 33 mL ammonia (Acros, p.a. 28-30 %). While uncoated gibbsite particles flocculate upon dispersion in ethanol, PVP-coated gibbsite is able to form a stable dispersion. To this dispersion 1.0 mL of TEOS (tetraethoxysilane: Fluka, purris $\geq 99.0\%$) was added under vigorous stirring. A transmission electron micrograph of the resulting particles is shown in Fig. 3.5a. The thickness of the silica shell can be adjusted easily by the amount of TEOS that is added to the system of PVP coated gibbsite particles. Therefore, in some of the systems an additional amount of TEOS was added, to make the silica coating thicker.

In order to demonstrate the versatility of gibbsite particles as a templating agent we also explored the use of larger particles. For this purpose gibbsite particles with $\langle d \rangle = 207$ nm were redispersed in the acidic mixture of aluminum alkoxides in water for a seeded growth procedure similar as described earlier [32]. After such a procedure the particles had grown to an average diameter $\langle d \rangle = 493 \pm 59$ nm, as was determined from measurements of the corner-to-corner distance of 400 platelets from transmission electron micrographs. These large particles were coated with a silica layer following the

same procedure as described above for the smaller particles. The result is a very turbid dispersion of platelets that shows shear-induced alignment upon stirring. In Fig. 3.5b a transmission electron micrograph of one of the resulting silica grafted gibbsite particles is shown. It is interesting to note that the gibbsite particle is coated with a silica layer that is slightly rougher than the gibbsite core. The average thickness of the silica layer in this system is determined by measuring more than 40 individual layers at the edges of the particles as visualized in Fig. 3.5b, yielding a thickness of 15 nm.

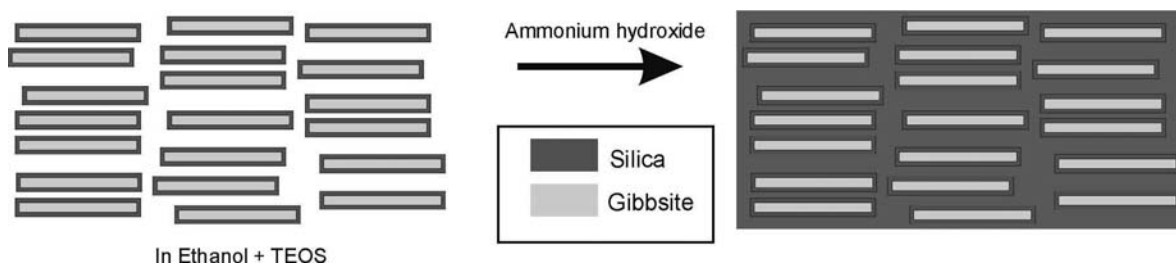


FIGURE 3.4. Artist's impression of the templating procedure of silica coated gibbsite in columnar liquid crystals within a solvent containing the silica precursor TEOS.

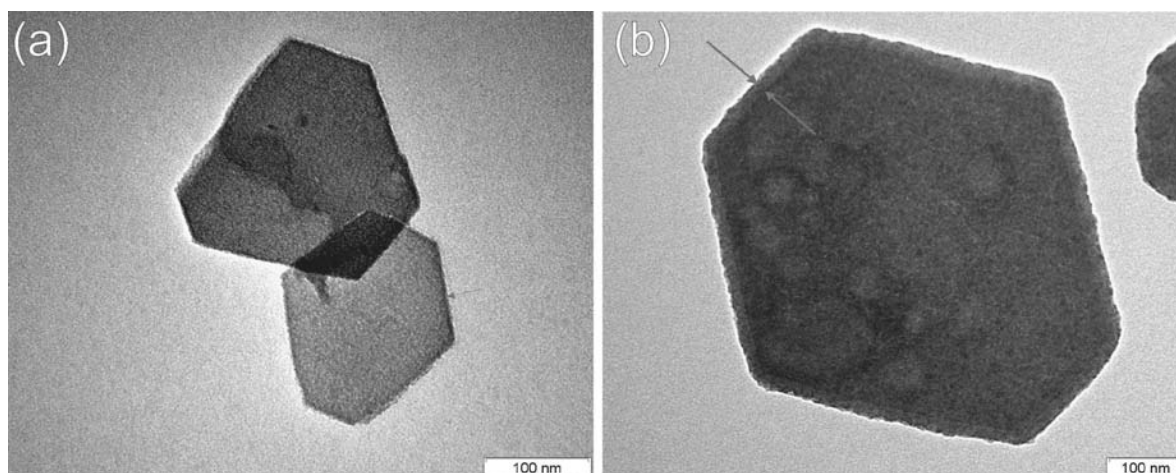


FIGURE 3.5. Transmission electron micrograph of silica coated gibbsite particles used in this study. A system of small gibbsite particles ($\langle d \rangle_{bare} = 210$ nm) was coated with a silica layer (average thickness 5 nm) (a). Performance of a seeded growth procedure for gibbsite leads to a larger average diameter ($\langle d \rangle_{bare} = 493$ nm, 12%) of the bare gibbsite platelets. Coating this larger system with silica (15 nm) leads to the system depicted in (b). The thickness of the silica coating is visible on the edges of the particles as indicated by the arrows.

3.5. HEXAGONAL COLUMNAR LIQUID CRYSTAL PHASES OF SILICA COATED GIBBSITE

The silica coated gibbsite particles, prepared as described in the previous section, form stable suspensions in water, ethanol and mixtures of ethanol and TEOS. The latter is of crucial importance since in order to be able to deposit silica on the liquid crystal colloidal particles there is a need to work in an environment where a significant amount of precursor (i.e., TEOS) is present. Solid material forming the pore walls is produced upon addition of an initiator. In all of the solvents mentioned above, centrifugation leads to the formation of a columnar liquid crystal as evidenced by the appearance of Bragg reflections. In Fig. 3.6 the results are shown for the system consisting of the small ($\langle d \rangle = 210$ nm) gibbsite particles coated with silica. Similarly in Fig. 3.7 the results are shown for the system containing the larger particles ($\langle d \rangle = 493$ nm). Dispersions of silica coated gibbsite particles in water were centrifuged and inspected under white illumination directly after stopping the centrifuge. Bright Bragg reflections became visible upon centrifugation of aqueous silica in ring shaped layers at the bottom of the centrifuge tubes. When the tubes are inspected upside down, the sediment will be perturbed by the tilt and becomes loose. A flow of previously sedimented material emerges along the walls of the tube. Even during flow, bright Bragg reflecting areas remain visible in the sediment. Similar phenomena were observed for dispersions in ethanol and mixtures of ethanol and TEOS. The centrifugal force and centrifugation time needed for the large particles was significantly smaller than for the smaller ones. Moreover, sedimentation of the large particles at 1 g for 4 days in a mixture of ethanol (40% v/v) and TEOS (60% v/v) already leads to beautiful Bragg reflections (Fig. 3.7d).

3.6. COLUMNAR LIQUID CRYSTALS OF SILICA COATED GIBBSITE PARTICLES AS TEMPLATES FOR DIRECTED GROWTH OF SILICA

To cast columnar liquid crystals in silica, first columnar pellets were obtained by sedimentation of silica coated gibbsite particles in a mixture of TEOS and ethanol as a solvent. After formation of such a sediment, the supernatant was removed and replaced by ammonium hydroxide (Acros p.a., 28-30%v/v) to start in situ polymerization of a silica network throughout the colloidal pellet. After addition of ammonia the colloidal crystals appeared fixated and no longer redispersed spontaneously. Optical Bragg reflections were still visible after this step. In order to prove the existence of the columnar phase and to characterize it in detail SAXS measurements were done on the solid system. So far, no conclusive results pertaining to the columnar phase could be extracted from these measurements. For the small gibbsite particles coated with a 5 nm layer of silica 20% v/v TEOS (and 80% v/v ethanol) was the maximum amount of silica precursor that could be used while keeping the system stable. To increase the amount

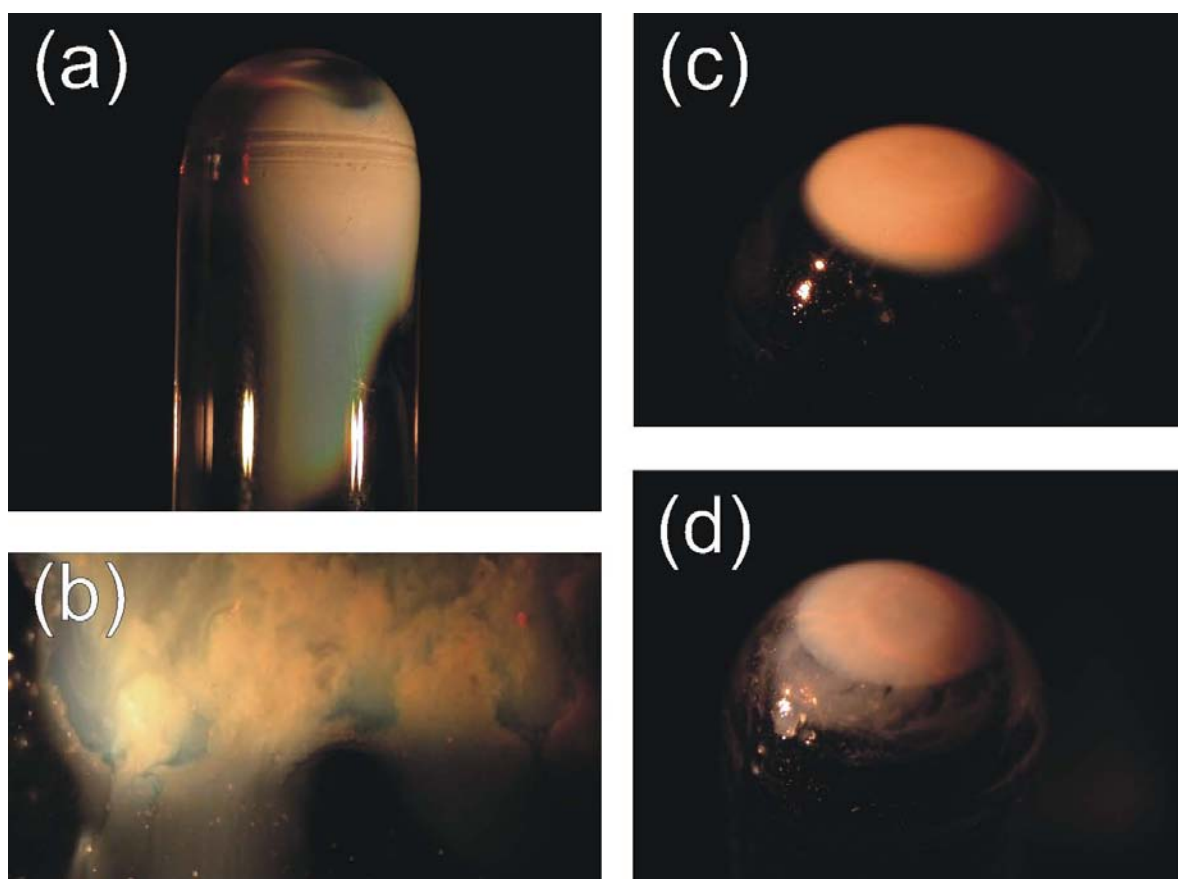


FIGURE 3.6. Centrifugation of the system of silica coated small gibbsite particles leads to the formation of columnar phases in various solvents as is observed from iridescence. Right before observation the test tubes were turned upside down for practical purposes. The sediments shown are formed in (a) water (2 hours, 185 g), (b) ethanol (17 hours, 185 g) and (c) TEOS (20% v/v) + ethanol (80% v/v, 2 hours, 447 g). Replacement of the supernatant in (c) with ammonia and subsequent infiltration with TEOS/ethanol followed by ammonia leads to the formation of a solid system (d).

of silica deposited upon addition of ammonium hydroxide, the silica precipitation procedure was repeated two more times by addition of a fresh reaction mixture consisting of ethanol and TEOS followed by addition of ammonium hydroxide. The resulting solid system, shown in Fig. 3.6d, is quite rigid.

The large particles, with a silica layer of 15 nm, were stable in a mixture of 60% v/v TEOS (and 40% v/v ethanol). In this case a single precipitation reaction step produced sufficient silica to form a rigid structure. The resulting structure was dried in air to remove the remaining solvent over several days. Upon drying the sediment slightly shrank, cracked and released from the walls of the sample tube. Careful examination showed that the resulting flakes of material still show Bragg reflections (Fig. 3.8). Depending on the angle of illumination, different columnar crystal domains show coloured

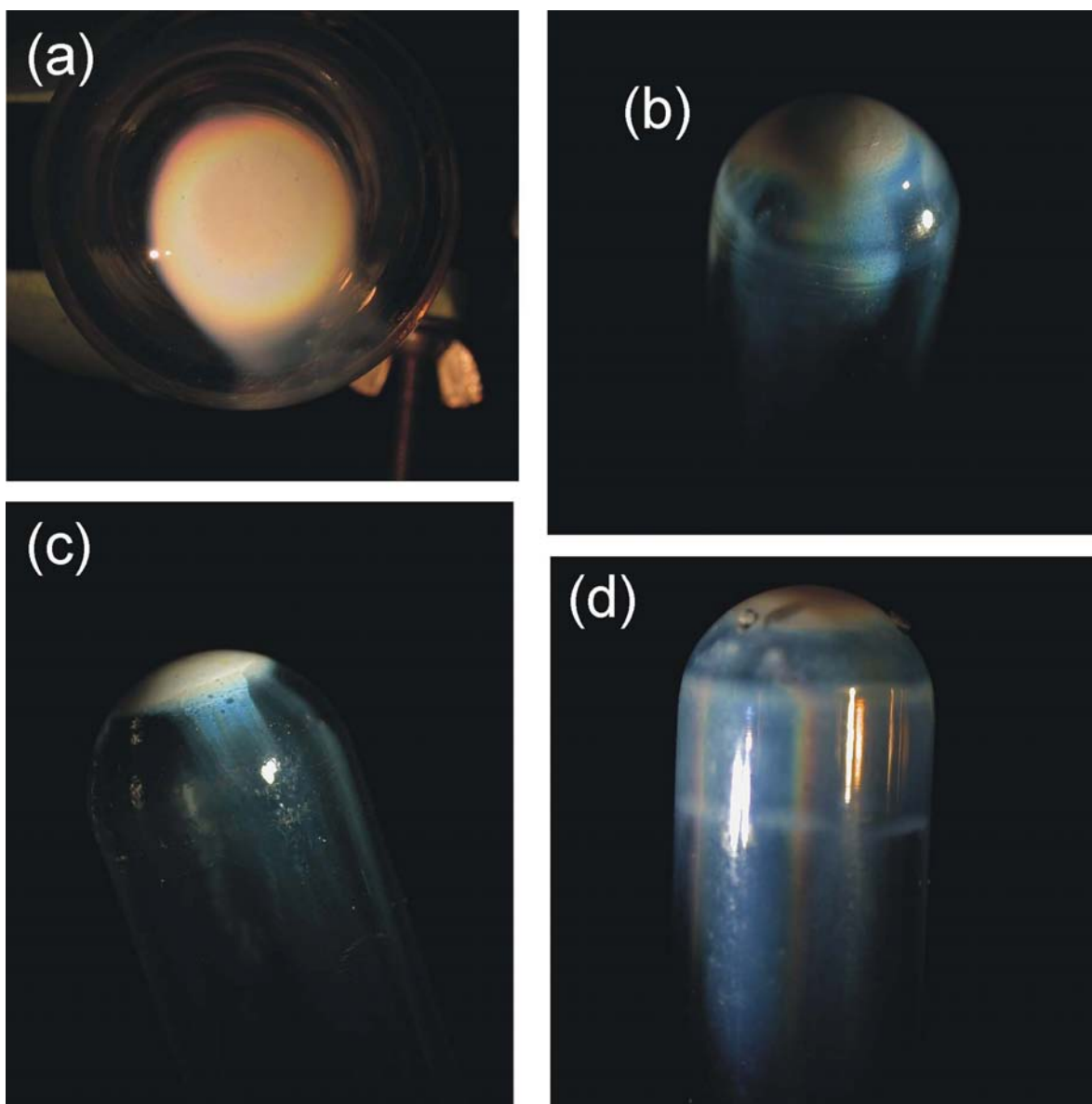


FIGURE 3.7. Centrifugation of the system of silica coated large gibbsite particles leads to the formation of columnar phases in various solvents as is observed from iridescence. Right before observation the test tubes were turned upside down for practical purposes. The sediments after centrifugation in (a) water (3 hours, 900g), (b) ethanol (30 minutes, 200g) and (c) TEOS (60% v/v) + ethanol (40% v/v) (30 minutes, 200g) are shown. After 4 days a columnar sediment is formed by normal gravity as is illustrated by the sample in 30% v/v TEOS + 70% v/v ethanol shown in (d).

reflections. Note that whereas in Fig. 3.2 blue iridescence is visible, this not the case in Fig. 3.8. This could be related to the fact that the particles in Fig. 3.2 have a diameter of 210 nm and in Fig. 3.8 the diameter of the particles is 493nm. To study

the effect of particle size on the wavelength of the reflections experiments with carefully controlled angles of illumination and reflection must be performed. Scanning electron microscopy (SEM) was performed on this material with a XLFEG30 (5kV, Philips). Prior to SEM experiments samples were sputter-coated with a layer of approximately 5 nm thickness of Pt/Pd alloy. The micrographs reveal that despite the large TEOS content before addition of ammonia, separate silica coated particles can still be distinguished (Fig. 3.9). This does not imply that the structure is loose. It is known that in the Stöber synthesis originally separated particles may grow together at too high concentrations of ammonia or TEOS, an effect that is exploited in the production of silica dumbbells [33]. A significant amount of silica has nucleated on the original silica coated gibbsite platelets making them appear much bulkier in SEM pictures. Although orientational order is clearly present and small stacks of platelets are visible, it is not obvious from SEM images that the platelets show hexagonal order. A possible explanation might be that whatever hexagonal order is present in this figure is masked by polydispersity. Moreover a limited amount of spherical particles is formed at the surface of the sediment. However, it is still unclear whether these spheres possess a gibbsite platelet as a core or if they are formed due to secondary nucleation.

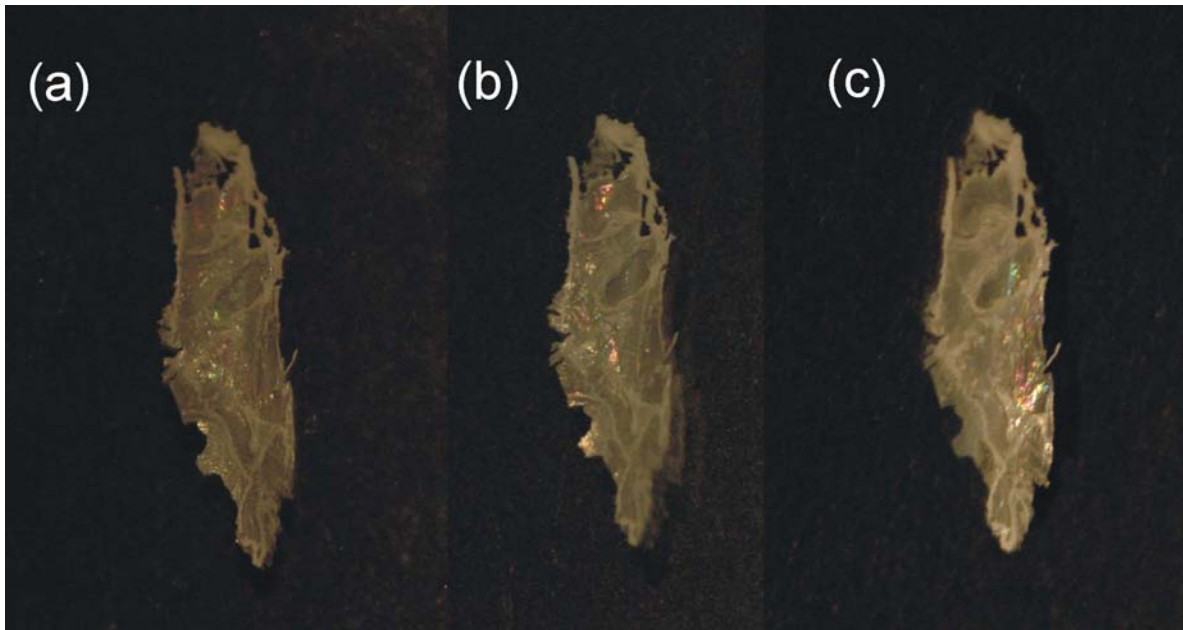


FIGURE 3.8. Solid flake of columnar silica coated gibbsite in silica. A columnar liquid crystal of silica coated gibbsite particles dispersed in TEOS (60% v/v) + ethanol (40% v/v) was solidified by addition of ammonium hydroxide and dried. Illumination by white light under various angles leads to reflections of various domains and colors.

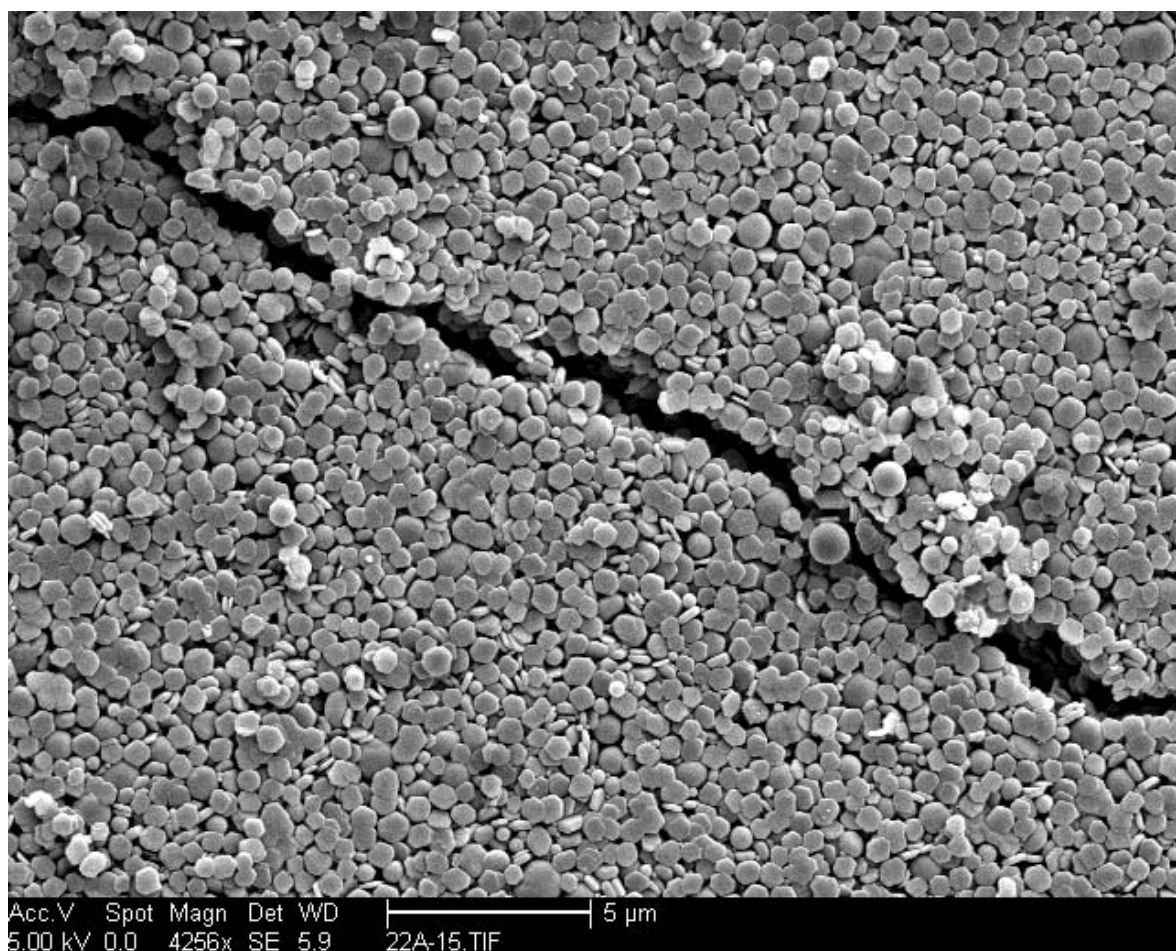


FIGURE 3.9. SEM image of silica coated gibbsite particles in the columnar phase after deposition of silica from the solvent and subsequent drying.

3.7. REMOVAL OF THE GIBBSITE CORES

The gibbsite core of a composite silica-gibbsite particle can be removed through the silica coating in solution by acid leaching the system in nitric acid, as was shown earlier by Wijnhoven [31]. Silica coated gibbsite particles were first transferred to water before concentrated nitric acid was added to the dispersion. After 4 days and 2 additions of a large excess of nitric acid, the system was investigated by TEM to see the result of the acid leaching on the particles. The leached particle displayed in Fig. 3.10a has an edge that is noticeably darker than the interior. Recall that the particles before leaching had the opposite contrast, being darker on the inside (Fig. 3.5b). From this we conclude that the gibbsite core has indeed been leached away. The dark edge has a thickness of approximately 17 nm, consistent with the thickness of the silica shell. The integrity of the silica coating seems unaffected by the leaching procedure. Even more conclusive information is provided by STEM EDX (Scanning Transmission Electron Microscopy Energy Dispersive X-ray) measurements on silica covered gibbsite platelets that were

leached. The dark-field STEM image displayed in Fig. 3.10b shows the location in a single particle where a spot EDX measurement was done. There is a large ratio between the signal attributed to Si and that attributed to Al in the corresponding EDX measurement that is displayed in Fig. 3.10c. This is in accordance with the removal of gibbsite. Since it is possible to leach out substantial amounts of aluminium from composite particles we have tried to use this acid leaching procedure for removal of the gibbsite cores in our dried, silica fixated columnar crystals. For this purpose flakes of Bragg reflecting material were immersed repeatedly for several days in concentrated nitric acid. SEM pictures reveal that the global appearance (Fig. 3.11a) of the system remains the same, but that individual platelets may show that they are hollow (Fig. 3.11b)

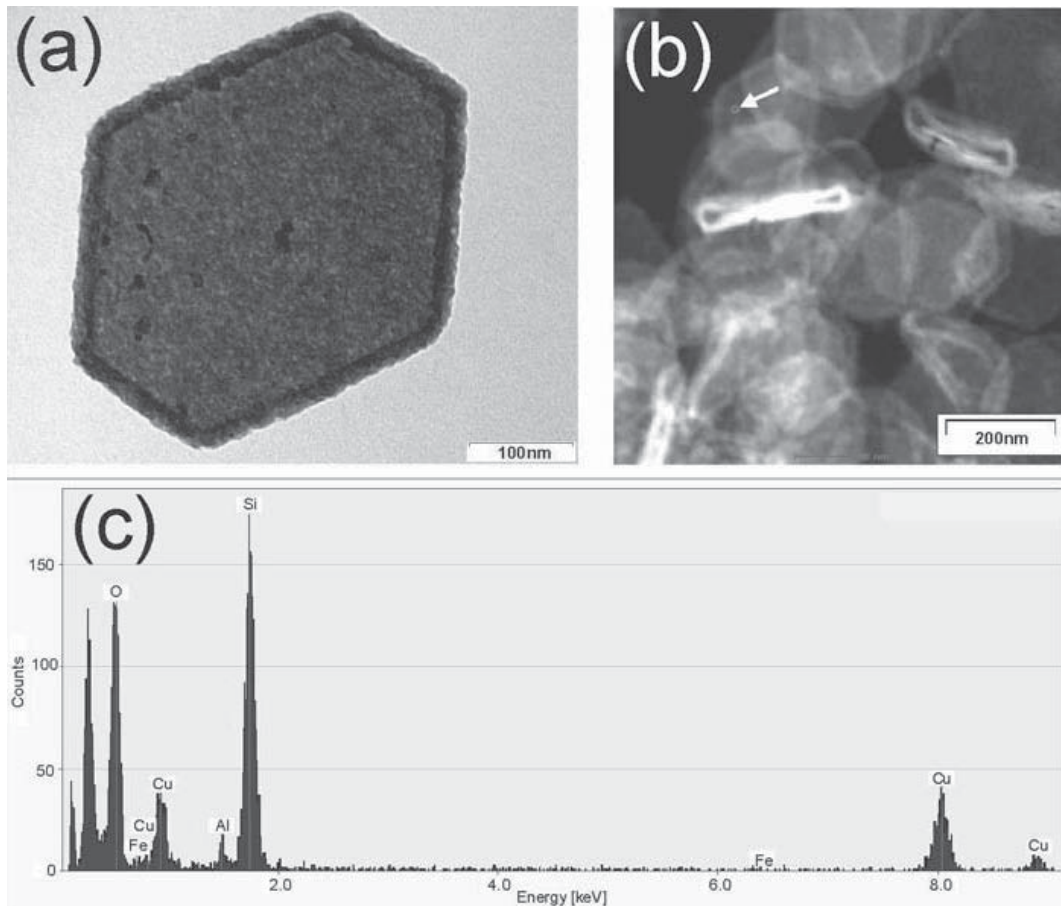


FIGURE 3.10. Acid leaching of silica-coated gibbsite can remove the gibbsite core through the silica coating, as can be seen in TEM (a). In (b) an STEM image is displayed. The arrow indicates the location in the particle where an EDX measurement was done. (c) EDX spectrum of the location in the leached silica coated gibbsite particle indicated in (b).

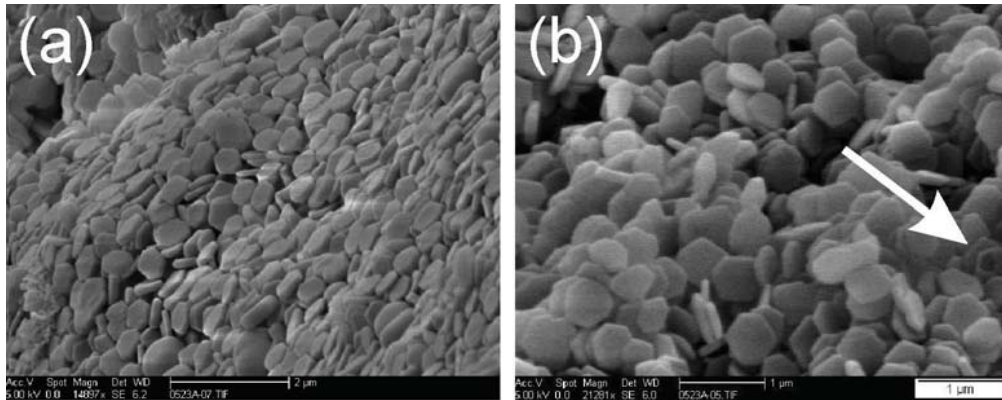


FIGURE 3.11. The result of acid leaching on a flake of columnar silica coated gibbsite particles that were fixated by in situ deposition of silica as observed in SEM. (a) The global appearance of the flake is similar to that before acid leaching (b) Detailed photograph of the system shown in (a). The arrow points at a particle that displays its hollow character.

3.8. CONCLUSIONS

In this work we have shown that colloidal liquid crystals of gibbsite particles do fulfill the three conditions (easy and fast formation of the colloidal liquid crystal, allowing adjustable thickness of the pore wall, possibility to remove the colloidal liquid crystal template) to act as a template for the preparation of an ordered macroporous material. Centrifugation appears to be a powerful tool to speed up the process of formation of liquid crystal phases from dilute suspensions of gibbsite particles. By coating the gibbsite particles with silica we have successfully used columnar liquid crystals as a template for the formation of inorganic composite materials with periodicity in the colloidal domain. The typical repeat distances of both components in the resulting material can be adapted. The original bare gibbsite particles can be grown to various sizes giving rise to different periodicities and the thickness of the silica shell can be adjusted before producing crystals. In situ growth of silica from alkoxides could stabilize and fixate the structure, such that the solvent could be removed. In this way synthetic opals of gibbsite in silica were produced. The resulting iridescent material can be treated with acid to leach out aluminium and therefore obtain macroporous silica with adjustable silica wall thickness.

3.9. ACKNOWLEDGEMENT

Esther Groeneveld, Peter de Lange, Chantal Vonk, Stefano Sacanna, Daniela Kraft and David van der Beek are acknowledged for their contributions. Hans Meeldijk, John Geus and Carlos van Kats are thanked for discussions.

Bibliography

- [1] C. T. Kresge, M. E. Leonowicz, W. J. Roth, J. C. Vartuli, and J. S. Beck. Ordered mesoporous molecular-sieves synthesized by a liquid-crystal template mechanism. *Nature*, 359(6397):710–712, 1992.
- [2] S. Inagaki, Y. Fukushima, and K. Kuroda. Synthesis of highly ordered mesoporous materials from a layered polysilicate. *Journal of the Chemical Society-Chemical Communications*, (8):680–682, 1993.
- [3] J. S. Beck, J. C. Vartuli, W. J. Roth, M. E. Leonowicz, C. T. Kresge, K. D. Schmitt, C. T. W. Chu, D. H. Olson, E. W. Sheppard, S. B. Mccullen, J. B. Higgins, and J. L. Schlenker. A new family of mesoporous molecular-sieves prepared with liquid-crystal templates. *Journal of the American Chemical Society*, 114(27):10834–10843, 1992.
- [4] G. S. Attard, J. C. Glyde, and C. G. Goltner. Liquid-crystalline phases as templates for the synthesis of mesoporous silica. *Nature*, 378(6555):366–368, 1995.
- [5] A. Corma. From microporous to mesoporous molecular sieve materials and their use in catalysis. *Chemical Reviews*, 97(6):2373–2419, 1997.
- [6] B. M. Weckhuysen, R. R. Rao, J. Pelgrims, R. A. Schoonheydt, P. Bodart, G. Debras, O. Collart, P. Van Der Voort, and E. F. Vansant. Synthesis, spectroscopy and catalysis of [cr(acac)(3)] complexes grafted onto mcm-41 materials: Formation of polyethylene nanofibres within mesoporous crystalline aluminosilicates. *Chemistry-a European Journal*, 6(16):2960–2970, 2000.
- [7] D. J. Lensveld, J. G. Mesu, A. J. van Dillen, and K. P. de Jong. Synthesis and characterisation of mcm-41 supported nickel oxide catalysts. *Microporous and Mesoporous Materials*, 44:401–407, 2001.
- [8] A. Taguchi and F. Schuth. Ordered mesoporous materials in catalysis. *Microporous and Mesoporous Materials*, 77(1):1–45, 2005.
- [9] S. A. Bagshaw, E. Prouzet, and T. J. Pinnavaia. Templating of mesoporous molecular-sieves by nonionic polyethylene oxide surfactants. *Science*, 269(5228):1242–1244, 1995.
- [10] D. Y. Zhao, J. L. Feng, Q. S. Huo, N. Melosh, G. H. Fredrickson, B. F. Chmelka, and G. D. Stucky. Triblock copolymer syntheses of mesoporous silica with periodic 50 to 300 angstrom pores. *Science*, 279(5350):548–552, 1998.
- [11] B. Smarsly and M. Antonietti. Block copolymer assemblies as templates for the generation of mesoporous inorganic materials and crystalline films. *European Journal of Inorganic Chemistry*, (6):1111–1119, 2006.
- [12] H. Friedrich, J. R. A. Sietsma, P. E. de Jongh, A. J. Verkleij, and K. P. de Jong. Measuring location, size, distribution, and loading of nio crystallites in individual sba-15 pores by electron tomography. *Journal of the American Chemical Society*, 129(33):10249–10254, 2007.
- [13] O. D. Velev, T. A. Jede, R. F. Lobo, and A. M. Lenhoff. Porous silica via colloidal crystallization. *Nature*, 389:447–448, 1997.
- [14] A. and D. J. Pine. Ordered macroporous materials by emulsion templating. *Nature*, 389:948–951, 1997.
- [15] J. E. G. J. Wijnhoven and W. L. Vos. Preparation of photonic crystals made of air spheres in titania. *Science*, 281(5378):802–804, 1998.
- [16] J. E. G. J. Wijnhoven, L. Bechger, and W. L. Vos. Fabrication and characterization of large macroporous photonic crystals in titania. *Chemistry of Materials*, 13(12):4486–4499, 2001.

- [17] F. M. van der Kooij, and H. N. W. Lekkerkerker, Formation of Nematic Liquid Crystals in Suspensions of Hard Colloidal Platelets. *Journal of Physical Chemistry B*, 102(40):7829–7832, 1998.
- [18] A. Blanco, E. Chomski, S. Grabtchak, M. Ibisate, S. John, S. W. Leonard, C. Lopez, F. Meseguer, H. Miguez, J. P. Mondia, G. A. Ozin, O. Toader, and H. M. van Driel. Large-scale synthesis of a silicon photonic crystal with a complete three-dimensional bandgap near 1.5 micrometres. *Nature*, 405(6785):437–440, 2000.
- [19] D. van der Beek and H. N.W. Lekkerkerker. Liquid crystal phases of charged colloidal platelets. *Langmuir*, 20(20):8582–8586, 2004.
- [20] J. E. G. J. Wijnhoven, D. D. van 't Zand, D. van der Beek, and H. N. W. Lekkerkerker. Sedimentation and phase transitions of colloidal gibbsite platelets. *Langmuir*, 21(23):10422–10427, 2005.
- [21] M. C. D. Mourad, J. E. G. J. Wijnhoven, D. D. Van 'T Zand, D. Van der Beek, and H. N. W. Lekkerkerker. Gelation versus liquid crystal phase transitions in suspensions of plate-like particles. *Philosophical Transactions of the Royal Society a-Mathematical Physical and Engineering Sciences*, 364(1847):2807–2816, 2006.
- [22] D. van der Beek, A. V. Petukhov, S.M. Oversteegen, G. J. Vroege, and H. N. W. Lekkerkerker. Evidence of the hexagonal columnar liquid crystal phase of hard colloidal platelets by high resolution saxs. *European Physical Journal E*, 16(3):253–258, 2005.
- [23] A. V. Petukhov, D. van der Beek, R. P. A. Dullens, I. P. Dolbnya, G. J. Vroege, and H. N. W. Lekkerkerker. Observation of a hexatic columnar liquid crystal of polydisperse colloidal disks. *Physical Review Letters*, 95(7):–, 2005.
- [24] D. van der Beek, P. B. Radstake, A. V. Petukhov, and H. N. W. Lekkerkerker. Fast formation of opal-like columnar colloidal crystals. *Langmuir*, 23(23):11343–11346, 2007.
- [25] W. Stöber, A. Fink, and E. Bohn. Controlled growth of monodisperse silica spheres in the micron size range. *Journal of Colloid and Interface Science*, 26(1):62, 1968.
- [26] A. M. Wierenga, T. A. J. Lenstra, and A. P. Philipse. Aqueous dispersions of colloidal gibbsite platelets: synthesis, characterisation and intrinsic viscosity measurements. *Colloids and Surfaces A*, 134:359–371, 1998.
- [27] F. M. van der Kooij. *Phase behaviour and dynamics of suspensions of hard colloidal platelets*. PhD thesis, Utrecht University, 2000.
- [28] D. van der Beek and H. N. W. Lekkerkerker. Nematic ordering vs. gelation in suspensions of charged platelets. *Europhysics Letters*, 61:702–707, 2003.
- [29] M. P. B. van Bruggen, M. Donker, H. N. W. Lekkerkerker, and T. L. Hughes. Anomalous stability of aqueous boehmite dispersions induced by hydrolyzed aluminium poly-cations. *Colloids and Surfaces A*, 150:115–128, 1999.
- [30] J. Bugosh. Colloidal alumina - the chemistry and morphology of colloidal boehmite. *Journal of Physical Chemistry*, 65:1789–1793, 1961.
- [31] J. E. G. J. Wijnhoven. Coating of gibbsite platelets with silica. *Chemistry of Materials*, 16:3821–3828, 2004.
- [32] J. E. G. J. Wijnhoven. Seeded growth of monodisperse gibbsite platelets to adjustable sizes. *Journal of Colloid and Interface Science*, 292(2):403, 2005.
- [33] P. M. Johnson, C. M. van Kats, and A. van Blaaderen. Synthesis of colloidal silica dumbbells. *Langmuir*, 21(24):11510–11517, 2005.

4

Lyotropic Hexagonal Columnar Liquid Crystals of Large Colloidal Gibbsite Platelets

ABSTRACT

We report the formation of hexagonal columnar liquid crystal phases in suspensions of large (570nm diameter), sterically stabilized, colloidal gibbsite platelets in organic solvent. In thin cells these systems display strong iridescence originating from columns that are aligned perpendicular to the cell walls. Small angle X-ray scattering and polarized light microscopy reveal significant column undulations and bending of the particle director particularly in the vertical direction. The fact that these phenomena are particularly pronounced in the bottom part of these systems points to the role of gravitational compaction.

4.1. INTRODUCTION

Colloidal suspensions display intriguing phase transitions between gas, liquid, solid and liquid crystalline phases. The structures that are formed by spontaneous self-organization on sub-micrometer scales in colloidal suspensions are of potential technological interest. For example, three-dimensional arrangements of spheres in colloidal crystals may serve as photonic materials intended to manipulate light[1].

Colloidal particles with non-spherical shapes (such as rods and plates) are of particular interest because of their ability to form liquid crystals. Nematic liquid crystals possess orientational order; smectic and columnar liquid crystals additionally exhibit positional order (in one and two dimensions respectively). The phase separation in suspensions of anisometric colloidal particles into an isotropic and a nematic phase was addressed theoretically by Lars Onsager [2] in the 1940s. He demonstrated that the thermodynamic stability of the nematic phase can be explained on a purely entropic basis by considering the competition between orientational entropy (favoring the isotropic state) and the entropy of the excluded volume (which favors the nematic state). As the latter becomes more important at higher concentrations, a first-order transition from an isotropic to a nematic phase may occur if the concentration of rods or plates is sufficiently high. Thus, even hard rods or plates may form a nematic phase. Evidence that a system of hard rods can form a thermodynamically stable smectic phase [3] and a system of hard platelets can form a thermodynamically stable columnar phase[4] was provided by computer simulations in 1980s and 1990s. While liquid crystal phase transitions in suspensions of rodlike particles have been observed for a long time it is only in the last ten years that firm experimental evidence for liquid crystal phase equilibria in suspensions of platelike particles was obtained [5, 6, 7, 8, 9, 10, 11, 12].

The liquid crystal phase behaviour of suspensions of colloidal gibbsite platelets has been explored extensively [6, 7, 13, 14]. These particles of approximately 150-200 nm in diameter can be synthesized conveniently by hydrothermal treatment of alumina alkoxides in acidic solution [15]. Suspensions of both sterically and charge stabilized gibbsite platelets synthesized in this way do display nematic and columnar phases upon increasing the concentration. The columnar phases of these colloidal gibbsite platelets produce strong Bragg reflections in the visible range[7, 13, 14] and have been used as templates for the generation of ordered silica structures[16]. It would be of great interest to produce photonic crystals of such material with arbitrary periodicities in the submicron range. Larger gibbsite particles can be grown using a seeded growth procedure[17]. Alternatively, such large particles can be synthesized by coprecipitation of aluminum nitrates[18] and subsequent hydrothermal treatment. Wijnhoven et al. observed that gibbsite platelets with an average diameter of 570nm in water upon sedimentation formed glassy sediments rather than columnar crystals[19]. Recently

Houghton and Donald provided detailed insight in similar structures of these platelets using environmental scanning electron microscopy[20].

In this paper we demonstrate that these large gibbsite particles that were sterically stabilized with polyisobutylene and suspended in tetralin do form beautiful columnar phases. In thin cells (thickness $\sim 0.15\text{mm}$) the columnar phase forms in a matter of hours and from the iridescence it would appear that the columns are uniformly ordered over centimeters perpendicularly to the glass walls of the sample cell. However detailed high resolution SAXS measurements indicate the presence of undulations in the columns. The column undulations are particularly pronounced in the bottom of the sample and are stronger in the vertical direction than in the horizontal direction. This points to the role of gravitational compaction of the flexible columns of the platelike particles, which is supported by similar SAXS observations on the columnar phase of small, charge stabilized in a centrifugal field [21].

4.2. EXPERIMENTAL

4.2.1. Synthesis

The colloidal, hexagonal gibbsite platelets used were prepared in a seeded growth experiment and characterized by Wijnhoven[17]. The platelet thickness and length (D) are measured to be 47 nm ($\pm 23\%$) and 570nm ($\pm 11\%$) by atomic force microscopy (AFM) and transmission electron microscopy (TEM, Fig. 4.1), respectively. The particle surfaces were grafted by amino modified poly-isobutylene chains (SAP230TP, Infineum UK Ltd.) following a novel approach developed by us and described in [23]. For this purpose aqueous gibbsite particles are mixed with an excessive amount of SAP230TP (1.5 g/g particles) dispersed in n-propanol (Acros, 99%). Subsequently the solvent is removed in a two-step process. First a substantial part of the water and n-propanol is extracted using a rotary evaporator, while raising the temperature to 40° C. Then the solvent remains are extracted by freezing the sample by immersion of the flask in liquid nitrogen followed by connection to a vacuum setup for freeze-drying. The sample is redispersed in toluene (J.T. Baker, 99.5%). Finally the excess of SAP230TP is removed by centrifugation of the particles followed by redispersion in toluene (repeated two times). This way allows for production of batches of polymer grafted inorganic particles to be produced with relative ease. The dispersion is centrifuged and redispersed twice in tetralin (1,2,3,4 tetrahydronaphtalene, Acros 98%).

4.2.2. Sample Preparation

Dilute suspensions of the sterically stabilized gibbsite particles were concentrated by moderate centrifugation (30min, 200g) and subsequent removal of the supernatant, followed by redispersion. The thus obtained concentrated suspensions were put in sample cells (inner dimensions of approximately $15 \times 15 \times 0.15$ mm) made of two

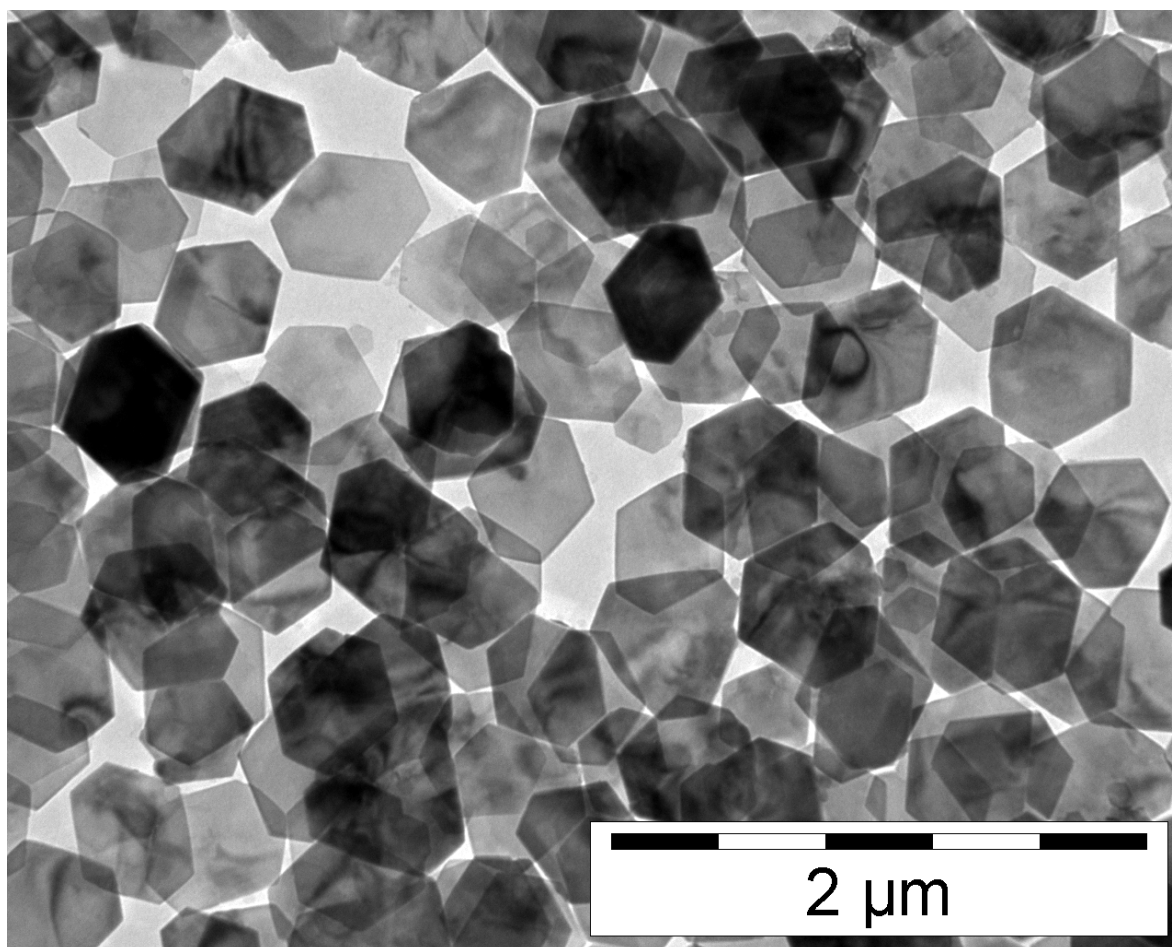


FIGURE 4.1. Transmission electron micrograph of the sterically stabilized gibbsite platelets.

glass plates (G. Menzel, Glasbearbeitungswerk GmbH, Germany, thickness 0,13 - 0,16 mm). The cells were held together by two-component tetralin insoluble epoxy resin (Araldit AW2101, Vantico AG, Switzerland) and were suitable for both optical as well as X-ray scattering experiments due to their small optical pathlength and limited glass wall thickness.

4.2.3. Polarization Microscopy

The liquid crystalline sample was studied using a Nikon polarization microscope (Eclipse LV100pol) equipped with a digital camera (QImaging, MP5). The optical birefringence was determined with the help of retardation filters (optical path difference 530 nm), inserted at an angle of 45° with respect to both the polarizer and analyzer.

4.2.4. Laser Diffraction

In order to study the periodicity in the liquid crystalline suspension laser diffraction experiments were performed using a variable wavelength Krypton-ion laser (Spectra

Physics, 2025-11) operated at a discharge current of 47.6A producing 0.11 Watt 476.5 nm wavelength light. The sample cell was mounted in the middle of a partly sandblasted round-bottom flask that was filled with toluene. In this way, reflections at the surface of the sample cell -which was oriented at an angle of 45 degrees with respect to the incoming laser beam- could be minimized (see also reference [24]). The flask was equipped with an entrance window for the laser beam. We can calculate the scattering angle θ (defined as the angle between the direct and the scattered beam) for the Bragg peaks by measurement of the distance between the direct and the diffracted laser beams over the surface of the flask and take into account the diameter of the flask. The d-spacings responsible for these diffractions can be calculated as follows:

$$d = \frac{\lambda}{2n_s \sin(\frac{\theta}{2})} \quad (4.1)$$

where λ is the wavelength of the laser *in vacuo*, n_s is the index of refraction of the solvent and θ the scattering angle.

4.2.5. Small Angle X-ray Scattering (SAXS)

Experiments were performed at the SAXS\WAXS station of the DUBBLE beamline BM-26B at the ESRF (Grenoble, France) using an earlier described setup [25]. A monochromatic 15 keV X-ray beam (wavelength $\lambda = 0.83 \text{ \AA}$, spectral width $\Delta\lambda / \lambda = 2 \times 10^{-4}$) was selected using a Si-111 monochromator and focused on the detector by a set of compound refractive lenses[26]. The sample was at 8m distance from the x-ray sensitive CCD detector (VHR Photonic Science, 4008x2671 pixels of 22×22 microns²). The sample cell was carefully displaced along the vertical direction in the X-ray beam by a step motor in order to probe the colloidal crystal at several heights in the dispersion.

4.3. RESULTS AND DISCUSSION

Directly after dispersion in tetralin the colloidal suspension of gibbsite platelets had a pale green color. The turbidity is remarkably low, despite the high concentration and the large platelet diameter. This is illustrated in Fig. 4.2a where it is shown that the dispersion is transparent. Within hours after transfer of the dispersion to the sample cell the colloidal suspension displayed bright Bragg reflections ranging from violet to red upon increase of the scattering angle. (Fig. 4.2b). Observed between crossed polarizers the middle of the sample appeared dark, in contrast to the edges of the sample cell which displayed strong birefringence (Fig. 4.2c). Apparently, in the middle part homeotropic anchoring of the platelets to the glass substrate (platelet surface parallel to substrate) caused this dark appearance. In this orientation of the particles the two identical indices of refraction of the uniaxial mineral are situated in the optical plane while the second index of refraction is oriented perpendicular to the walls. This leads to absence of birefringence in the optical configuration employed here.

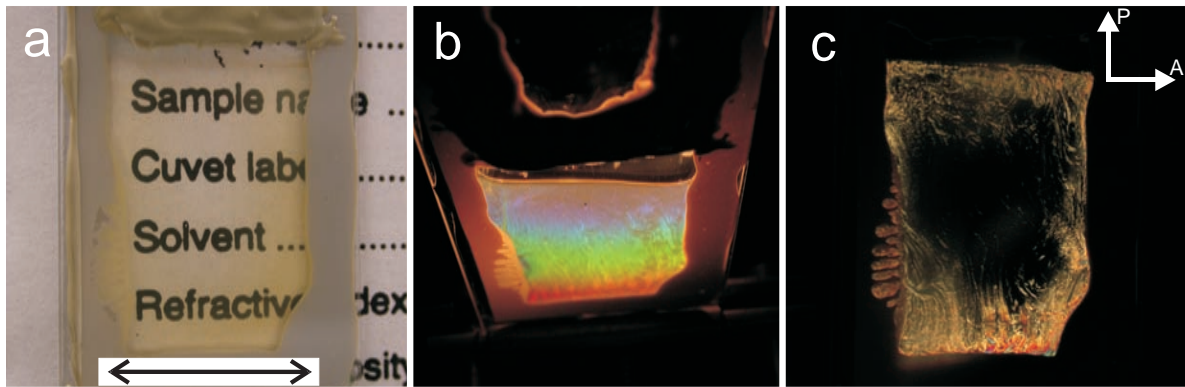


FIGURE 4.2. In panel (a) the translucent properties of the sample are demonstrated. The arrow denotes 17 mm, which corresponds to the width of the cell. Panel (b) depicts the cell illuminated by a white light source. The variation of the colors is related to the variation in the viewing angle. Panel (c) shows the sample in between crossed polarizers (indicated in the upper right corner by P and A , respectively)

200 μm

This is confirmed by the fact that tilting the glass cell along a vertical rotation axis such that the glass walls are not oriented parallel to the polarizers anymore made the cell appear birefringent, as the second index of refraction of the mineral now entered the optical plane. At the sides of the sample cell birefringence is clearly visible. This we ascribe to the additional effect of the side walls on the orientation of the platelets. Since the gibbsite particles are large the typical periodicities in the sample associated with the iridescence can be measured conveniently by laser light diffraction. Three Bragg peaks could be discerned visually on the round-bottom flask. Measurement of the positions of the diffraction peaks in the horizontal plane leads to scattering angles of 37.8° , 67.6° and 76.4° . Assuming 1.54 for n_s , this leads to d -values of 478 nm, 278 nm and 250 nm. The ratio of the related d -values (1:0.58:0.52) is in close agreement with the ratios (1: $\sqrt{1/3}$: $\sqrt{1/4}$) of the d_{100} , d_{110} and d_{200} spacings in a hexagonal lattice. This we ascribe to the formation of a hexagonal columnar liquid crystal.

A more detailed picture was obtained by small angle X-ray diffraction. In Fig. 4.3a typical X-ray scattering intensity profiles and a 2D X-ray scattering pattern of the iridescent sample 5 months after preparation are displayed. At low q -values up to four rings of Bragg reflections were observed. The ratios of the corresponding q -values were in agreement with the characteristic ratios of 1: $\sqrt{3}$: $\sqrt{4}$: $\sqrt{7}$ of a hexagonal lattice. Moreover, at higher q a liquid-like Bragg peak for the (intracolumnar) 001 reflection is visible (typically around 70 nm in this sample).

Upon going from the top to the bottom of the sample the q -values of the intercolumnar reflections slightly increase indicating compaction of the structure (Fig. 4.3b). Moreover, the low q reflections become increasingly elliptical. This is surprising since the

gravitational length of the gibbsite platelets ($l_g = k_B T / (\Delta m g) = 30 \mu\text{m}$, where $k_B T$ is the thermal energy, Δm is the buoyant mass of the particles in the solvent and g is the gravitational acceleration) is much larger than the structure period so that no direct influence of the gravity on the structure can be expected. Even more surprisingly, the d -values $d_{hkl} = 2\pi/q_{hkl}$ calculated from the Bragg peak positions appear smaller than those expected for an ideal hexagonal columnar structure with the intercolumnar distances equal to the average particle diameter D : $d_{100}^{\text{ideal}} = D\sqrt{3}/2$ and $d_{110}^{\text{ideal}} = D/2$.

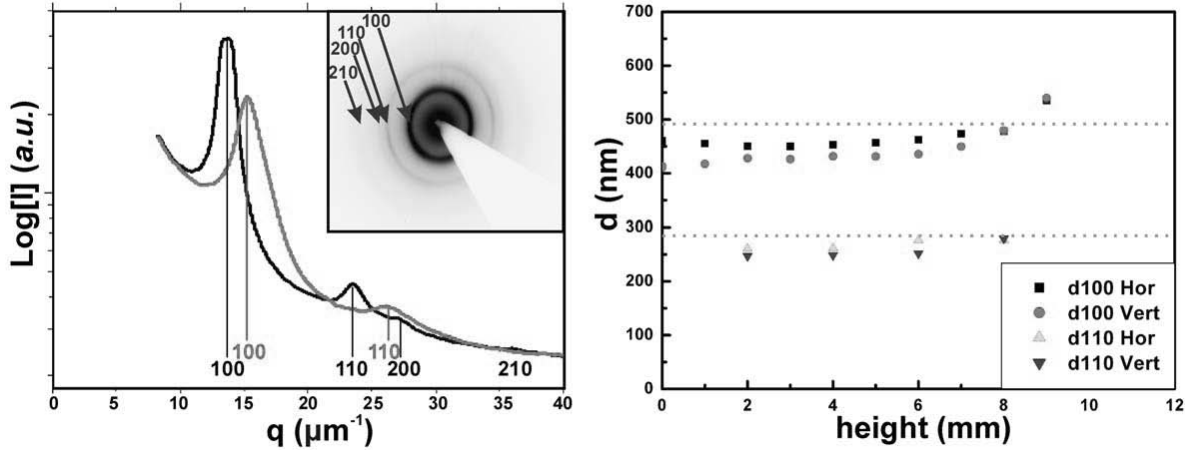


FIGURE 4.3. Panel (a) depicts the profiles of the X-ray scattering intensity in the horizontal (black curve) and vertical (red curve) direction. The inset shows the 2D high resolution SAXS pattern. Panel (b) shows the d_{100} and d_{110} recorded in the horizontal (Hor) and vertical (Vert) direction at different heights above the bottom of the sample. The dashed lines indicate the d_{100}^{ideal} and d_{110}^{ideal} assuming an intercolumnar distance equal to the diameter of the platelets (570nm).

To rationalize these surprising results, we have assumed that columns can significantly undulate while locally preserving the average particle orientation \mathbf{n} as sketched in Fig. 4.4a. Similar column undulations have been seen in computer simulations of hard discs [27]. An example of such a result, which is shown in Fig. 4.4b, was kindly provided to us by Tanja Schilling. In the diffraction domain, such column undulations can reduce the separation between column axes to $a = D \cos \phi$, where ϕ is the angle between the platelets normal and the column axis. Column undulations in the domain 1 sketched in Fig. 4.4a can significantly broaden the Bragg diffraction spot in the y direction, along the average orientation of the particle normal \mathbf{n} as schematically shown in Fig. 4.4c. The tails of such a broadened reflection are then found at larger q -values, which correspond to smaller intercolumn separation a .

We have further assumed that the average particle orientation \mathbf{n} can also fluctuate within the X-ray beam. This will in turn lead to appearance of domains with slightly

different orientations, such as the domains 2 and 3 sketched in Fig. 4.4*a*. The overall diffraction pattern from the columnar crystal possessing significant shorter-scale column undulations and larger-scale fluctuations of the particle orientation will be determined by the sum of all regions within the beam. As one can see in Fig. 4.4*c*, the observed peak position can be thus shifted to a larger q value.

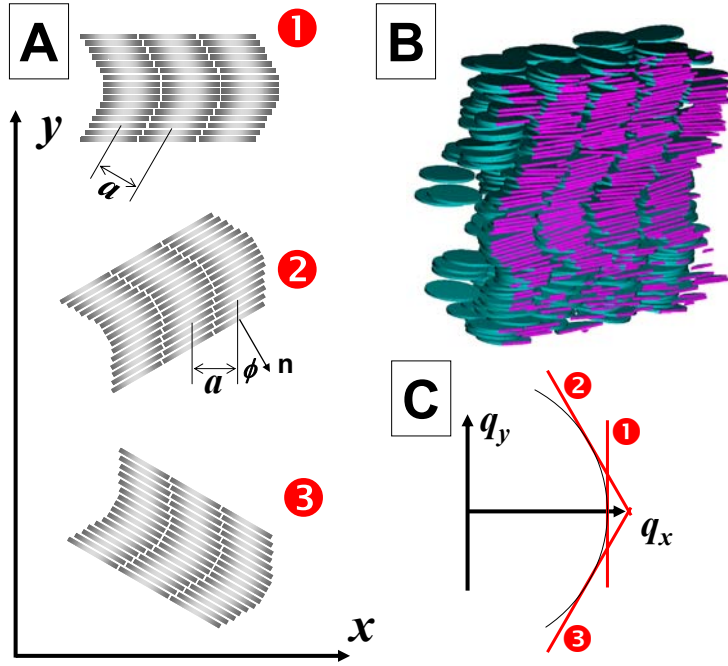


FIGURE 4.4. Panel (A) depicts cartoons of three hexagonal columnar domains with different particle orientations. Due to column undulations the column axis makes an angle ϕ with the particle director \mathbf{n} , such that the intercolumnar spacing \mathbf{a} becomes smaller than the particle diameter. Panel (B) shows an intersection of a snapshot from a hexagonal columnar phase in computer simulations on hard disks, kindly provided by Tanja Schilling, with significant column undulations. In Panel (C) the broadening of the diffraction spots originating from the three domains sketched in Panel (A) is illustrated giving rise to a shift of the Bragg peak to larger q -values.

SAXS measurements were carried out again 5 months later. The results of this experiment closely resemble the results of the first set of measurements. This supports the long-term stability of the proposed structures. We have experimentally observed that rotation of the sample within the X-ray beam by angles up to 50° along the vertical axis does not lead to significant changes in the position of the intercolumnar Bragg

reflections, while their intensity slowly reduces. This is consistent with the model and suggests that both column undulations *and* variations of the particle director by approximately 30° should be present in the sample. The higher q value in the vertical direction can thus be caused by stronger column undulations in the vertical rather than horizontal direction. This difference in the amplitude of the orientational fluctuations in the two directions may be related to the growth history. In the course of time a slow structure rearrangement (e.g., annealing of growth defects) can lead to a slow densification of the structure, which can induce slow settling of the structure in the *vertical* direction. If this process is non-uniform, it can enhance column undulations in the vertical direction. In our system the column undulations are particularly pronounced in the bottom of the sample, which points to the role gravitational compaction in the rearrangement of the liquid crystalline structures.

We note that undulation effects of this type are not necessarily limited to colloidal platelets. For example, considerable layer undulations and variation of the particle orientation have been observed in the lyotropic smectic phase of colloidal β -FeOOH rods in scanning electron microscopy images[28].

Support for the hypothesis that undulations are stronger in the vertical than in the horizontal direction comes from polarization microscopy. In this technique the optical path difference (OPD) of transmitted polarized light can be determined [29]. Insertion of a retardation filter (λ -plate), oriented at 45° with respect to the polarizer and analyzer, leads to a new offset of the OPD. Depending on the orientation of the anisotropic particles with respect to the orientation of the retardation filter different interference colors will be visible. When the orientation of the particle director is parallel to the slow axis of the retardation filter the OPD of the particles will be added to the OPD of the retardation filter, leading to a large observable OPD. In contrast, when the orientation of the particle director is perpendicular to the slow axis of the retardation filter the OPD of particles will be subtracted from the OPD of the retardation filter leading to a small observable OPD. In Fig. 4.5 polarization micrographs of the columnar crystal with and without retardation filter are displayed. From Fig. 4.5 (a) and (b) it appears that there are particle directors present at orientations parallel and perpendicular with respect to the retardation filter leading to the interference colors blue and orange in Fig. 4.5 (b), respectively. Clear indication that the particle director deviates preferentially in the vertical direction of the sample, is found upon rotation of the sample by 45° (Figs 4.5 (c) and (d)). Now, higher interference colors (light blue) appeared in case the vertical direction in the sample coincides with the slow axis of the retardation filter (Fig. 4.5c). In contrast, lower interference colors (yellow) are observed in case the vertical direction in the sample is oriented perpendicularly to the slow axis of the retardation filter (Fig. 4.5d). So the interference colors point towards a preferential

orientation of the slow axis of the index of refraction and thus of the particle director in the vertical direction rather than in the horizontal direction in this columnar phase.

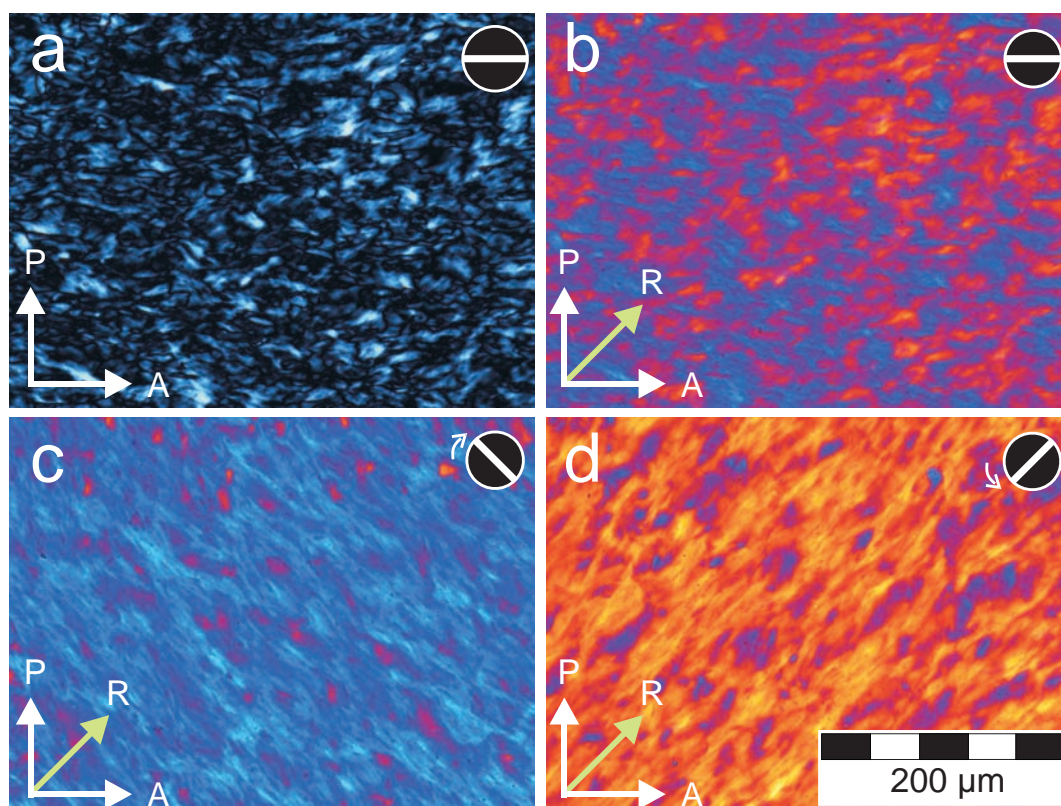


FIGURE 4.5. Polarized light micrographs of the system without (a) and with (b, c, d) retardation plate of 530 nm. The orientation of the polarizer and analyzer are indicated by P and A , respectively, while the slow axis of the retardation filter is indicated as R . In the upper right corner the horizontal direction is indicated: the cell was tilted by 45° clockwise (c) and counter-clockwise (d) giving rise to different interference colors.

In one of the samples the columnar phase was concentrated further by very slow evaporation of the solvent (the sample was not dried out completely after a period of 2 years). This dispersion displayed a higher turbidity, but did not lose its striking iridescence. SAXS experiments were now performed on this 2.5 year old sample (Fig. 4.6). The long range hexagonal order is decreased. The 100, 110 and 001 were the only Bragg peaks to be seen and appeared broader than before drying. These experiments indicate a similar difference between scattering in the horizontal and vertical direction (Fig. 4.6 (b)) as described before.

The textures observable in polarization microscopy had significantly changed after the slow evaporation of solvent. Rather than granular patterns periodically undulating textures appeared (Fig. 4.7) that show broad similarities to earlier published patterns

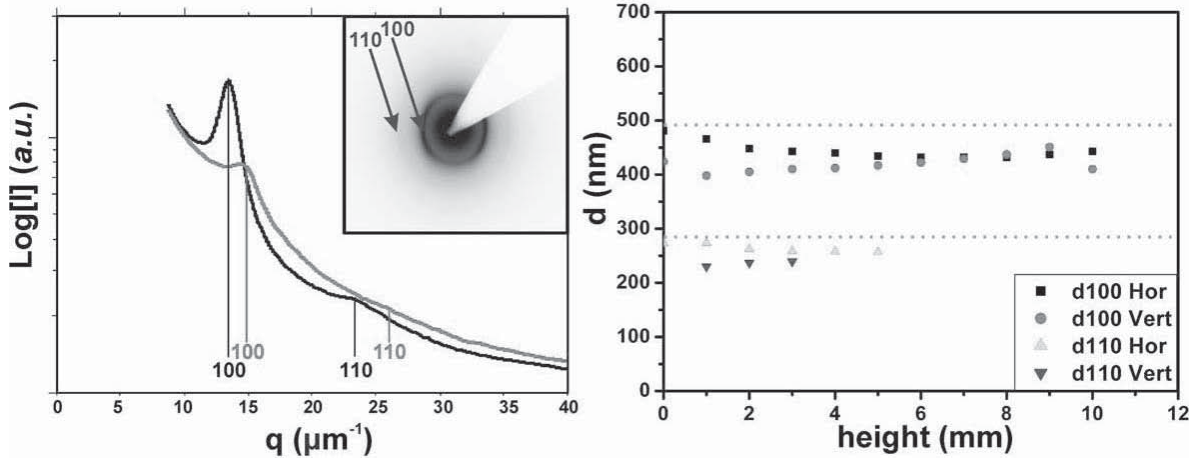


FIGURE 4.6. Panel (a) depicts the profiles of the X-ray scattering intensity in the horizontal (black curve) and vertical (red curve) direction of the concentrated sample. The inset shows the 2D high resolution SAXS pattern. Panel (b) shows the d_{100} and d_{110} recorded in the horizontal (Hor) and vertical (Vert) direction at different heights above the bottom of the sample. The dashed lines indicate the d_{100}^{ideal} and d_{110}^{ideal} assuming an intercolumnar distance equal to the diameter of the platelets (570nm).

of columnar phases of colloidal rods[30, 31]. The undulating patterns have a periodicity of about 10 micrometers in the vertical direction and 50 micrometers in the horizontal direction. The retardation colors in Fig. 4.7a and b compared to those in Fig. 4.7c and d clearly indicate that the particle director deviates preferentially in the vertical direction and has some components along the horizontal direction as described above. Moreover, rotation of the sample with respect to the polarizers indicated that these dark lines correspond to the regions in which the platelets are homeotropically oriented with respect to the glass walls.

4.4. CONCLUSIONS

Concentrated suspensions of large sterically stabilized gibbsite particles form hexagonal columnar phases in flat sample cells in a matter of hours. The iridescence points to a uniformly oriented structure in which the columns are oriented perpendicular to the glass walls of the cell. SAXS and polarization microscopy clearly indicate the presence of column undulations. Furthermore, the difference in undulations in the vertical direction compared to the horizontal direction imply the strong effect of gravitational compaction in the structure indicating that these phenomena are particularly pronounced in the columnar phase of large platelets.

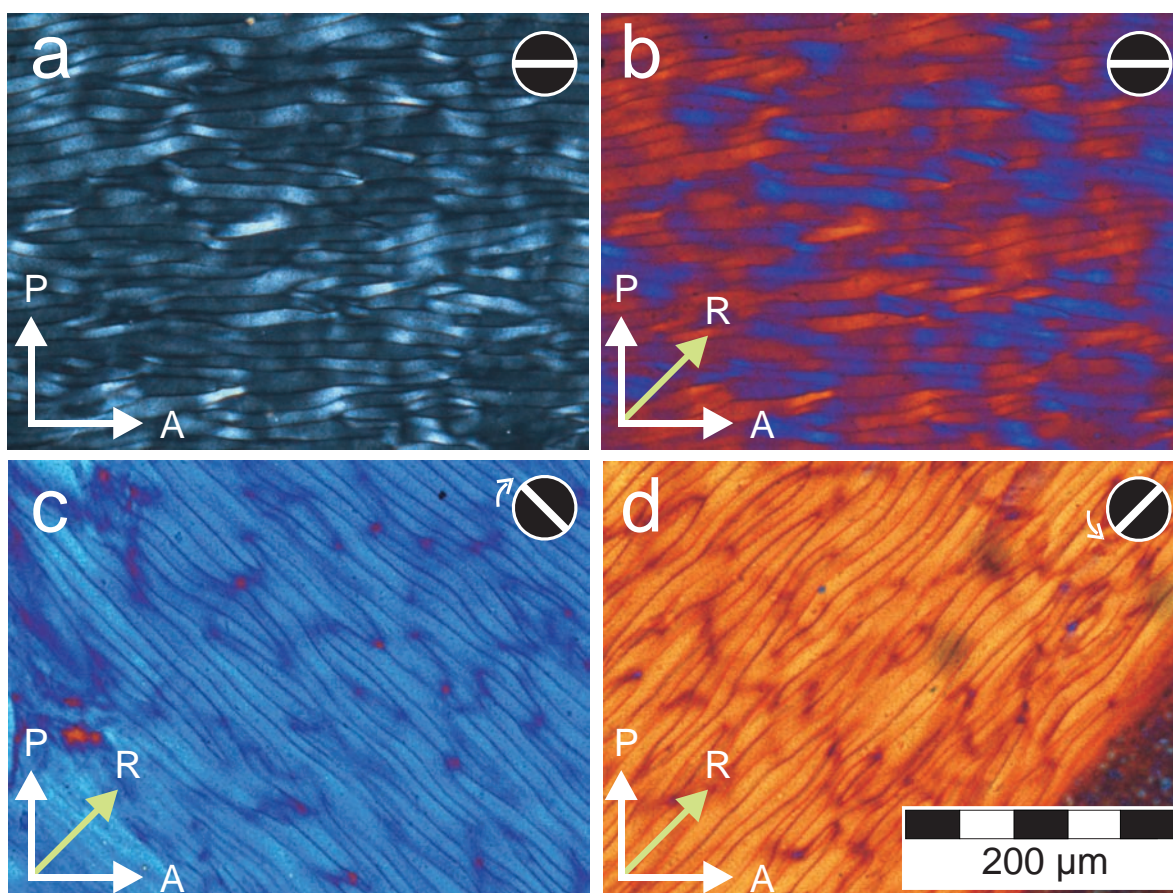


FIGURE 4.7. Polarized light micrographs of the concentrated system without (a) and with (b, c, d) retardation plate of 530 nm. The orientation of the polarizer and analyzer are indicated by P and A , respectively, while the slow axis of the retardation filter is indicated as R . In the upper right corner the horizontal direction is indicated: the cell was tilted by 45° clockwise (c) and counter-clockwise (d) giving rise to different interference colors.

4.5. ACKNOWLEDGEMENT

Bonny Kuipers is acknowledged for help in the laser diffraction measurements. Judith Wijnhoven is acknowledged for providing the aqueous gibbsite sample and Tanja Schilling for sharing her simulation data. Job Thijssen, Hans Meeldijk and Lia Verhoeff are thanked for discussions.

Bibliography

- [1] J. E. G. J. Wijnhoven and W. L. Vos, *Science* 1998, *281*, 802-804
- [2] L. Onsager, *Annals of the New York Academy of Sciences* 1949, *51*, 627-659
- [3] D. Frenkel, H. N. W. Lekkerkerker and A. Stroobants, *Nature* 1988, *332*, 822-823
- [4] J. A. C. Veerman and D. Frenkel, *Physical Review A* 1992, *45*, 5632-5648
- [5] A. B. D. Brown, S. M. Clarke and A. R. Rennie, *Langmuir* 1998, *14*, 3129-3132
- [6] F. M. van der Kooij and H. N. W. Lekkerkerker, *Journal of Physical Chemistry B* 1998, *102*, 7829-7832
- [7] F. M. van der Kooij, K. Kassapidou and H. N. W. Lekkerkerker, *Nature* 2000, *406*, 868-871
- [8] S. Liu, J. Zhang, N. Wang, W. Liu, C. Zhang and D. Sun, *Chemistry of Materials* 2003, *15*, 3240-3241
- [9] D. van der Beek and H. N. W. Lekkerkerker, *Europhysics Letters* 2003, *61*, 702-707
- [10] D. van der Beek and H. N. W. Lekkerkerker, *Langmuir* 2004, *20*, 8582-8586
- [11] J. O. Fossum, E. Gudding, D. d. M. Fonseca, Y. Meheust, E. DiMasi, T. Gog and C. Venkataraman, *Energy* 2005, *30*, 873
- [12] L. J. Michot, I. Bihannic, S. Maddi, S. S. Funari, C. Baravian, P. Levitz and P. Davidson, *PNAS* 2006, *103*, 16101-16104
- [13] F. M. van der Kooij, D. van der Beek and H. N. W. Lekkerkerker, *Journal of Physical Chemistry B* 2001, *105*, 1696-1700
- [14] D. van der Beek, A. V. Petukhov, S. M. Oversteegen, G. J. Vroege and H. N. W. Lekkerkerker, *Eur Phys J E* 2005, *16*, 253-258
- [15] A. M. Wierenga, T. A. J. Lenstra and A. P. Philipse, *Colloids and Surfaces A* 1998, *134*, 359-371
- [16] M. C. D. Mourad, E. Groeneveld, P. J. de Lange, C. Vonk, D. v. d. Beek and H. N. W. Lekkerkerker, *Journal of Materials Chemistry* 2008, *18*, 3004-3010
- [17] J. E. G. J. Wijnhoven, *Journal of Colloid and Interface Science* 2005, *292*, 403
- [18] S. Shen, P. S. Chow, F. Chen, S. Feng and R. B. H. Tan, *Journal of Crystal Growth* 2006, *292*, 136
- [19] J. E. G. J. Wijnhoven, D. D. van 't Zand, D. van der Beek and H. N. W. Lekkerkerker, *Langmuir* 2005, *21*, 10422-10427
- [20] H. A. Houghton and A. M. Donald, *Scanning* 2008, *30*, 223-227
- [21] D. van der Beek, P. B. Radstake, A. V. Petukhov and H. N. W. Lekkerkerker, *Langmuir* 2007, *23*, 11343-11346
- [22] A. M. Wierenga, T. A. J. Lenstra and A. P. Philipse, *Colloids and Surfaces A* 1998, *134*, 359-371
- [23] M. C. D. Mourad, E. J. Devid, M. M. van Schooneveld, C. Vonk and H. N. W. Lekkerkerker, *J. Phys. Chem. B* 2008, *112*, 10142-10152

- [24] J. Sanders, *Acta Crystallographica Section A* 1968, *24*, 427-434
- [25] A. V. Petukhov, J. H. J. Thijssen, D. C. 't Hart, A. Imhof, A. van Blaaderen, I. P. Dolbnya, A. Snigirev, A. Moussaid and I. Snigireva, *Journal of Applied Crystallography* 2006, *39*, 137-144
- [26] A. Snigirev, V. Kohn, I. Snigireva and B. Lengeler, *Nature* 1996, *384*, 49
- [27] D. van der Beek, T. Schilling and H. N. W. Lekkerkerker, *Journal of Chemical Physics* 2004, *121*, 5423-5426
- [28] H. Maeda and Y. Maeda, *Langmuir* 1996, *12*, 1446-1452
- [29] P. C. B. Robinson, S., *Qualitative Polarized Light Microscopy*, Oxford University Press - Royal Microscopical Society:Oxford, 1992, Ch. 2
- [30] F. Livolant and Y. Bouligand, *Journal de Physique* 1986, *47*, 1813-1827
- [31] E. Grelet, *Physical Review Letters* 2008, *100*, 168301

5

The Nematic Phase of Sterically Stabilized Gibbsite Platelets as Template for Ordered Polymer Nanocomposites

ABSTRACT

We study the formation of ordered nanostructures of colloidal gibbsite platelets in polymer making use of the nematic liquid crystal forming properties of these anisometric particles in dispersion. Two systems of colloidal gibbsite platelets were used, one with average diameter 232 nm and one with average diameter 574 nm. The platelets were made organophilic by polymer grafting with amino modified polyisobutylene stabilizer. At high particle concentrations these platelets form nematic liquid crystal phases in divinylbenzene (monomer) solution. *In situ* polymerization is induced by a UV-sensitive initiator. The resulting polymer-gibbsite nanocomposites contained nematically ordered gibbsite platelets, as is confirmed by polarizing microscopy. Furthermore, combined focused ion beam-scanning electron microscopy and transmission electron microscopy shows the dispersion of the platelets in the nanocomposite. Both polarizing microscopy and electron microscopy show that the larger platelets have a significantly higher degree of orientational ordering in the nanocomposite than the smaller gibbsite platelets.

5.1. INTRODUCTION

The design and assembly of platelet reinforced polymer nanocomposites is a topic of great current interest [1]. Inspiration in this field comes from the nanostructures found in nature that are produced by organisms in the process of biomineralization [2]. A beautiful example of such a structure is found in nacre, that consists of more than 90 % wt of calcium carbonate, in the form of aragonite, in an organic matrix composed predominantly of glycoproteins [3]. Interestingly, such natural nanocomposites exhibit a generic mechanical structure in which the nanometer size of mineral particles ensures optimum strength and maximum tolerance of flaws (robustness) [4]. Most work done so far on platelet-polymer nanocomposites concerns systems in which the platelets are exfoliated smectite clay lamellae. Recently, attempts have been made to obtain ordered structures of platelets in a polymer matrix. Several groups have successfully applied layer-by-layer deposition techniques to obtain lamellar polymer nanocomposites of micron sized platelets such as montmorillonite with polyelectrolytes [5] or with polyvinyl-alcohol [6] and aluminium oxide with the biopolymer chitosan [7]. These nanocomposites were shown to be strong, stretchy and light-weight. While giving rise to a desirable nacre-like material the disadvantage of the layer-by-layer deposition method is that it requires adaptation to make it suitable for bulk manufacturing. A simple and rapid process to obtain biomimetic nanocomposites is electrophoretic deposition developed by Lin *et al.* [8] and applied for the production of gibbsite platelets-polyvinylalcohol nanocomposites.

Here, we make use of the self-assembly of sterically stabilized gibbsite platelets in apolar solvents [9] to obtain ordering of the mineral platelets. *In situ* polymerization of the dispersing phase of the organophilic mineral platelets (as demonstrated for clays and organoclays [10, 11]) leads then to composite materials. In our procedure, the nematic liquid crystal phase formation of the platelets is responsible for the ordering in the final nanocomposite, giving rise to nematically ordered gibbsite platelet-polymer nanocomposites. We compare the formation of nanocomposites from colloidal gibbsite systems with two different average platelet diameters.

5.2. EXPERIMENTAL

5.2.1. Particle preparation.

In this work we will use two systems of colloidal gibbsite particles. The first system was prepared hydrothermally from aluminium alkoxides in acidic solution as described in Chapter 2. The second system consisted of the larger particles that were presented in Chapter 4. This system was synthesized via a seeded growth procedure of aluminium alkoxides in acidic solution, resulting in a larger average platelet diameter. The surface area (A) of well over 250 individual particles was measured with imaging software

(i)TEM, soft imaging system GmbH). An average equivalent circular diameter ($\langle D \rangle$) was calculated as:

$$\langle D \rangle = \sqrt{\frac{4A}{\pi}} \quad (5.1)$$

where A is the measured surface area. It is determined that the platelets of the first system have an equivalent circular diameter ($\langle D \rangle$) of 232 nm and will be referred to as $G232$, while the platelets of the second system have $\langle D \rangle$ equal to 574 nm and will be referred to as $G574$.

Described in chapter 4 is also the method to graft amino-modified polyisobutylene stabilizer (SAP 230 TP, Infineum, U.K.) on aqueous gibbsite via freeze drying, that has been applied to both systems used here. After freeze-drying, the dispersions of polymer grafted gibbsite particles were obtained in toluene. Finally, the solvent was replaced by three cycles of centrifugation (2 h, 900g) and redispersed in monomer solution. For the monomer solution the following chemicals were used as-received: Divinylbenzene (DVB, Merck) and photoinitiator (2,4,6-trimethylbenzoyl, Irgacure 819), obtained from CIBA Holding AG, Switzerland. Two different monomer solutions were used: (MS1) was used for $G232$ and consisted of 99 % wt DVB + 1 % wt Irgacure, while (MS2), composed of 98 % DVB + 2 % Irgacure, was used to disperse $G574$. Transmission electron microscopy (FEI, Tecnai 10 kV, the Netherlands) was used to obtain micrographs (Figure 5.1) from dried suspensions of the polymer grafted platelets.

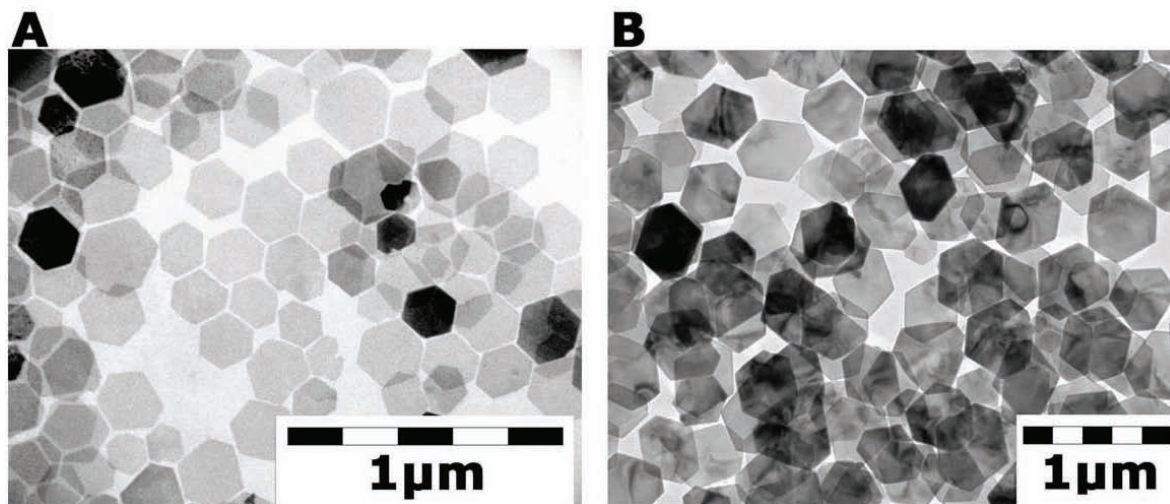


FIGURE 5.1. Transmission electron microscopy on dried suspensions of sterically stabilized colloidal gibbsite platelets. Panel (a) displays a micrograph of platelet system $G232$ ($\langle D_A \rangle = 232$ nm), while Panel (B) displays platelet system $G574$ ($\langle D_B \rangle = 574$ nm)

5.2.2. Sample preparation.

Homemade glass cells with inner dimensions $10 \times 10 \text{ mm}^2$ and approximately $145 \text{ }\mu\text{m}$, held together by glue (Araldit AW2102/HW2951, Huntsman Advanced Materials, Belgium) were used to store unpolymerized samples. These are well suited for polarizing microscopy and the initiation of the polymerization reaction and can be disassembled to recover polymerized samples for inspection with Focused ion beam-scanning electron microscopy (FIB-SEM). After equilibration time for at least 48 hours, the samples were polymerized by illumination with UV-light ($\lambda = 365 \text{ nm}$, 10 W) for 2 hours. After polymerization, samples were inspected by polarization microscopy. Some of the samples were removed from the sample cell in order to inspect them by electron microscopy.

5.2.3. Polarizing Microscopy.

A Nikon polarization microscope (Eclipse LV100pol) equipped with a digital camera (QImaging, MP5) was used to inspect the samples. A retardation filter (optical path difference 530 nm) was inserted at an angle of 45° with respect to both the polarizer and analyzer in order to determine the optical path difference of the samples.

5.2.4. Focused ion beam-scanning electron microscopy (FIB-SEM).

The inside of the nanocomposite samples was analyzed in a dual-beam Focused ion beam-scanning electron microscope (FEI, Nova Nanolab 600, the Netherlands). All scanning electron images were based on the detection of secondary scattered electrons. The focused Gallium ion beam is used to create nanometer smooth sectioning of the composite at specific sites and under designated orientation. Ion milling of the samples by the focused ion beam was employed to cut out thin sections (approximate size $10 \times 10 \times 0.1 \text{ }\mu\text{m}$) from the specimen that are suitable to be transferred and observed in a transmission electron microscope. In order to achieve this the sections are first connected to the tip of a sample needle by platinum welds. These were deposited *in situ* by decomposition of organo-platinum gas under irradiation of the focused ion beam. Then the sample was transferred by the needle to the vicinity of a copper grid. The sample was attached again with platinum welds to the grid and released from the needle by ion milling. Finally, the sample is trimmed to a lamella of approximately 100 nm thickness by ion milling. After this procedure, the grid was removed from the sample stage of the microscope and transported conveniently to the transmission electron microscope (see [12] for an extensive review on this procedure).

5.2.5. Transmission electron microscopy (TEM).

Thin sections of the gibbsite-polymer nanocomposite were inspected in TEM (FEI, Tecnai 20 kV, the Netherlands), which is most suitable to image colloidal particles with one dimension on the order of tens of nanometers. Furthermore, tilt series were made in order to investigate the orientation of the platelets within the sections.

5.3. RESULTS

The formation of nanocomposites of gibbsite in a polyvinylbenzene network was achieved in two steps: first a stable dispersion of the particles was prepared in a solvent composed of monomer and photoinitiator followed by two days of equilibration, then the polymerization was started by illumination with UV-light. It was checked by transmission electron microscopy on dried samples that the particles are not aggregated both after grafting with PIB (Figure 5.1) and after redispersion in monomer solution. The resulting dispersions were translucent and appeared pale yellowish. We first describe the results for the *in situ* polymerization of *G232*. For the suspension in monomer at low particle concentrations, flow birefringence was observed, while at high particle concentrations permanent birefringence was observed (Figure 5.2). Polarization micrographs before and after polymerization (Figure 5.3) display structures reminiscent of nematic liquid crystal phases. Although small cracks emerged throughout the sample the birefringence pattern and the retardation colors remained largely unchanged. Macroscopically, the polymerization process only led to subtle changes in the appearance of the samples: the translucency decreased and the colors slightly faded. Despite these macroscopic observations the polarizing microscopy images of the system before and after polymerization point out almost no changes in texture. Therefore, we suggest that the structures formed by the platelets in solution did not change significantly by the polymerization process. It appears that the dynamics of the system were quenched to yield a nanocomposite which comprises the original platelet structure.

We now discuss the results for the polymerization of the samples that contain *G574*. The polarization micrographs (Figure 5.4) of the polymerized sample shows birefringent patterns which are homogeneously colored. Rotation of the sample with respect to the polarizers and retardation filter revealed the presence of a preferential orientation of the director within the area included in the micrograph. Moreover, the retardation colors are of higher order in comparison with the polymerized samples prepared from *G232*. For both systems *G232* and *G574* the gibbsite-polymer nanocomposites had a pale yellowish color and were still translucent despite a somewhat higher turbidity in comparison with the dispersions in monomer (Figure 5.5). Moreover the materials had shrunk a few percent, which led to decreased contact with the walls of the cell. The polymerized samples could be removed intact from the sample cell and were rigid. A novel and convenient way to explore the structure of such nanocomposites in real space is by use of a dual-beam Focused ion beam-scanning electron microscope (FIB-SEM)[12]. High quality imaging can be performed with the scanning electron beam. Figure 5.6 displays micrographs that were obtained by electron imaging in FIB-SEM. These micrographs display closely packed stacks of particles against a dark background. For *G232*, the length of the stacks appears to be of the same order of the average platelet diameter. It



FIGURE 5.2. Birefringent phase of sterically stabilized colloidal gibbsite platelets in DVB monomer solution placed in between crossed polarizers and illuminated from the back.

appears that the platelets of *G574* are more uniformly ordered than *G232*. Thin slices of the material were removed by focused ion beam sectioning (milling) and transferred to the transmission electron microscope. Figure 5.7 displays transmission micrographs of both polymerized systems. Here, individual platelets are easily recognized and the presence of stacks formed by several platelets in the sample is unambiguous. Although the particles are separated from each other by several nanometers at minimum, the polymer density in between the faces of stacked platelets seems to be lower than the background, as higher intensity is observed at these spots in the transmission images. Some of the particles are not entirely flat, but display slight bending of their surface. It was shown by tilting the specimen within the microscope stage with respect to the electron beam, that several small nematic domains are present in the polymer sample of system *G232*. These have nematic directors that can be orthogonal even for neighboring domains, as is substantiated by transmission electron micrographs obtained under various tilting angles of the sample.

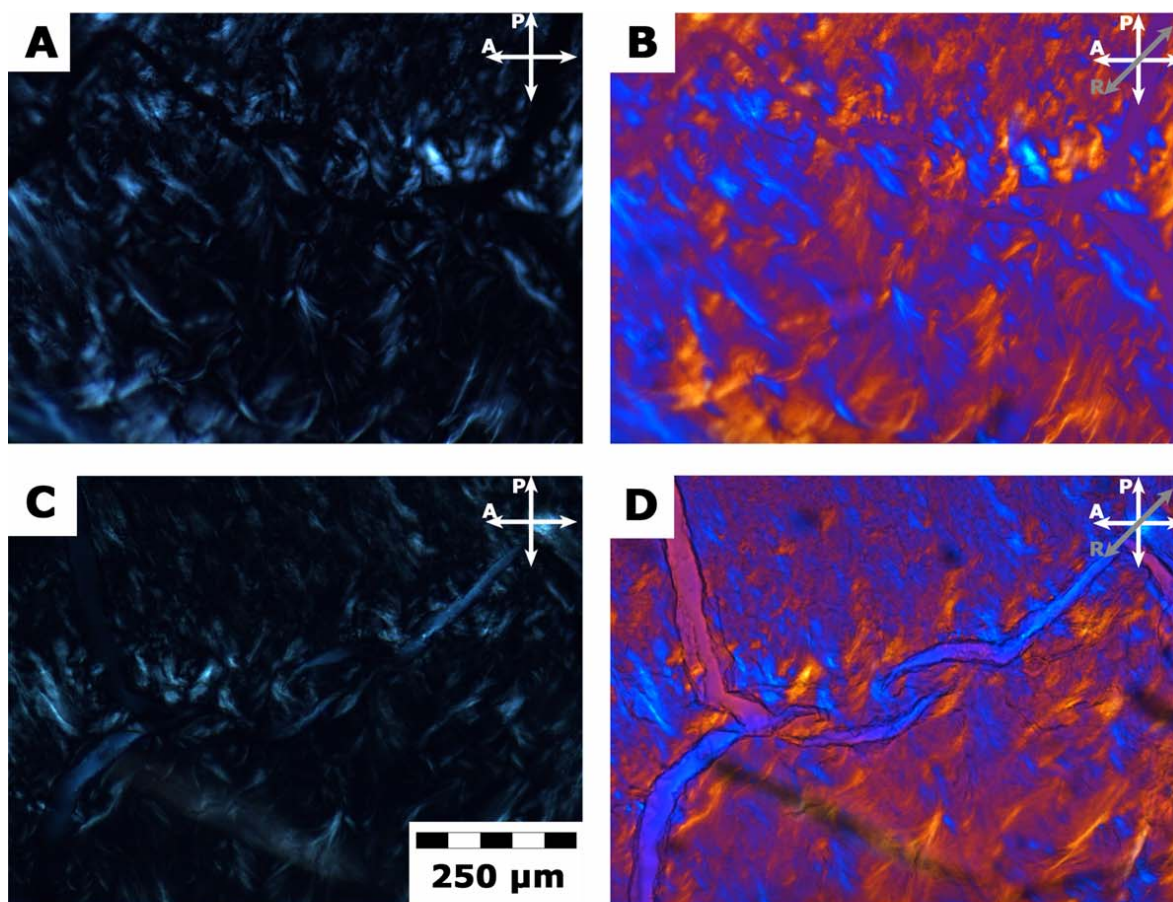


FIGURE 5.3. Polarizing micrographs of sterically stabilized gibbsite platelets (system *G232*) before (Panels A, B) and after (Panels C, D) polymerization of the solvent. Panels B and D display the micrographs obtained after insertion of the retardation filter. In the upper right corner of the micrograph is indicated the orientation of the polarizer (P), analyzer (A) and retardation filter (R).

5.4. DISCUSSION AND CONCLUSIONS

Colloidal gibbsite platelets that are grafted with PIB stabilizer easily form nematic liquid crystal phases in apolar solvents such as toluene at sufficient volume fractions [9]. By centrifugation and redispersion this solvent can be replaced by apolar monomer solutions containing photoinitiator. The resulting dispersions are still able to form nematic phases as is evidenced by their birefringence (Figure 5.2). Furthermore, these dispersions can be used as precursors for bulk polymer that comprises PIB-grafted gibbsite. Interestingly, it was evidenced by polarizing microscopy that polymerization of the dispersions by UV illumination did not change the ordering of the particles in the dispersion significantly, as the micrographs before and after initiation bear similarity both in texture and in interference color (Figure 5.3). Therefore we conclude that the ability of sterically stabilized colloidal gibbsite platelets to form nematic liquid

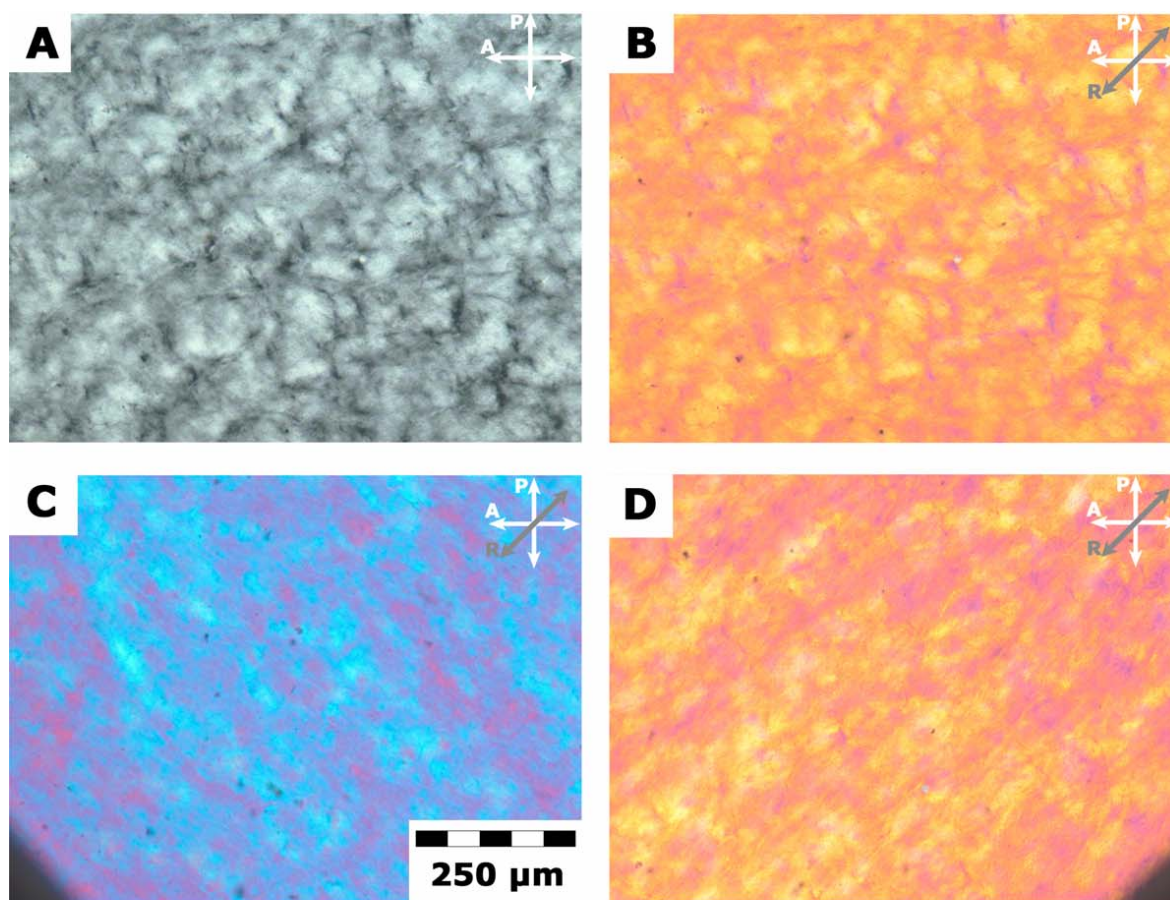


FIGURE 5.4. Polarizing micrographs of sterically stabilized gibbsite platelets (system *G574*) after polymerization of the solvent. Panel A displays the micrograph obtained without retardation filter, while panels B, C and D are obtained with retardation filter. The sample was rotated over 45 degrees clockwise (panel C) and counterclockwise (panel D). In the upper right corner of the micrograph is indicated the orientation of the polarizer (P), analyzer (A) and retardation filter (R).

crystal phases can be deployed as a mold for the formation of nematically ordered nanocomposites of mineral platelets in bulk polymer. Polymerization did slightly change the macroscopic properties of the samples, giving rise to somewhat less transparent samples. Upon insertion of a retardation filter the samples containing system *G232* displays complementary interference colors (ranging from pale yellow to light blue), as well as neutral (approximately 530nm) interference colors, indicating that there are small nematic domains oriented independent of each other. Although on different length scales the same phenomenon is observed in the scanning (Figure 5.6A) and transmission (Figures 5.7 A - B) electron micrographs, where the platelets are piled up in short but pronounced stacks that are randomly oriented.

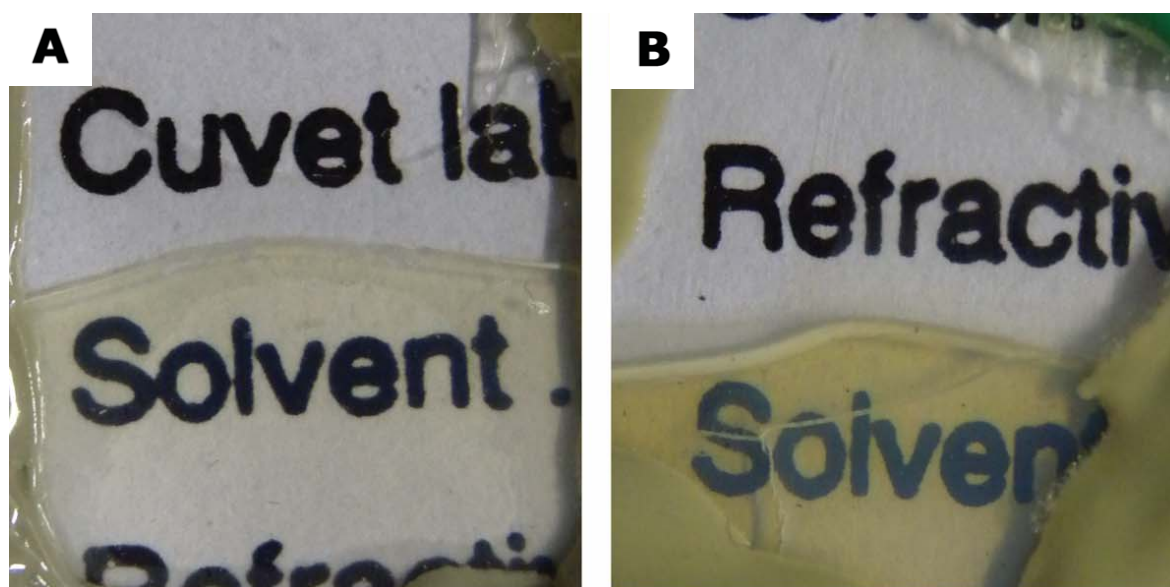


FIGURE 5.5. Gibbsite-polymer nanocomposites of approximately $150\ \mu\text{m}$ thickness. Panel A shows the nanocomposites of system $G232$ and panel B shows the nanocomposites of system $G574$. The upper half of the images displays the empty part of the sample cell as a reference and the width of the images corresponds to approximately $1.5\ \text{cm}$.

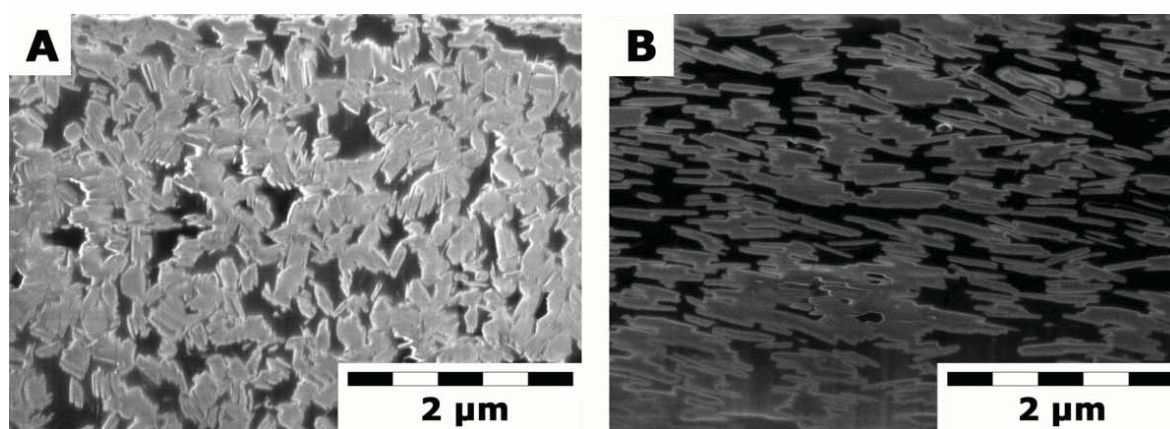


FIGURE 5.6. Scanning electron micrograph on gibbsite-polymer nanocomposites. Panel A displays the composite containing gibbsite platelet system $G232$ and panel B displays the composite containing the gibbsite platelet system $G574$. Both intersections were obtained by milling of the specimen by a focused ion beam.

On the other hand samples containing system $G574$ (Figure 5.4) have more homogeneously colored interference patterns. Rotation of the sample within the polarizing microscope indicated that the director pattern of the nematic has a preferential direction in this sample. Rotation of the sample such that the vertical orientation of the

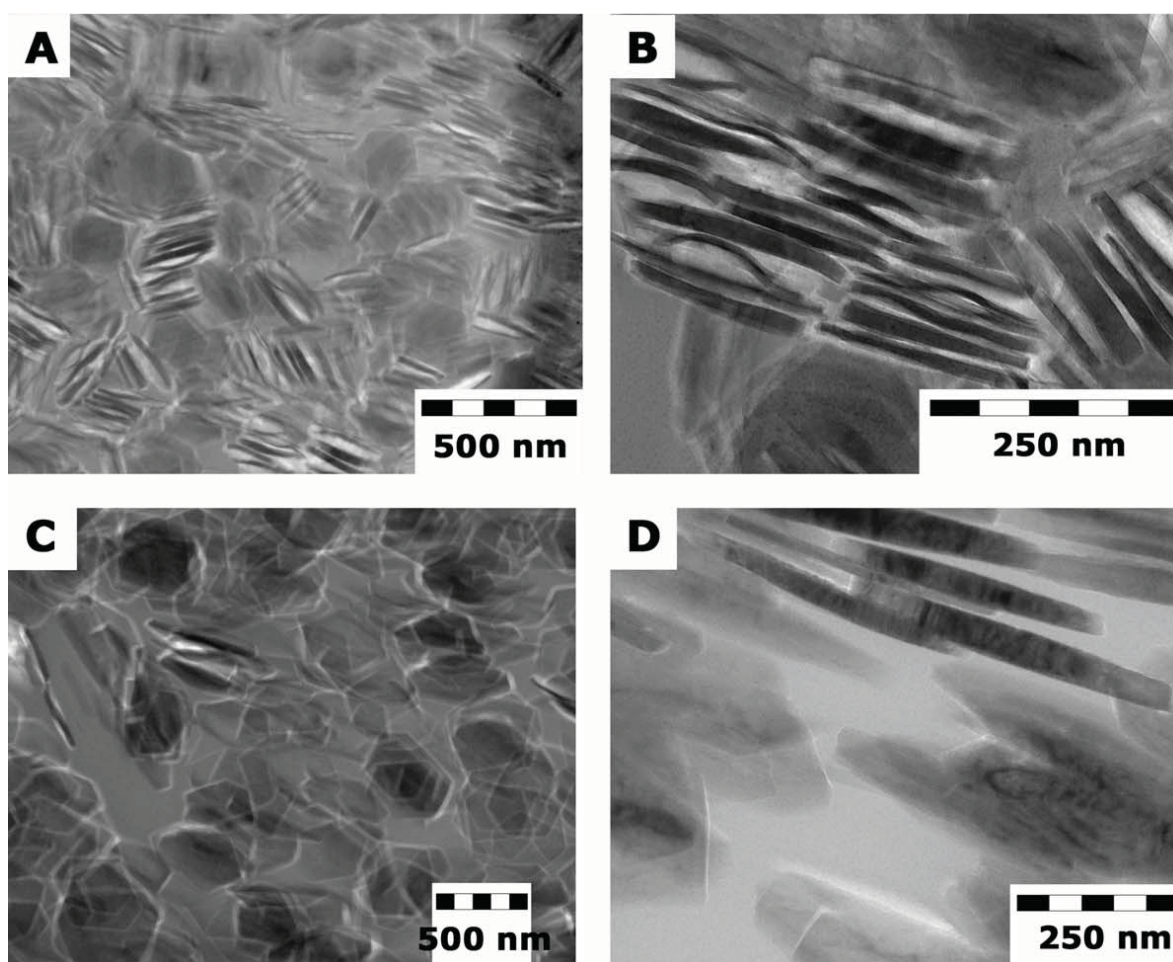


FIGURE 5.7. Transmission electron micrographs of gibbsite-polymer nanocomposites. Panels A and B (close-up) display the nanocomposite containing gibbsite platelet system $G232$, while Panels C and D (close-up) display the nanocomposites containing the gibbsite platelets of system $G574$.

samples aligns with the slow axis of the retardation filter leads to higher order interference colors (light blue), indicating net alignment of the slow axis of the platelets in this direction. Rotation of the sample such that the vertical orientation of the samples is perpendicularly oriented with respect to the slow axis of the retardation filter led to lower order interference colors (whitish yellow). This confirms the presence of a net orientation of the director in the sample of the platelets of system $G574$ along the vertical direction. The scanning electron micrograph shown in Figure 5.6 displays a rather uniform alignment of the platelets, with particle directors that typically vary over 30 to 40 degrees at maximum.

The mineral platelets are well dispersed throughout the polymer as is evidenced by the scanning electron micrographs in Figure 5.6. Although to a large degree they are piled up, no aggregates are formed. Inspection with TEM (Figure 5.7) shows that the

structures of gibbsite are intercalated by the polymer. Furthermore, the transmission micrographs show that the nanocomposite is filled with closely packed structures of platelets. The particles are better resolved in the TEM than in the SEM images, particularly those which are not oriented perpendicular to the imaging plane.

We conclude that the system *G574* has more homogeneous ordering of the mineral platelets within the nanocomposite than system *G232*, presumably due to the larger average platelet diameter. This is substantiated by additive experimental techniques that extend over different length scales. Polarization microscopy indicated the (in)homogeneity of the nematic platelet ordering over length scales of millimeters. It shows that over such length scales system *G232* has orthogonally oriented nematic domains, while on the same length scale system *G574* has a single net orientation of the nematic director. Inspection with FIB-SEM yields results on the ordering of the platelets in the micrometer regime and can resolve stacks of platelets. Here it is confirmed that in the nanocomposites of system *G232* orthogonally oriented short stacks of platelets occur. Additionally, information on the typical length scale and on the distribution of such stacks is obtained. Finally, further information on the local ordering of the colloidal platelets in the nanocomposites was obtained by TEM imaging of a lamella that was prepared in FIB-SEM. Here, location, orientation and deformation of single platelets can be discerned. The platelets can be nearly touching or separated by about 10 nanometers within a stack, indicative of a good dispersion in the polymer matrix. Stacks are predominant in the sample of system *G232*, while nematic order is predominant in the sample of system *G574*. The stacks in system *G232* appear to be closely packed. Some of the thinner platelets (in system *G232*) are slightly bent.

There have been other approaches to obtain nematic ordering of anisometric particles in polymer in literature such as layer-by-layer deposition [5, 6, 7], pressure molding [13], centrifugation [14] and electrophoretic deposition followed by infiltration [8]. Our approach, on the other hand involves a cast of the composite that is formed based on the self-assembling properties of the constituents themselves: organophilic mineral platelets. Additionally, lyotropic liquid crystals of such platelets are easy to direct by external fields, which may eventually help to get control over the ordering of the casting structures. Hopefully, this approach opens up routes to the challenging manufacturing of highly orientationally and periodically ordered polymer-mineral nanocomposites with high mineral contents in bulk amounts.

5.5. ACKNOWLEDGEMENT

Hans Meeldijk and Matthijs de Winter are acknowledged for their contributions. Laurent Heux and Chris Schneijdenberg are thanked for discussions.

Bibliography

- [1] T. J. Pinnavaia and G. W. Beall, *Polymer clay nanocomposites*, Wiley, New York, 2001.
- [2] S. Mann, *Biomineralization*, Oxford University Press, Oxford, 2001.
- [3] N. Watabe, *The Mollusca, Form and Function: Shell Structure*, Vol. 11, Academic Press, New York, 1988.
- [4] H. Gao, B. Ji, I. L. Jäger, E. Arzt, and P. Fratzl, *Proceedings of the National Academy of Sciences of the United States of America*, 2003, **100**(10), 5597–5600.
- [5] Z. Tang, N. A. Kotov, S. Magonov, and B. Ozturk, *Nat Mater*, 2003, **2**(6), 413–418.
- [6] P. Podsiadlo, A. K. Kaushik, E. M. Arruda, A. M. Waas, B. S. Shim, J. Xu, H. Nandivada, B. G. Pumplun, J. Lahann, A. Ramamoorthy, and N. A. Kotov, *Science*, 2007, **318**(5847), 80–83.
- [7] L. J. Bonderer, A. R. Studart, and L. J. Gauckler, *Science*, 2008, **319**(5866), 1069–1073.
- [8] T.-H. Lin, W.-H. Huang, I.-K. Jun, and P. Jiang, *Electrochemistry Communications*, 2009, **11**(1), 14–17.
- [9] F. M. van der Kooij and H. N. Lekkerkerker, *Philosophical Transactions of the Royal Society of London*, 2001, **359**, 985–995.
- [10] C. Decker, K. Zahouily, L. Keller, S. Benfarhi, T. Bendaikha, and J. Baron, *Journal of Materials Science*, 2002, **37**(22), 4831–4838.
- [11] L. Keller, C. Decker, K. Zahouily, S. Benfarhi, J. M. Le Meins, and J. Mieke-Brendle, *Polymer*, 2004, **45**(22), 7437–7447.
- [12] M. L. Richard, *Microscopy Research and Technique*, 2006, **69**(7), 538–549.
- [13] C. Özdilek, E. Mendes, and S. J. Picken, *Polymer*, 2006, **47**(6), 2189–2197.
- [14] R. Chen, C.-a. Wang, Y. Huang, and H. Le, *Materials Science and Engineering: C*, 2008, **28**(2), 218–222.

6

Formation of Nematic Liquid Crystals of Sterically Stabilized Layered Double Hydroxide Platelets

ABSTRACT

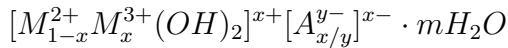
Colloidal platelets of hydrotalcite, a layered double hydroxide, have been prepared by coprecipitation at pH 11-12 of magnesium nitrate and aluminum nitrate at two different magnesium to aluminum ratios. Changing the temperature and ionic strength during hydrothermal treatment, the platelets were tailored to different sizes and aspect ratios. Amino modified poly-isobutylene molecules were grafted onto the platelets following a convenient new route involving freeze-drying. Organic dispersions in toluene were prepared of the particles with the largest size and highest aspect ratio. The colloidal dispersions prepared in this way showed isotropic-nematic phase transitions above a limiting concentration in a matter of days. The number density at the transition and the width of the biphasic region were determined and compared to theory. The orientation of the platelets in nematic droplets (tactoids) and at the isotropic-nematic interface were analyzed by polarization microscopy. It was observed that sedimentation induces a nematic layer in samples that are below the limiting concentration for isotropic-nematic phase separation. Only after years, nematic phases were observed in the aqueous suspensions of the charged particles.

Reproduced in part with permission from M.C.D. Mourad, E.J. Devid, M.M. van Schooneveld, C. Vonk and H.N.W. Lekkerkerker, J. Phys. Chem. B 112 (2008) 10142. Copyright 2008 American Chemical Society.

6.1. INTRODUCTION

The isotropic to nematic transition in dispersions of anisotropic mineral colloids has been subject of renewed interest during the last 20 years [1, 2]. After the first observations of such a transition for V_2O_5 [3], α -FeOOH [4] and californite [5], which nowadays is recognized as hectorite [6] and the consequent theoretical treatment of the phenomenon by Onsager [7], there has been a considerable silence in the experimental field. In recent years however the so-called mineral liquid crystals have re-emerged and isotropic to nematic transitions have now been observed as well for aqueous boehmite [8, 9], imogolite [10], akaganeite [11, 12], goethite [14, 13], gibbsite [15], layered double hydroxides [16] and nontronite [17] and sterically stabilized boehmite [9], gibbsite [18] and sepiolite [19].

The layered double hydroxides (LDH) platelets are particularly interesting since they form an easy-to-synthesize class of colloidal, disk shaped materials that can be adapted chemically to contain different metal ions and intercalated anions. The general formula for LDH is:



with M^{2+} , M^{3+} the divalent and trivalent metal cations, respectively. The structure is obtained when part of the divalent cations is substituted by trivalent cations with a similar ionic radius while the brucite like structure is maintained. The ability of introducing significant amounts of trivalent cations make that the LDH particles have interesting tunable optical and magnetic properties. Hydrotalcite is the LDH that consists of Mg^{2+} and Al^{3+} . This mineral is easy to synthesize and the preparation is well described [20, 21, 22].

Sun *et al.* demonstrated the ability of water dispersed hydrotalcite platelets to phase separate into nematic [16] and lamellar [23] structures. Moreover, addition of a depletion agent by means of non-adsorbing polymer, led to multi-phase equilibria [24]. The interaction between the individual particles in these experiments is dominated by the repulsion of the particles through their charge, and in the latter case by the depletion attraction. The contribution of the electrostatical double layer to this interaction decreases the effective anisotropy [15] and may result in phase behavior not expected on entropic grounds [15, 25, 26]. In contrast, polymer grafted particles may be regarded as elements with almost hard interactions for which entropy dominates the phase behavior.

In the work presented here the synthesis of hydrotalcite is performed by alkaline coprecipitation of metal nitrates [22]. Furthermore, experiments at different temperatures and peptization were performed to control the size [21]. The average particle diameter plays an important role: the presence of an electric double layer or a grafted polymer layer will decrease the aspect ratio (size over thickness: d/l). The larger the size of

the platelet the smaller the effect of these layers on the aspect ratio is. Computer simulations [27] predict that for $(d/l) \leq 7$ the isotropic-nematic transition is no longer thermodynamically stable and is replaced by an isotropic-columnar transition. This is demonstrated in experiments with nickel hydroxide platelets [28]. Moreover, in case of columnar liquid crystals, a particle diameter that is too small will cause Bragg reflections to occur at wavelengths below the visible range. On the other hand, too large particle sizes have been observed to prevent phase separation in sedimentation experiments [25].

Using a novel approach the hydrotalcite particles were grafted with amino-functionalized poly-isobutylene (PIB) chains which are known for their successful stabilization of inorganic particles. PIB proved its use in other liquid crystal forming systems [9, 18, 19]. Dispersions of sterically stabilized hydrotalcite particles in toluene have a very low turbidity due to refractive index matching and are able to phase separate in a few days, compared to months for similar aqueous systems [16]. Earlier, non-aqueous suspensions of liquid crystal forming mineral particles were obtained by an elaborate method which involves a gradual solvent substitution upon addition of the stabilizing polymer [29, 30]. Here we describe an alternative method in which the particles are freeze dried in the presence of the stabilizer as has been applied before successfully to graft surfactants on cellulose whiskers [31]. The resulting organophilic hydrotalcite particle maybe a useful starting material in the preparation of polymer colloid nanocomposites [32].

6.2. EXPERIMENTAL

6.2.1. Preparation

Colloidal hydrotalcite platelets were synthesized by coprecipitation at pH 11-12. $\text{Mg}(\text{NO}_3)_2 \cdot 6\text{H}_2\text{O}$ (Acros Organics, p.a.) and $\text{Al}(\text{NO}_3)_3 \cdot 9\text{H}_2\text{O}$ (Aldrich, 98+ % p.a.) with the total concentration of the Mg and Al ion content equal to 0.5M, were added dropwise to an equal volume of alkaline solution containing 1.1M NaOH (Merck, p.a.) and 0.15M NaNO_3 (Merck, p.a.) [22]. All water used for the preparation was Millipore (Synergy, Millipore company) or doubly distilled water. Two magnesium to aluminium ratios of the reactants were used to obtain different systems: 2:1 and 4:1.

After coprecipitation some of the suspensions were hydrothermally treated in their mother liquid, while others were centrifuged (900g, 40 minutes) and redispersed in water before. This treatment is expected to improve the growth and crystallinity of the resulting particles [21]. The mixtures were stirred at fixed temperature (of 22°C, 85°C and 150°C, respectively) for 3 days. For each batch the ratio of the reactants, the temperature during hydrothermal treatment and the insertion of a redispersion step are presented in Table 6.1. Finally the suspensions were dialyzed in tubes (regenerated

TABLE 6.1. The average diameter and the relative standard deviation of the diameter as measured by electron microscopy on hydrotalcite platelets synthesized at various experimental conditions. Variables are the mole fraction of $\text{Mg}^{2+}:\text{Al}^{3+}$ and the insertion of a step in which the precipitate is sedimented by centrifugation and redispersed in Millipore water before hydrothermal treatment.

System	Ratio $\text{Mg}^{2+}:\text{Al}^{3+}$	θ ($^{\circ}\text{C}$)	Centrifuged	d [nm]	σ_d
A	2:1	22	-	46	0.33
B	2:1	85	-	65	0.27
C	2:1	150	yes	146	0.26
D	4:1	85	-	51	0.29
E	4:1	85	yes	69	0.35
F	4:1	150	yes	133	0.33

TABLE 6.2. Crystallographic data for hydrotalcite systems obtained via various synthetic routes. The crystallographic unit cell was calculated by fitting the diffractograms to the R3-m space group.

System	a [\AA]	b [\AA]	c [\AA]	remarks
C	6.35	6.37	47.92	
D	6.28	6.56	49.40	some contamination
E	6.32	6.43	49.34	some contamination
F	6.31	6.43	49.00	additional bayerite phase present

cellulose, Visking, MWCO 12000-14000) against demineralized water until the conductivity dropped below $10 \mu\text{S}/\text{cm}$, and centrifuged in order to concentrate and fractionate (typically at 1000g, 17h; Beckman Coulter, Avanti J20-XP).

The system with the largest hydrotalcite platelets (system C, as indicated in Table 6.1) was grafted with steric stabilizer in order to obtain an organophilic system. The polymer used to graft the mineral material is amino modified poly-isobutylene stabilizer SAP 230 TP having two tails of approximately 17 isobutylene subunits. A mixture of 1-propanol (80ml Acros, 99+%) and SAP 230 TP (Infineum, UK, 10 gram) was stirred mechanically until the polymer appeared well dispersed. Aqueous hydrotalcite dispersion (100 ml , $79\text{g}/\text{dm}^3$) was added dropwise to the mixture. Then the solvent was removed by a rotational vacuum evaporator until a highly viscous paste was obtained. The product was spread out as a film at the inside of a round bottom flask and was frozen in liquid nitrogen and connected to a vacuum setup. After freeze-drying a mixture of hydrotalcite

particles and stabilizing polymer was obtained, which was easily redispersable in toluene (J.T.Baker, 99.5 +%). Finally, excess SAP 230TP was removed by three cycles of centrifugation (2h, 900g) and redispersion in toluene. Concentration series of sterically stabilized hydrotalcite dispersions in toluene were made with overall concentrations ranging from 300 to 700g/dm³ by centrifugation and redispersion.

6.2.2. Particle characterization

Individual platelets were studied by transmission electron microscopy (TEM) and atomic force microscopy (AFM). For TEM, hydrotalcite particles were dried on polymer films which were sputter coated with carbon for enhanced electrical conductance and supported on copper grids. The electron microscopes (Tecnai 10 and Tecnai 12, FEI Company) were operated at 100 and 120 KeV, respectively. The size of the particles was measured with imaging software (iTEM, soft imaging system GmbH). The surface area (A) of well over 250 individual particles was measured. An equivalent spherical diameter was calculated as:

$$d = \sqrt{\frac{4A}{\pi}} \quad (6.1)$$

where A is the measured surface area. The polydispersity in the calculated diameters is expressed by means of the relative standard deviation

$$\sigma_d = \frac{\sqrt{\langle d^2 \rangle - \langle d \rangle^2}}{\langle d \rangle} \quad (6.2)$$

AFM measurements were performed using a scanning probe microscope (Digital Instruments) in tapping mode equipped with a TESP silicon tip (Digital Instruments) on a hydrotalcite suspension dried on freshly cleaved mica. In addition to the diameter the thickness and its relative standard deviation (σ_l) of the platelets was measured from AFM images using WSxM (Nanotec electronica S.L.).

Further characterization of the platelets was done by X-ray diffraction (XRD) using CoK $_{\alpha}$ radiation (1.79026 Å) on a Bruker-AXS D8 operated at 30 kV and 45 mA. The powder X-ray diffractograms were compared with a powder diffraction database (International Centre for Diffraction Data, 2000) and Pawley fits were made in order to calculate the crystallographic unit cell constants using Topas (Bruker AXS, Delft, The Netherlands).

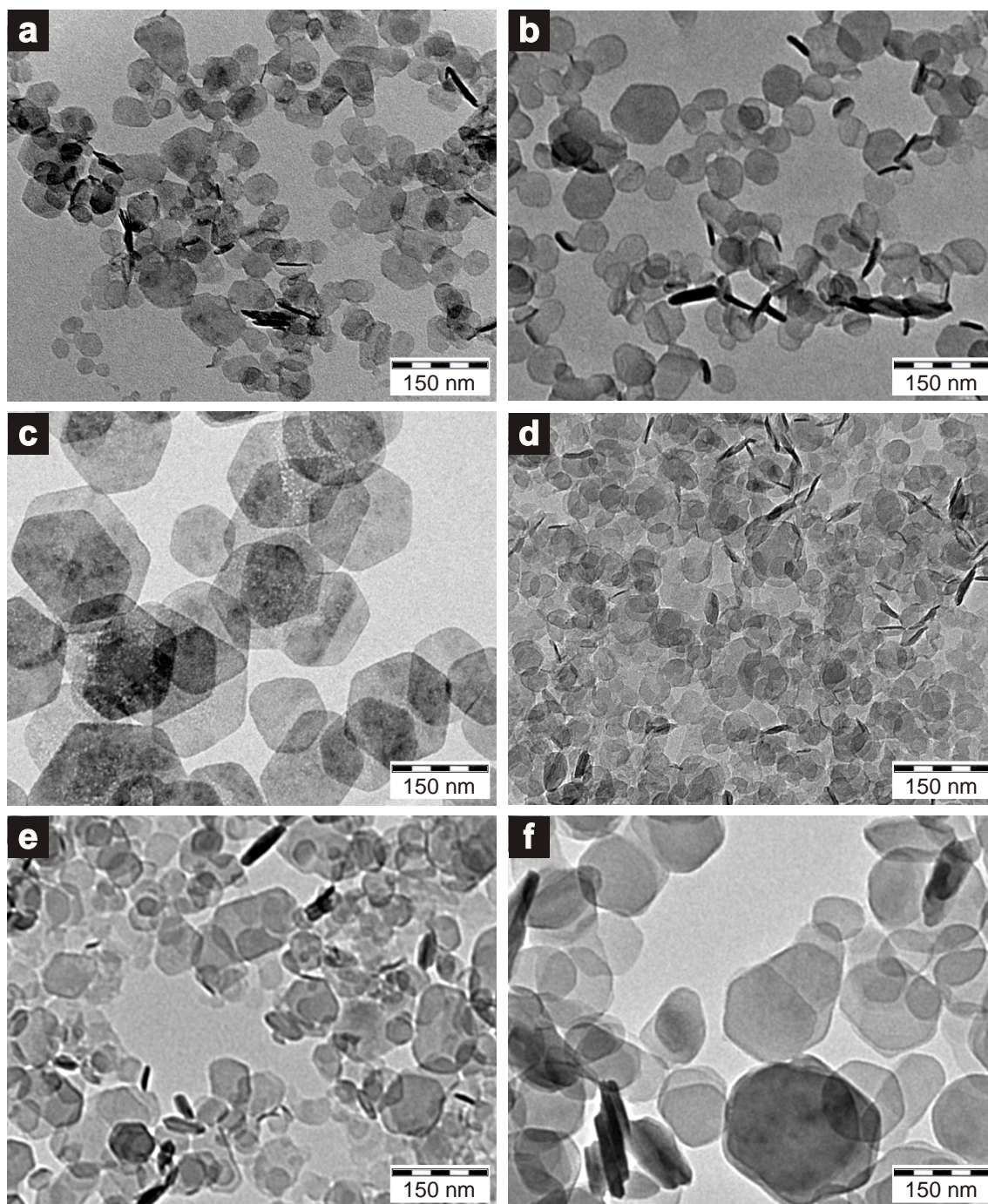


FIGURE 6.1. Transmission electron micrographs of the hydrothermalite platelets synthesized. Figures (a) to (f) correspond to systems A to F as defined in Table 6.1. Clearly visible is the hexagonal shape with slightly rounded corners for all systems.

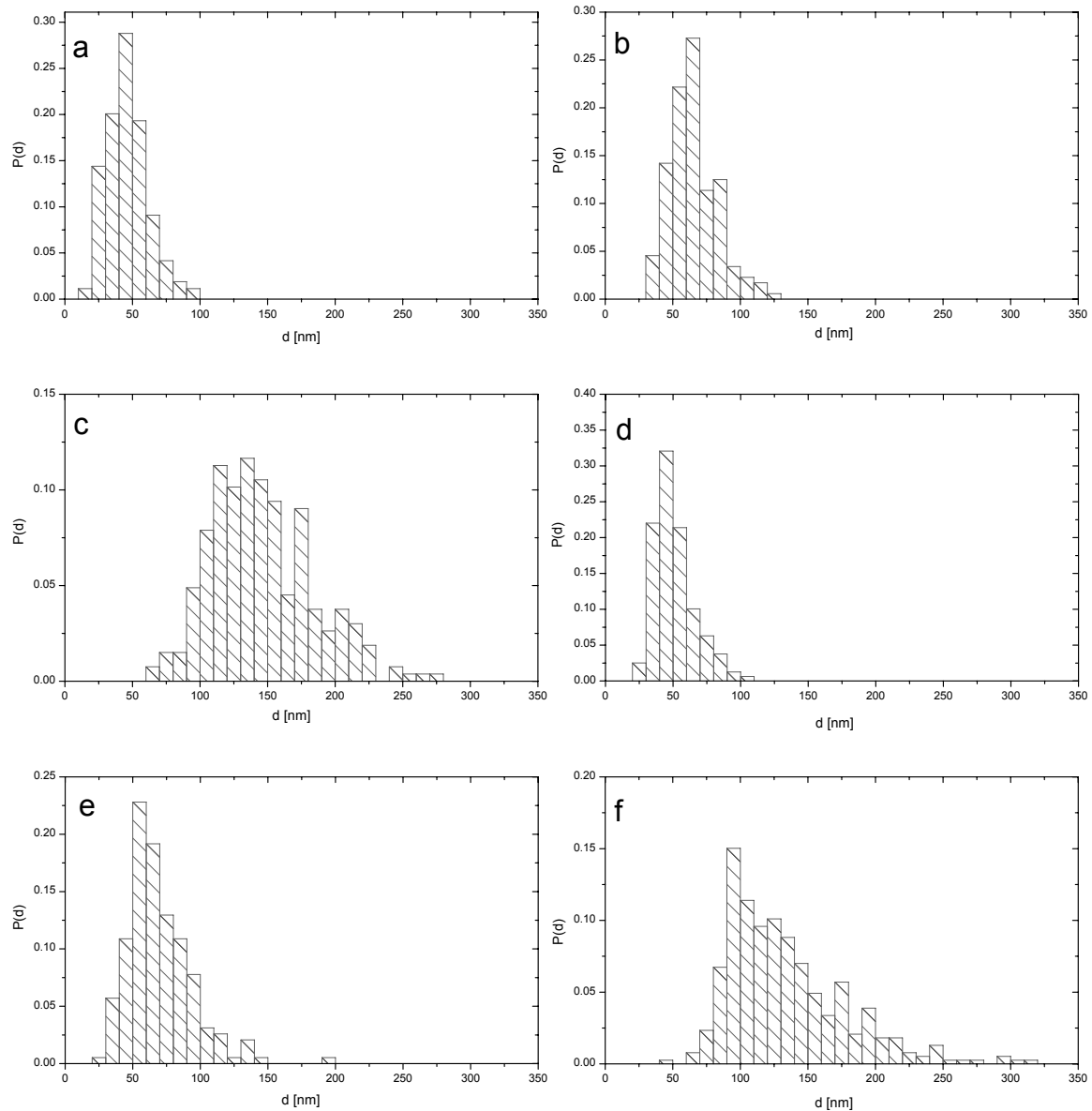


FIGURE 6.2. Diameter distributions of hydrotalcite platelets. Transmission electron micrographs were analyzed using the method described in section 6.2.2. Figures (a) to (f) correspond to systems A to F as defined in Table 6.1.

6.2.3. Sedimentation

The hydrotalcite platelets that were most likely to form nematic phases due to their large average diameter and therefore large (d/l) even in combination with an electric double layer were concentrated by centrifugation and redispersion in NaCl solutions. It is well known that changing the ionic strength influences the interaction potential of charged particles and disk shaped particles in particular[33]. Therefore a concentration series of 50 to 200 g/dm³ was made in solutions of 10⁻³ M and 10⁻⁴ M NaCl. The series

was transferred into capillaries (Vitrocom, 100mm x 4mm, optical path: 100 μ m) that were flame sealed and stored in vertical position for sedimentation over several months. All samples were stored in a dark, thermostatted room and inspected regularly under normal illumination and between crossed polarizers.

Samples of PIB-stabilized hydrotalcite were prepared by centrifugation and redispersion in toluene in optical cells (10 \times 10 \times 40 mm, Hellma). These were inspected under normal illumination and between crossed polarizers during the first days after preparation and were stored upright for sedimentation during several months. Part of these samples was transferred to round borosilicate Mark tubes (diameter 2mm, W. Muller, Schonwalde bei Berlin, Germany) suitable for small angle X-ray scattering experiments. Another part of these samples was transferred into homemade glass cuvetts of inner dimensions 10 \times 10 mm and approximately 145 μ m for polarization microscopy.

6.2.4. Polarization microscopy

A Nikon polarization microscope (Eclipse LV100pol) equipped with a digital camera (QImaging, MP5) was used to follow the phase separation process. A retardation filter (optical path difference 530 nm) was inserted at an angle of 45 degrees with respect to the polarizer and analyzer in order to determine the optical birefringence. Photographs were taken during the process of phase separation starting 2 hours after homogenization.

6.3. AQUEOUS DISPERSIONS

6.3.1. Temperature controlled synthesis of nanoplatelets

After alkaline coprecipitation crystalline platelets of hydrotalcite were hydrothermally treated. The effect of temperature and salinity during this hydrothermal treatment and the ratio of Mg and Al ions on the size of the particles was determined by measurements of the average particle diameter. Figure 6.1 shows typical transmission electron micrographs of the systems obtained with hydrothermal treatment at different temperatures. The platelets have a hexagonal shape with rounded corners. There are no signs of aggregation visible in the micrographs.

Size distributions (as shown in Figure 6.2) were constructed from measurements on well over 250 particles and the average diameter and the relative standard deviation were obtained (Table 6.1). The average diameter $\langle d \rangle$ ranges from 49 to 146 nm and became larger when hydrothermal treatment was performed at 150 $^{\circ}$ C instead of 85 $^{\circ}$ C as has been reported earlier [21].

System C which has the largest particles and the lowest polydispersity in diameter was selected for further study. As a first step we determined the thickness (l) and diameter (d) of the particles of this system by AFM. Images and histograms of (l) and (d) based

on 100 particles are given in Figure 6.3. Using these results we find an average thickness $\langle l \rangle = 12.7$ nm with a relative standard deviation $\sigma_l = 0.36$ and an average diameter $\langle d \rangle = 182$ nm with relative standard deviation $\sigma_d = 0.23$. The average diameter is larger than the value found by TEM. This may be related to the sampling. These AFM data allow us to investigate to what extent the diameter and thickness are correlated. The correlation coefficient

$$R_{d,l} = \frac{\langle dl \rangle - \langle d \rangle \langle l \rangle}{\langle d \rangle \langle l \rangle} \quad (6.3)$$

turns out to be 0.04. The product was identified to be hydrotalcite from the obtained powder X-ray diffraction patterns. One of the samples (F) shows signs of a bayerite phase in addition to hydrotalcite. (D) and (E) have some minor unidentified peaks (see Figure 6.4). The sample that was hydrothermally treated without replacement of the mother liquid (D) appears less crystalline in comparison to (E) as individual widths of reflections are increased. The patterns were fitted to the R3-m space group using the Pawley fit algorithm to yield a, b and c parameters for the crystallographic unit cell (shown in Table 6.2). In Figure 6.5 the x-ray powder diffractogram of system F and the corresponding fitted diffractogram are provided.

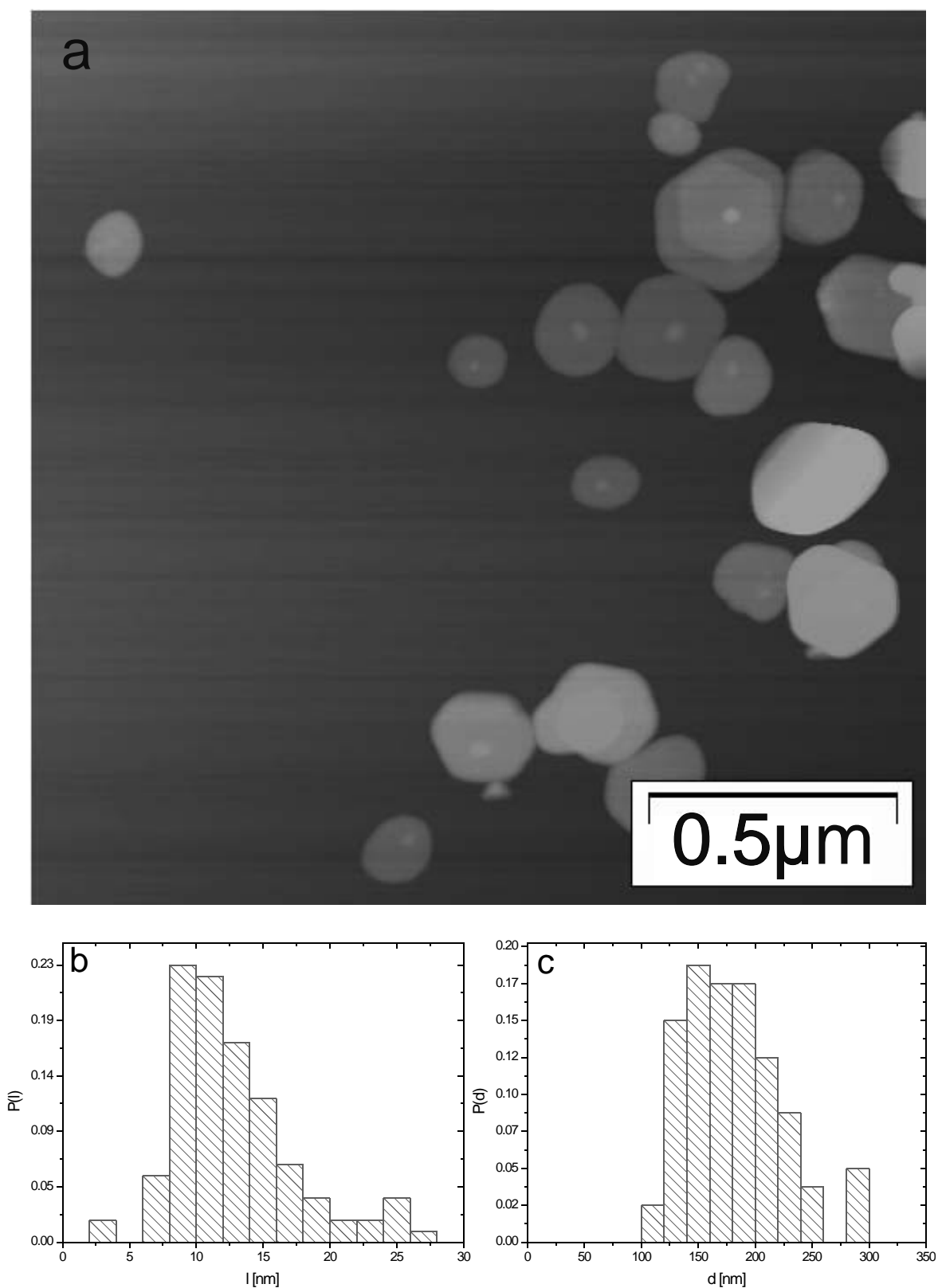


FIGURE 6.3. AFM measurements on hydrotalcite platelets. In (a) an AFM image of hydrotalcite platelets on a mica support is displayed. In (b) a histogram of the thickness of the platelets, as measured by AFM, is shown ($\langle l \rangle = 12.7$ nm with $\sigma_l = 0.36$). In (c) the platelet diameter distribution from AFM is depicted ($\langle d \rangle = 182$ with $\sigma_d = 0.23$).

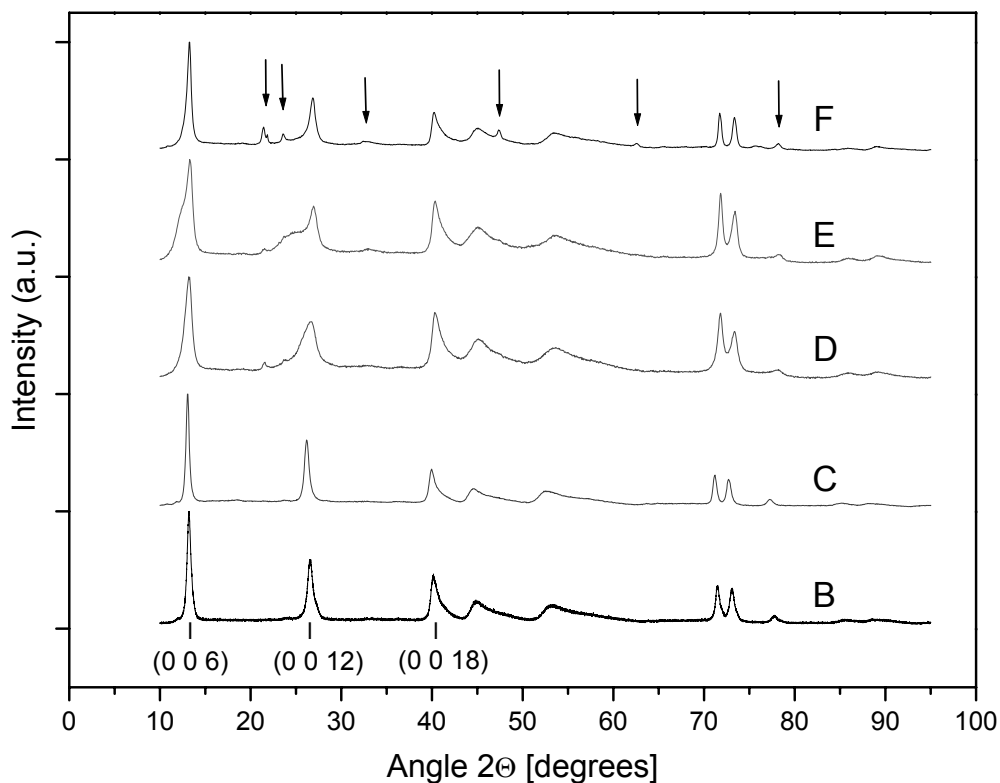


FIGURE 6.4. X-ray powder diffractograms of the different hydroxaltes studied (B to F, as defined in Table 6.1). The baseline of the diffractograms was shifted vertically for clarity. Arrows indicate peaks that are attributed to the presence of a bayerite phase.

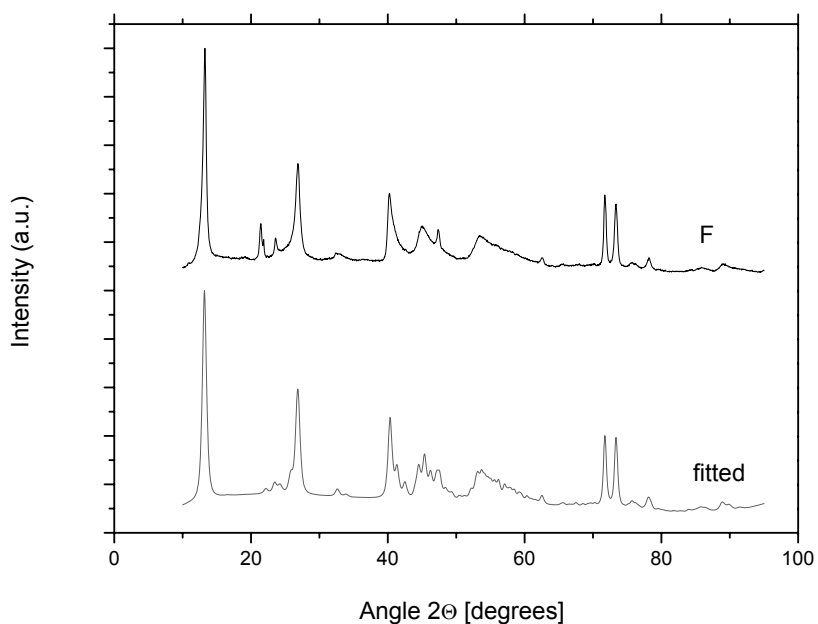


FIGURE 6.5. X-ray powder diffractogram of system F (Table 6.1) and the fitted diffractogram.

6.3.2. Sedimentation

By centrifugation and redispersion hydrotalcite samples of system C were prepared at concentrations from 50 g/dm^3 to 200 g/dm^3 and at ionic strengths ranging from 10^{-4} to 10^{-2} M NaCl in flat optical capillaries. The colloidal suspensions are stable both with and without the NaCl added and do not show any signs of aggregation. The sample at 200 g/dm^3 and 10^{-3} M NaCl was too viscous to be transferred into an optical capillary. Gravity induces sedimentation of the stable suspensions within days. After a few weeks a remarkably complex pattern of layers is formed within the sediment. The layers are not separated by flat and horizontal interfaces although distinct transitions between regions with a large variation in turbidity can be discerned. These patterns bear some resemblance to those described by Fossum *et al.* for sodium fluorohectorite [34], [35]. Moreover the sedimented samples are highly viscous and have deformed suspension-air interfaces. Figure 6.6 shows the samples 10 months after preparation between crossed polarizers. Apart from depolarized scattering only few birefringent speckles, typically sized 3 to $10\text{ }\mu\text{m}$, were observed in these samples. After 2 years, however, sharp and strongly birefringent interfaces are formed in the upper part of the sediments (Figure 6.7).

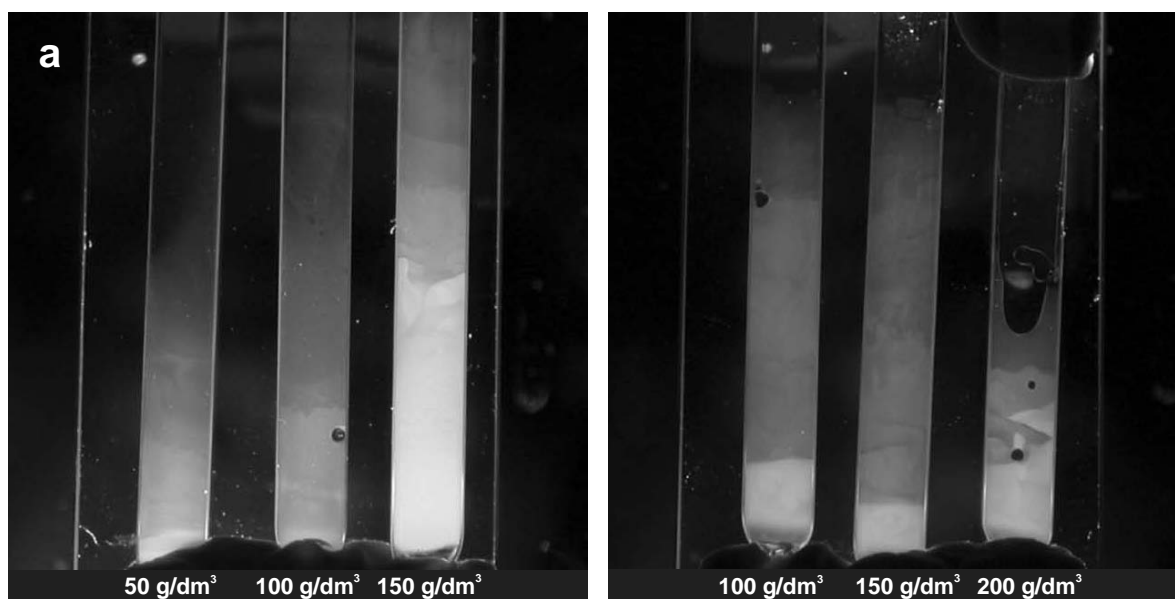


FIGURE 6.6. Sedimentation profiles of aqueous hydrotalcite between crossed polarizers at (a) 10^{-3} M NaCl added, from left to right $50, 100$ and 150 g/dm^3 hydrotalcite and (b) 10^{-4} M NaCl added salt and from left to right $100, 150$ and 200 g/dm^3 hydrotalcite respectively.

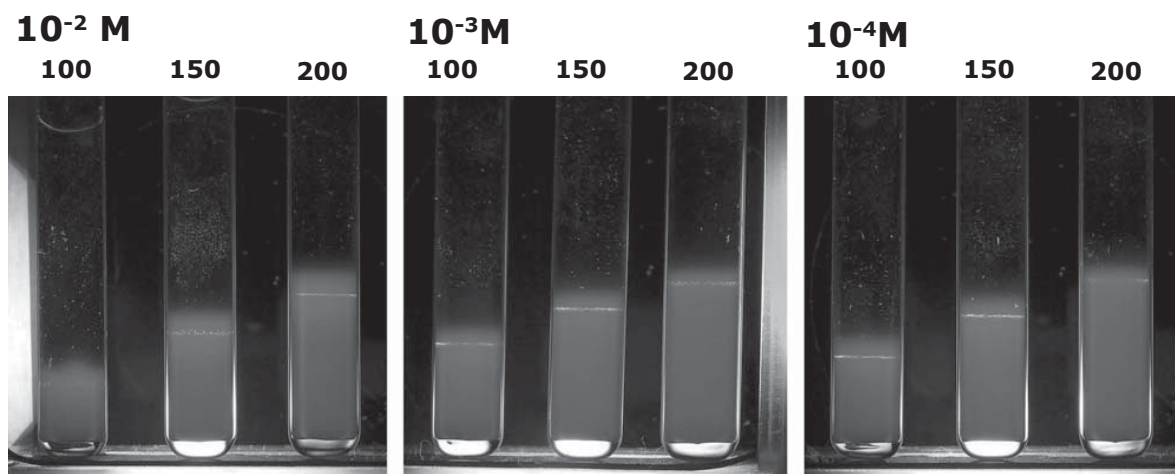


FIGURE 6.7. Samples of aqueous hydrotalcite between crossed polarizers at 10^{-2} - 10^{-4} M NaCl added and particle concentration of 100 - 200 g/L (indicated above) displaying birefringent phases 2 years after preparation .

6.4. ORGANIC DISPERSIONS

6.4.1. Synthesis of organophilic nanoplatelets

Freeze-drying a mixture of the aqueous system C with stabilizing SAP 230 TP polymer in 1-propanol yielded a sticky paste which easily dissolved in toluene. In three cycles of centrifugation and redispersion in toluene the excess of polymer is removed and a stable, transparent dispersion of hydrotalcite in toluene remains. Dilute suspensions are coloured yellow by optical absorption due to the SAP 230 TP and show birefringence upon stirring. As the index of refraction of hydrotalcites is close to that of toluene (≈ 1.50) the dispersion has a very low turbidity. Transmission electron micrographs (Figure 6.8a) were analyzed to determine the dimensions of the particles. The average diameter of the polymer grafted hydrotalcite particles is represented by the histogram in Figure 6.8b. The organophilic system has a larger average diameter and smaller polydispersity ($\langle d \rangle = 167$, $\sigma_d = 0.22$) compared to the original aqueous system, probably due to the size selective character of repetitive centrifugation and decanting. In Figure 6.9 we present an AFM image of the organophilic hydrotalcite platelets. Compared to the aqueous system, presented in Figure 6.3 the spreading of the organophilic particles on mica is rather poor, leading to overlaps. This makes determination of the diameter difficult, while the thickness could be sampled at the free edges of particles. The measurements reveal an average thickness $\langle l \rangle = 19.2$ nm with a relative standard deviation $\sigma_l = 0.22$. Compared to the bare hydrotalcite particles the SAP 230 TP covered hydrotalcite particles are on average 6.5 nm thicker, which is in reasonable agreement with twice the estimated thickness (3-4 nm) of the poly-isobutylene grafting layer [39, 30].

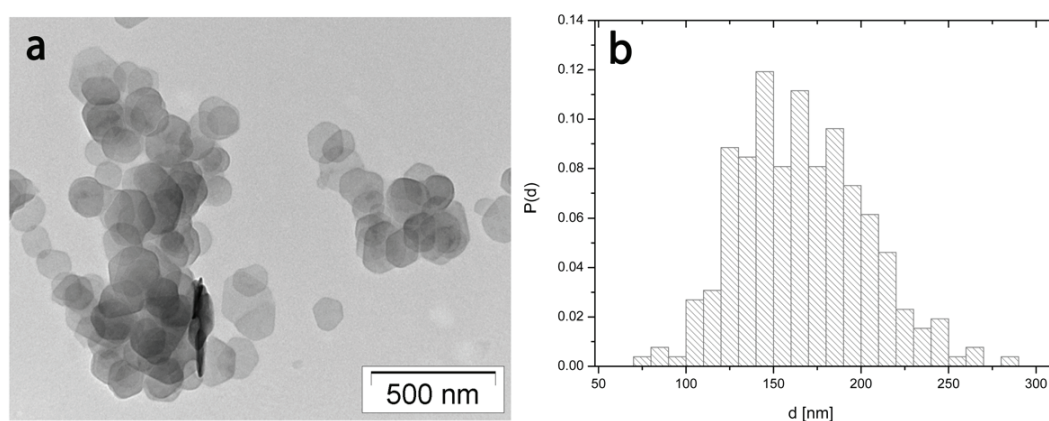


FIGURE 6.8. (a) Transmission electron micrograph of PIB grafted hydrotalcite platelets. The particle diameter was obtained from similar micrographs of the polymer grafted system yielding $\langle d \rangle = 167$ nm and $\sigma = 0.22$ for the mineral core visible by TEM. (b) shows a histogram of the average particle diameter distribution for the polymer grafted system as obtained by measurements on several electron micrographs as described in section 6.2.2.

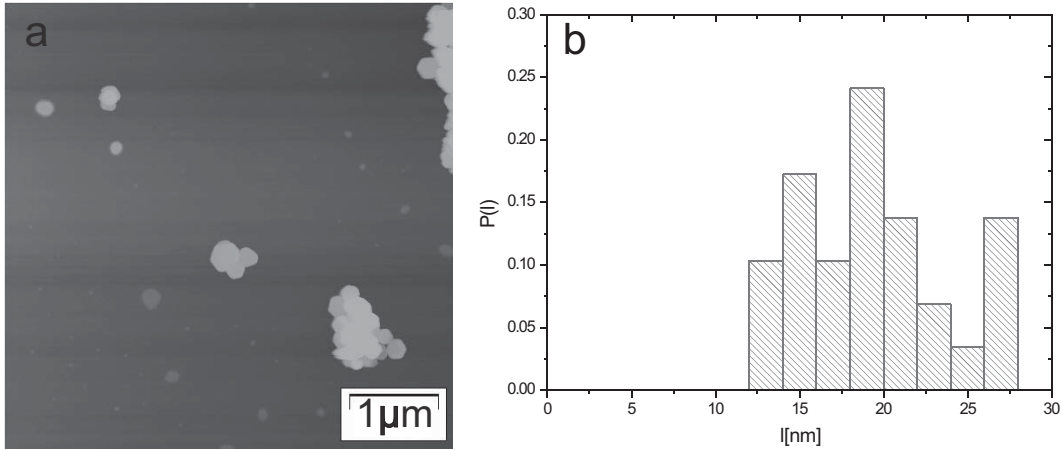


FIGURE 6.9. AFM measurements on polymer grafted hydrocalcite platelets. In (a) an AFM image of the poly-isobutylene stabilized hydrocalcite platelets on a mica support is displayed. In (b) a histogram of the thickness of the grafted platelets, as measured by AFM, is shown ($\langle l \rangle = 19.2\text{nm}$ with $\sigma_l = 0.22$).

6.4.2. Isotropic-nematic phase separation

A series of concentrated non-aqueous dispersions of hydrocalcite was prepared in order to study phase separation of the platelets. Within one day macroscopic phase separation is visible and samples split into a lower birefringent and a upper non-birefringent phase (Figure 6.10a-e). The latter phase shows flow induced birefringence when the cuvet is gently displaced (Figure 6.10f). The interface between the isotropic and nematic phase moves along when the cuvetts are tilted. After 3 days, the relative phase volumes were measured and presented in Figure 6.11.

In order to compare with other systems the experimental value at which dispersions were at high enough concentration to undergo the isotropic-nematic transition can be converted in a so-called dimensionless density ($n \langle d^3 \rangle$, where n represents the number density (N/V) and d the diameter of the platelets). The experimental volume fraction for a polydisperse system, ϕ , can easily be converted to dimensionless number densities. The particles are assumed to have a disk shape with diameter d and thickness l , so the volume fraction can be described as

$$\phi = \frac{\pi}{4} n \langle d^2 l \rangle \quad (6.4)$$

The dimensionless number density can now be written as:

$$n \langle d^3 \rangle = \frac{4}{\pi} \phi \frac{\langle d^3 \rangle}{\langle d^2 l \rangle} \quad (6.5)$$

Starting from this equation, sample calculations based on the obtained AFM data show that the dimensionless number density is rather accurately given by

$$n \langle d^3 \rangle \simeq \frac{4}{\pi} \phi \frac{\langle d \rangle}{\langle l \rangle} \quad (6.6)$$

TABLE 6.3. Comparison of nD^3 for the concentration of the isotropic to nematic transition as found in this study and in literature. The value $n_I < d^3 >$ refers to the lower boundary of the biphasic gap while $n_N < d^3 >$ refers to the higher boundary.

reference	experiment	(d/l)	$n_I < d^3 >$	$n_N < d^3 >$
-	PIB grafted hydrotalcite	9	2.75	4.70
[30]	PIB grafted gibbsite	11	2.5	2.7
[46]	Monte Carlo	∞	4.04	4.12
[47]	Monte Carlo cut spheres	10	3.82	3.87
[48]	Monte Carlo cut spheres	10	4.03	4.17
[42]	Monte Carlo cut spheres	15	3.68	4.11
[48]	Monte Carlo cut spheres	20	3.90	4.17
[49]	Monte Carlo, 25% polydispersity	∞	3.53	4.97

Combining the TEM and AFM measurements we use $\langle d \rangle = 173.5$ nm and $\langle l \rangle = 19.2$ nm. The quoted value for $\langle d \rangle$ is based on the TEM value (167nm) plus the thickness of the stabilizing poly isobutylene layers (6.5nm) inferred from AFM measurements. The volume fraction ϕ is calculated as the solid mass content of the dispersion per volume divided by the particle density (ρ) of the composite hydrotalcite-polymer particle. The composite particle density was estimated at 1.70 kg/dm³ by taking into account a 12.7nm thick disk of mineral hydrotalcite with mass density 2.13 kg/dm³ and a total thickness of 6.5 nm of the poly-isobutylene stabilizing layers with density 0.87 kg/dm³. The threshold concentration at which the biphasic region starts is estimated by extrapolation of the data in Figure 6.11 to be 0.400 kg/dm³ (the origin of the small nematic phase observed after 3 days at an overall concentration of 300 g/dm³ is ascribed to sedimentation) This mass density corresponds to a volume fraction $\phi_I = 0.24$ and hence $n_I < d^3 \rangle = 2.75$. Similarly a value of $\phi_N = 0.41$ and hence $n_N < d^3 \rangle = 4.70$ is found after insertion of the mass concentration at which samples are fully nematic (0.700 kg/dm³). In Table 6.3 this value is compared with experimental and computer simulation data for isotropic-nematic phase separating systems of platelets. Computer simulations for monodisperse systems give a relative width of the biphasic gap of about 10 percent or slightly less, whereas for a 25 percent polydisperse system the width of the biphasic gap is 40 percent. The experimental system studied here gives a width of the biphasic region of 75 percent. This is higher than the theoretical value for infinitely thin platelets and clearly indicates the importance of polydispersity in experimental systems.

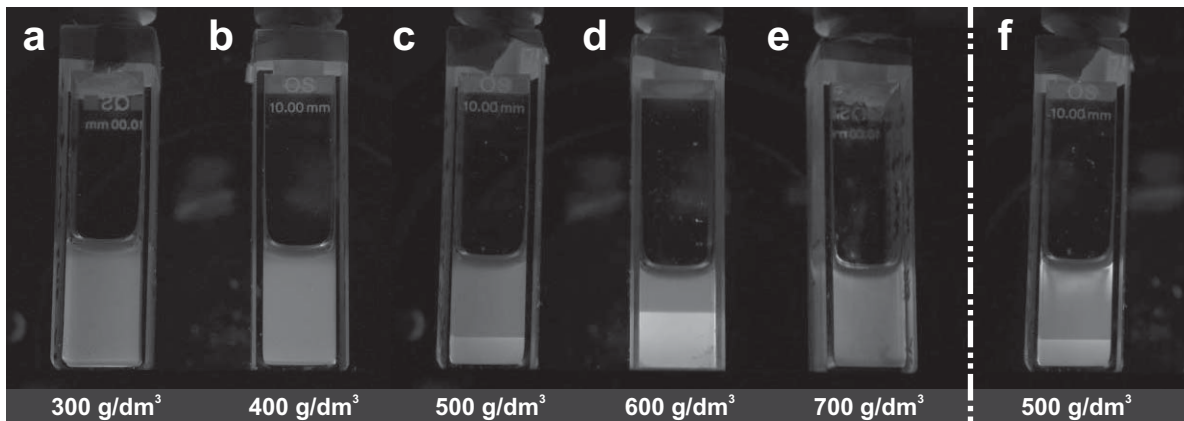


FIGURE 6.10. Isotropic-nematic phase separation of poly-isobutylene stabilized hydrocalcite platelets in toluene as observed between crossed polarizers two days after homogenization. At concentrations of 300 (a) and 400 g/dm^3 (b) mainly isotropic phase is visible. At (c) 500 and (d) 600 g/dm^3 a nematic phase appears clearly at the bottom of the cuvet which extends over the entire cuvet at 700 g/dm^3 (e). The lower phase is permanent birefringent, the upper phase shows birefringence when flow is induced by gently displacing the cuvet over millimeters, which is shown for 500 g/dm^3 in (f).

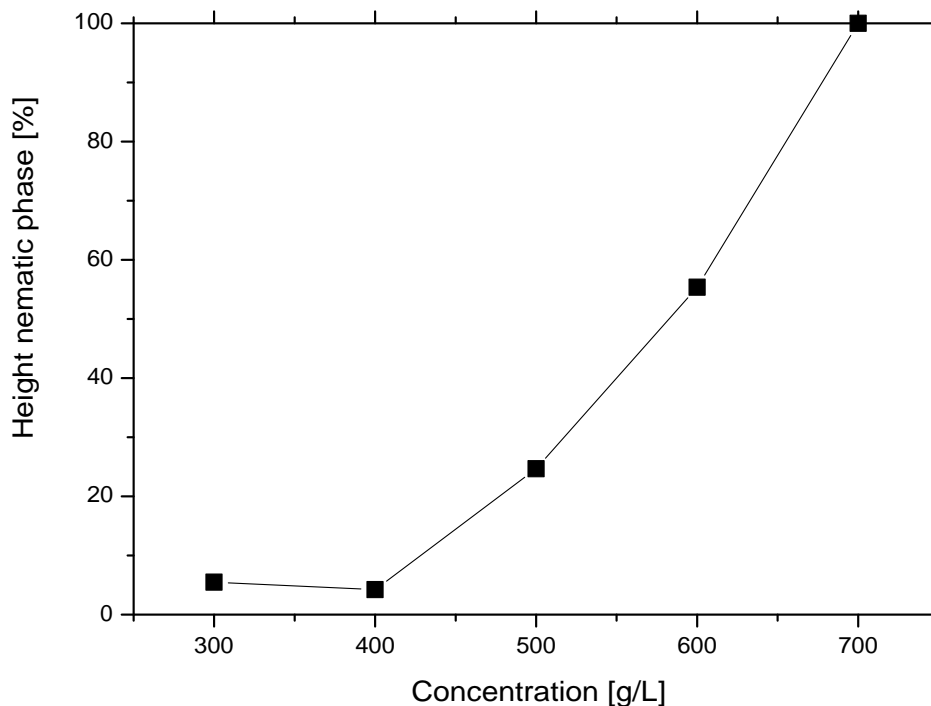


FIGURE 6.11. Phase volume of the nematic as part of the total volume for the samples shown in Figure 6.10. Three days after homogenization the height of the nematic phase as part of the total volume in the capillaries was measured.

6.4.3. Nematic tactoids

Nematic tactoids are observed to nucleate and sediment in the isotropic phase. Typically they have dimensions ranging from 20 to 70 micrometers in diameter and are found to have a rather round shape that is elongated giving rise to tails along the direction of sedimentation. This is exemplified in Figure 6.12 where a microscopy image of the isotropic phase close to the isotropic-nematic interface in a biphasic sample between crossed polarizers is shown. To identify the structure of the nematic tactoids retardation plates were used.

Hydrotalcite is a uniaxial negative material ($n_\epsilon=1.494$, $n_\omega=1.511$, [40] and references included). This means that the slow axes are directed along the surface of the platelets. Since the difference in refractive indices of the solvent toluene ($n=1.496$), and hydrotalcite ($n \simeq 1.5$) is very small, the birefringence of the nematic phase will be determined by the intrinsic birefringence of the mineral platelets themselves [41]. This means that in the nematic phase the slow axes are perpendicular to the director, which is defined as the vector perpendicular to the surface of the platelets. Therefore polarization microscopy pictures taken with a retardation filter in the optical system will display higher interference colors if the director is oriented perpendicular to the slow axis of the retardation filter and the optical axis of the microscope. It should be noted that no contribution to birefringence and therefore no interference color comes from those particles with a director parallel to the microscope axis or parallel to one of the polarizers.

The orientation of the director at different locations within the nematic tactoids may now be determined. From the interference colors with and without a retardation filter we deduce that the platelets align parallel to the interface of the tactoids in agreement with the observations done by van der Beek *et al.* on the orientation of sterically stabilized gibbsite platelets at the macroscopic isotropic-nematic interface [42].

The blue interference color observed with retardation filter on the left and right side of the tactoid corresponds to an optical path difference of 680nm (Michel-Levy color chart). Subtracting the contribution of the retarder means that the optical path difference Γ is 150nm. Since

$$\Gamma = \Delta n s \quad (6.7)$$

we find using a path length (s) of 50 μm a Δn equal to 0.003. Comparing this to the estimated theoretical value,

$$\Delta n = |n_\epsilon - n_\omega| \phi_{core} S_2 \quad (6.8)$$

using for the volume fraction of hydrotalcite cores $\phi_{core} = 0.25$ and for the order parameter $S_2 \simeq 0.8$ we find $\Delta n=0.0033$. This is in good agreement with the value that follows from polarization microscopy and confirms our analysis. In the lower part of the tactoid we observe an orange-yellow interference color of 380nm. This corresponds

to an optical difference of 150nm again, but now in the subtraction mode. Combining the observation described above, a sketch of the particle orientation at the surface of the tactoid can be made (Figure 6.13). The interference color in the core of the tactoid however, is more complex to analyse due to the cumulative character of the interference colors and is therefore not analysed.

Interestingly it seems that the nematic tactoids are reluctant to merge with the nematic phase upon arrival at the interface. In Figure 6.14 the sample at 500 g/dm^3 is presented, 4 months after preparation. On top of the initial interface a new layer of birefringent material is deposited. If we observe this at a microscopical level we find that there is an extended layer of tactoids present on top of the interface.

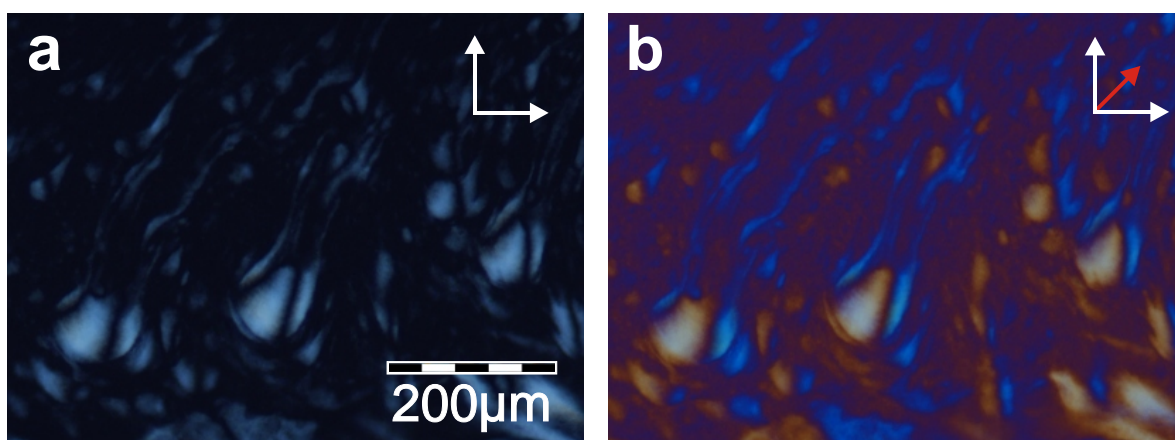


FIGURE 6.12. Polarizing microscopy images of nematic tactoids in the isotropic phase (a) shows the tactoids ranging in size from approximately 20 to $75 \mu\text{m}$ in diameter. In (b) the same tactoids are depicted after insertion of a retardation filter of optical path difference 530 nm (slow axes indicated).

6.4.4. Sedimentation

Samples with overall concentrations of 275 g/dm^3 and 350 g/dm^3 that initially are in the isotropic phase develop nematic phases due to sedimentation. The first signs of this sedimentation induced isotropic-nematic transition are observed already after few days. The nematic phase just below the interface consists of many small nematic domains with a typical size in the order of $10 \mu\text{m}$. In time the nematic domains merge and the interface becomes more smooth and flat. Figure 6.15 shows polarization microscopy images of the sedimentation induced isotropic to nematic transition at 350 g/dm^3 after 4 months when full sedimentation equilibrium appears to have been reached.

When the crossed polarizers are oriented parallel and perpendicular with respect to the interface (Figure 6.15a) no birefringence at the interface is observed, indicating that the director of the platelets at the interface is directed along one of the crossed polarizers. This is confirmed by the appearance of interference colors at the interface

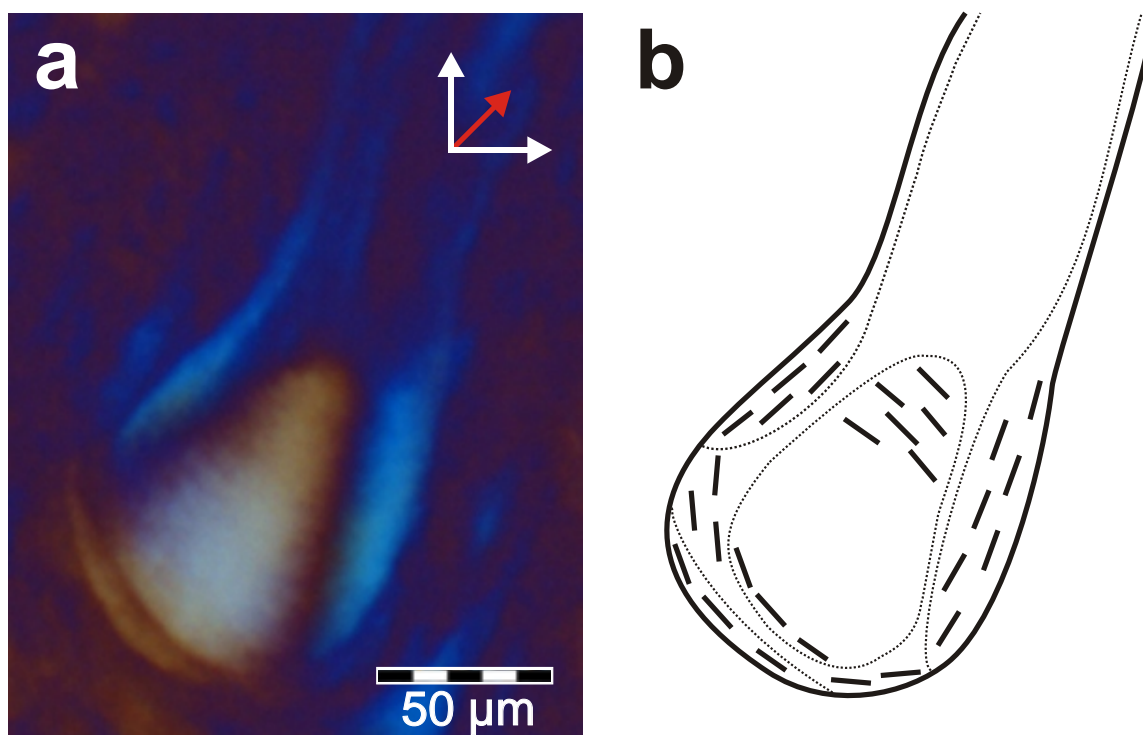


FIGURE 6.13. (a) Close up of one of the tactoids presented in Figure 6.12b. (b) Artist impression of the orientation of the platelets within the intersect of the nematic tactoid represented in panel (a) as deduced from the interference colors in combination with the orientation of the retardation filter.

upon rotation of the polarizers by 45 degrees (Figure 6.15b). Insertion of a 530 nm retardation filter at 45 degrees with respect to the polarizers leads to appearance of higher interference colors blue and green indicating that the slow optical axis is parallel to the interface (Figure 6.15c). This in turn means that the particles are parallel to the interface as was observed for colloidal gibbsite [43, 42].

In the case of the sample at $275\text{g}/\text{dm}^3$ the volume fraction of nematic phase is 0.208, in the case of $350\text{g}/\text{dm}^3$ this fraction is 0.283 in sample cells with a height of 12mm. Assuming the concentration of the nematic phases to be equal to $700\text{g}/\text{dm}^3$ we find for the average concentration in the isotropic phase $163\text{g}/\text{dm}^3$ in the case of an overall concentration of $275\text{g}/\text{dm}^3$ and $212\text{g}/\text{dm}^3$ for an overall concentration of $350\text{g}/\text{dm}^3$. This means that there is a large difference in the overall concentrations of isotropic phases in equilibrium with a sedimentation induced nematic phase. Using the equations of state for osmotic pressure as obtained from Monte Carlo simulations the concentration profiles in the various phases can be calculated.

For a monodisperse colloidal suspension the balance between the osmotic pressure gradient and the gravitational force can be written as:

$$\frac{\partial \Pi}{\partial z} = -nm^*g \quad (6.9)$$

where Π is the osmotic pressure, z is the height of the phase, n is the particle number density (number of particles per volume, N/V), m^* is the buoyancy corrected mass of the colloidal hydroxide particles and g the gravitational force constant. Equation 6.9 can be rewritten in the form

$$\left(\frac{\partial \Pi}{\partial n} \right)_{T, \mu_0} \frac{\partial n}{\partial z} = -nm^*g \quad (6.10)$$

where T refers to the absolute temperature and μ_0 to the chemical potential of the solvent. For the case of sterically stabilised gibbsite the heights of the phases were

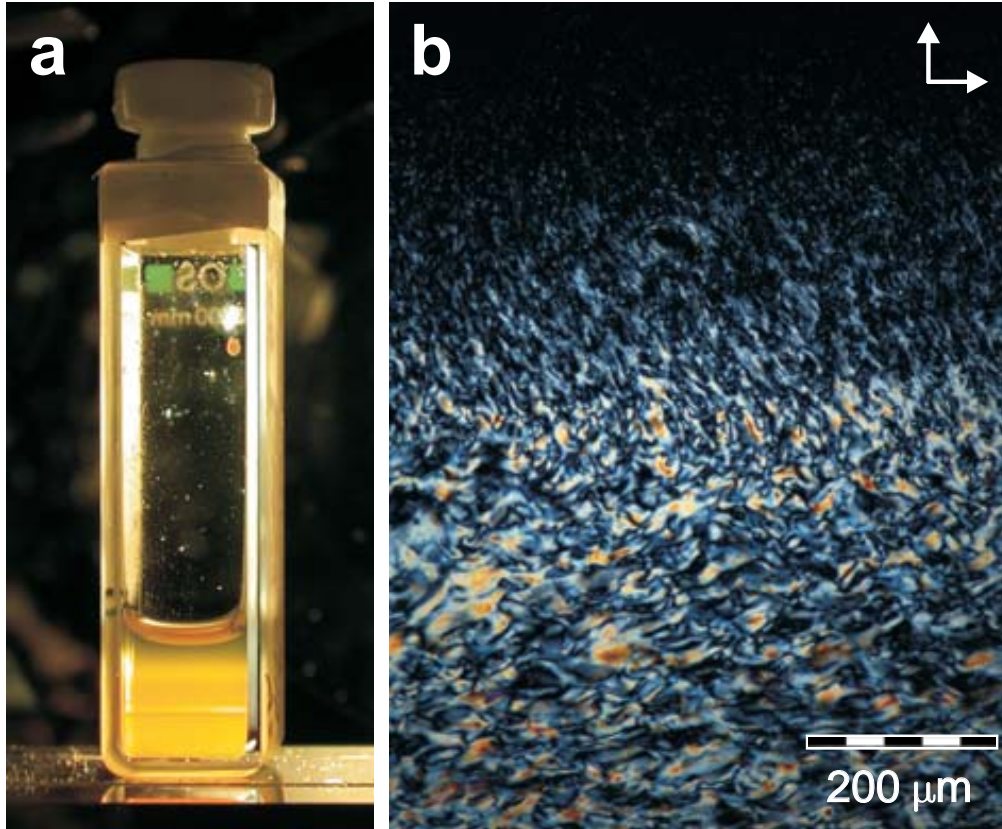


FIGURE 6.14. Macroscopic(a) and microscopic(b) observations of the isotropic-nematic interface at 500 g/dm^3 between crossed polarizers (indicated by the arrows), four months after homogenization. (a) On top of the initial interface a millimeter thick layer of birefringent material is visible. (b) The initially sharp interface is coarsened such that there is no sharp interface between the nematic and the isotropic phase anymore, but a diffuse layer of tactoids instead.

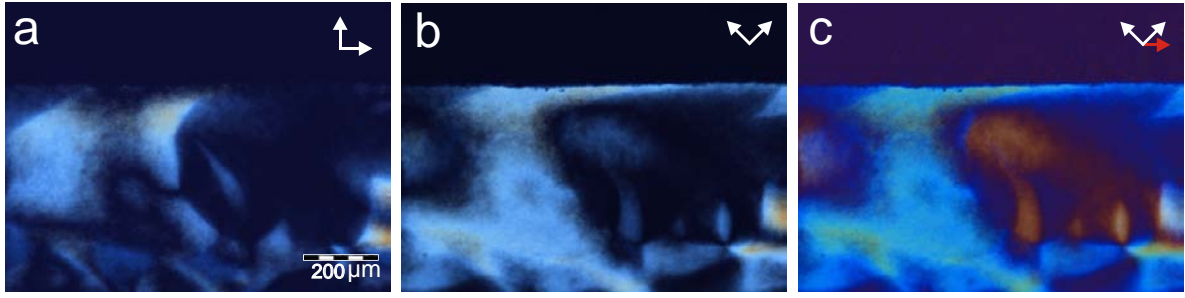


FIGURE 6.15. Polarization microscope images of the sedimentation induced isotropic-nematic interface of polymer grafted hydrotalcite. In (a) the crossed polarizers are oriented parallel and perpendicular with respect to the interface. (b) Rotation of the polarizers by 45 degrees results in a clear visibility of the interface and therefore indicates that the particles have a preferential orientation with respect to the interface. (c) Insertion of a retardation filter at 45 degrees with respect to the polarizers reveals the orientation of the particles at the interface: higher interference colors blue and green are observed which are related to the slow axis of the particles being parallel to the interface.

calculated and reasonable agreement with experiments was obtained [42].

For the present system polydispersity plays a significant role as is exemplified from the width of the biphasic gap. In order to take the effect of polydispersity into account one has to define a balance equation of the different species [44]:

$$\frac{\partial \mu_j}{\partial z} = -m_j^* g \quad j = 1, \dots, c \quad (6.11)$$

which in turn can be written as

$$\sum_{k=1}^c \left(\frac{\partial \mu_j}{\partial n_k} \right)_{T, \mu_o, n_l} \frac{\partial n_k}{\partial z} = -m_j^* g \quad j = 1, \dots, c \quad (6.12)$$

Although for binary mixtures of hard spheres good expressions for the thermodynamic derivatives

$$\left(\frac{\partial \mu_j}{\partial n_k} \right)_{T, \mu_o, n_l}$$

exist and therefore concentration profiles could be calculated [45], the required thermodynamic derivatives for platelets are not known and similar calculation could not be performed.

6.5. CONCLUSIONS

In this work, double layered hydroxides were synthesized from magnesium and aluminum nitrates controlling the size of the platelets to tailor them to platelet sizes applicable for lyotropic liquid crystal formation by adjustment of the reactants and

the temperature of hydrothermal treatment. The aqueous colloidal suspensions are highly stable and on prolonged standing (10 months) interesting sedimentation profiles are formed, but no liquid crystal transitions were observed. Liu *et al.* [16] report on similar sedimentation profiles in which nematic phases are formed after several weeks as evidenced by clear birefringence and tactoid formation. It should be noted that the concentrations of the suspensions that formed nematic phases were very close to the sol-gel transition [36]. Apparently in our system, like in most natural and synthetic aqueous clay systems, the sol-gel transition occurs before the isotropic-nematic phase separation [37, 38]. Using a novel approach involving freeze-drying, amino-functionalized polyisobutylene was grafted on the inorganic platelets. This stabilizer proved its use in other liquid crystal forming systems [9, 18, 19]. The organophilic disks prepared here also showed isotropic-nematic phase transitions at very short time scales. This transition occurs at a concentration similar to comparable systems found in literature, although the biphasic gap is wider than observed so far. Moreover, nematic tactoids are observed in polarization microscopy. Nematic phases were induced by gravity in initially isotropic samples yielding sharp isotropic-nematic interfaces. As has been argued in [19] the grafting with PIB leads to (nearly) hard particle interactions, which makes the suspension less susceptible to gelation allowing for the isotropic-nematic phase transition to be observed.

6.6. ACKNOWLEDGEMENTS

Edwin Devid, Matti van Schooneveld, Chantal Vonk, Marjan Versluijs-Helder and Annemieke ten Brinke are acknowledged for their contributions. Hans Meeldijk, Chris Schneijdenberg and John Geus are acknowledged for discussions.

Bibliography

- [1] A. S. Sonin, *J. Mater. Chem.* 1998, *8*, 2557
- [2] P. Davidson and J.-C. P. Gabriel, *Curr. Opin. Colloid Interface Sci.* 2005, *9*, 377
- [3] H. Zocher, *Z. Anorg. Allg. Chem.* 1925, *147*, 91
- [4] K. Coper and H. Freundlich, *Trans. Faraday Soc* 1937, *33*, 348
- [5] I. Langmuir, *J. Chem. Phys.* 1938, *6*, 873
- [6] I. Bihannic, L. J. Michot, B. S. Lartriges, D. Vantelon, J. Labille, F. Thomas, J. Susini, M. Salomé and B. Fayard, *Langmuir* 2001, *17*, 4144
- [7] L. Onsager, *Ann. N. Y. Acad. Sci.* 1949, *51*, 627
- [8] J. Bugosh, *J. Phys. Chem.* 1961, *65*, 1789
- [9] P. A. Buining, A. P. Philipse and H. N. W. Lekkerkerker, *Langmuir* 1994, *10*, 2106
- [10] K. Kajiwara, N. Donkai, Y. Hiragi and H. Inagaki, *Makromol. Chem.* 1986, *187*, 2883
- [11] Y. Maeda and S. Hachisu, *Colloids Surf.* 1983, *6*, 1

- [12] H. Maeda and Y. Maeda, *Phys. Rev. Lett.* 2003, *90*, 018303
- [13] B. J. Lemaire, P. Davidson, D. Petermann, P. Panine, I. Dozov, D. Stoenescu and J. P. Jolivet, *EPJ E* 2004, *13*, 309
- [14] B. J. Lemaire, P. Davidson, J. Ferré, J. P. Jamet, P. Panine, I. Dozov and J. P. Jolivet, *Phys. Rev. Lett.* 2002, *88*, 125507
- [15] D. van der Beek and H. N. W. Lekkerkerker, *Europhys. Lett.* 2003, *61*, 702
- [16] S. Liu, J. Zhang, N. Wang, W. Liu, C. Zhang and D. Sun, *Chem. Mater.* 2003, *15*, 3240
- [17] L. J. Michot, I. Bihannic, S. Maddi, S. S. Funari, C. Baravian, P. Levitz and P. Davidson, *PNAS* 2006, *103*, 16101
- [18] F. M. van der Kooij, K. Kassapidou and H. N. W. Lekkerkerker, *Nature* 2000, *406*, 868
- [19] Z. X. Zhang and J. S. van Duijneveldt, *J. Chem. Phys.* 2006, *124*, 154910
- [20] A. Vaccari, *Catal. Today* 1998, *41*, 53
- [21] L. Hickey, J. T. Klopogge and R. L. Frost, *J. Mater. Sci.* 2000, *35*, 4347
- [22] G. Lagaly, O. Mecking and D. Penner, *Colloid Polym. Sci.* 2001, *279*, 1090
- [23] N. Wang, S. Liu, J. Zhang, Z. Wu, J. Chen and D. Sun, *Soft Matter* 2005, *1*, 428
- [24] W. Zhu, D. Sun, S. Liu, N. Wang, J. Zhang and L. Luan, *Colloids Surf.* 2007, *301*, 106
- [25] J. E. G. J. Wijnhoven, D. D. van 't Zand, D. vanderBeek and H. N. W. Lekkerkerker, *Langmuir* 2005, *21*, 10422
- [26] M. C. D. Mourad, J. E. G. J. Wijnhoven, D. D. Van 'T Zand, D. Van der Beek and H. N. W. Lekkerkerker, *Philos. Trans. R. Soc. London, A* 2006, *364*, 2807
- [27] J. A. C. Veerman and D. Frenkel, *Phys. Rev. A* 1990, *41*, 3237
- [28] A. B. D. Brown, S. M. Clarke and A. R. Rennie, *Langmuir* 1998, *14*, 3129
- [29] P. A. Buining and H. N. W. Lekkerkerker, *J. Phys. Chem.* 1993, *97*, 11510
- [30] F. M. van der Kooij and H. N. W. Lekkerkerker, *J. Phys. Chem. B* 1998, *102*, 7829
- [31] L. Heux, G. Chauve and C. Bonini, *Langmuir* 2000, *16*, 8210
- [32] X. Fu and S. Qutubuddin, *Polymer* 2001, *42*, 807
- [33] E. J. W. Verwey and J. T. G. Overbeek, *Theory of the Stability of Lyophobic Colloids*, 1948
- [34] J. O. Fossum, *Physica A (Amsterdam)* 1999, *270*, 270
- [35] J. O. Fossum, E. Gudding, D. d. M. Fonseca, Y. Meheust, E. DiMasi, T. Gog and C. Venkataraman, *Energy* 2005, *30*, 873
- [36] J. Zhang, L. Y. Luan, W. X. Zhu, S. Y. Liu and D. J. Sun, *Langmuir* 2007, *23*, 5331
- [37] A. Mourchid, A. Delville, J. Lambard, E. Lécolier and P. Levitz, *Langmuir* 1995, *11*, 1942
- [38] J. C. P. Gabriel, C. Sanchez and P. Davidson, *J. Phys. Chem.* 1996, *100*, 11139
- [39] M. P. B. van Bruggen, F. M. van der Kooij and H. N. W. Lekkerkerker, *J. Phys.: Condens. Matter* 1996, *8*, 9451
- [40] C. Frondel, *Am Miner* 1941, *26*, 295
- [41] W. L. Bragg and A. B. Pippard, *Acta Crystallographica* 1953, *6*, 865
- [42] D. van der Beek, T. Schilling and H. N. W. Lekkerkerker, *J. Chem. Phys.* 2004, *121*, 5423
- [43] D. van der Beek and H. N. W. Lekkerkerker, *Langmuir* 2004, *20*, 8582
- [44] A. Vrij, *J. Chem. Phys.* 1980, *72*, 3735
- [45] T. Biben, J. P. Hansen and J. L. Barrat, *J. Chem. Phys.* 1993, *98*, 7330
- [46] R. Eppenga and D. Frenkel, *Mol. Phys.* 1984, *52*, 1303
- [47] J. A. C. Veerman and D. Frenkel, *Phys. Rev. A* 1992, *45*, 5632
- [48] S.-D. Zhang, P. A. Reynolds and J. S. van Duijneveldt, *J. Chem. Phys.* 2002, *117*, 9947
- [49] M. A. Bates, *J. Chem. Phys.* 1999, *111*, 1732

7

Isotropic-to-Nematic Phase Transition of Sterically Stabilized Hectorite Platelets and Hectorite-Polymer Nanocomposites

ABSTRACT

Natural hectorite clay particles were sterically stabilized by amino-modified polyisobutylene polymer chains and formed stable colloidal suspensions when dispersed in apolar solvents. In toluene, the polymer-grafted lath-like hectorite particles display tactoid formation and isotropic-to-nematic liquid crystal phase separation. The particles were transferred to divinylbenzene monomer solution. Polymer-hectorite nanocomposites were made by *in situ* polymerization of this dispersing phase. These nanocomposites could be sectioned and imaged in focused ion beam/scanning electron microscopy. Samples from the specimen were prepared and transferred to a transmission electron microscope. In this way single- and multi-layered hectorite particles could be resolved in high resolution electron micrographs.

7.1. INTRODUCTION

The grafting of surfaces of inorganic colloidal particles by amino-modified poly-isobutylene polymer chains (PIB) has proven a successful method to stabilize such particles in apolar solvents, such as toluene [1]. The resulting organophilic colloids behave to a large extent as hard-interacting particles. The grafting of colloids with PIB has allowed studying the liquid crystal phase behavior of hard-interacting systems of anisometric particles in organic suspension, such as boehmite [2], gibbsite [3], sepiolite [4], goethite [5] and hydrotalcite [6].

Interestingly, the formation of nematic phases in (ungrafted) aqueous suspensions of these particles is not without complications. While at sufficient particle concentration liquid crystal phases are formed in aqueous suspensions of boehmite [7], gibbsite (see [8, 9], Chapter 2) and hydrotalcite [10, 11] this only happens in a limited range of particle and salt concentrations. Outside of this liquid crystal phase region (birefringent) gels, in which the macroscopic phase separation processes are hampered, are formed. For aqueous suspensions of sepiolite no liquid crystal phase formation has been reported. Gelation is ubiquitous in suspensions of clay particles [12, 13, 14]. This may be a reason that only few reports on liquid crystal phase separation in suspensions of charged clay particles have appeared so far, for hectorite [15] and nontronite [16, 17]. Although Langmuir [15] reported on isotropic-nematic phase coexistence in aqueous suspensions of natural hectorite (which he himself called *California bentonite*), a lath-like smectite clay [18, 19], this observation appeared difficult to reproduce, even by Langmuir himself.

We will demonstrate the applicability of the PIB-grafting method via freeze-drying, introduced in Chapter 4, and the dispersion of the resulting particles in toluene to circumvent gelation in suspensions of hectorite clay. Isotropic-nematic phase separation and nematic tactoid formation of these suspensions are studied.

As has been shown for gibbsite particles (see Chapter 5), PIB-grafting enables the dispersion of inorganic particles in DVB monomers. These suspensions of particles in monomers can be polymerized in order to obtain solid nanocomposites. Besides the potential of platelet reinforced polymer materials themselves [20], there are two more advantages to these materials. In the first place real space images of the structures formed by the particles in the bulk of the inorganic dispersions can be studied conveniently using a dual beam focused ion beam-scanning electron microscopy (FIB-SEM) to trim and image the materials. Furthermore, samples can be removed from the specimens and prepared for transmission electron microscopy (TEM) analysis. In the case of hectorite laths this enables study of the intraparticle structure of single hectorite particles.

7.2. EXPERIMENTAL

Hectorite, SHCa-1, was supplied by the Clay Minerals Society, Source Clays Repository and was purified before use and dispersed in water as described in [19]. This treatment of the hectorite consisted of dispersion and prehydration in demineralized water for 48 hours. The largest particles were removed from the sample by three cycles of centrifugation for 20 minutes at 400 g. After each centrifugation step the supernatant was collected, while the pellet was redispersed in demineralized water and centrifuged again. The collected supernatant was dialyzed against demineralized water for 14 days. Transmission electron micrographs of the hectorite particles were taken on a Tecnai 12 (FEI, the Netherlands). The clay laths are shown to be well dispersed. The sizes and polydispersity of these particles were measured by ten Brinke *et al.* to be average 288 nm in length (polydispersity 47%), 43 nm in width (polydispersity 24%) on basis of electron micrographs, in agreement with Bosbach *et al.* [18]. The average thickness of the particles was estimated to be 6 nm.

The hectorite particles were sterically stabilized by polymer grafting with amino modified polyisobutylene (SAP 230TP, Infineum, U.K.). The grafting method described in chapter 4 is used to graft these onto the hectorite. After freeze-drying, polymer grafted hectorite particles were redispersed in toluene. Finally, the dispersions were washed in three cycles by centrifugation (2 h, 900g) and redispersion and toluene (for phase separation samples) and monomer solution (for nanocomposite samples). The monomer solution was composed of 99% 4 Divinylbenzene (DVB, Merck) and 1% UV curable photoinitiator (2,4,6-trimethylbenzoyl, Irgacure 819), obtained from CIBA Holding AG, Switzerland. Finally, transmission electron micrographs were taken from dried suspensions of the polymer grafted platelets in order to inspect them for aggregates. Translucent, light brown suspensions of PIB-hectorite in toluene were obtained. The index of refraction of hectorite (1.49-1.52) is close to that of toluene (1.49), leading to relatively clear suspensions.

Samples in the concentration range that phase separation occurs were transferred into optical cells (10×10×40 mm, Hellma). These were observed illuminated by white light and between crossed polarizers during the first days after preparation. Some of these phase separating samples and some of the nanocomposite samples were transferred to homemade glass cell of inner dimensions 10×10 mm and approximately 145μm. These cells were glued together (Araldit AW2102/HW2951, Huntsman Advanced Materials, Belgium). Nanocomposites were obtained by illumination of these sample cells for 2 hours by UV light. Polymerized samples could be extracted from the sample cells.

A Nikon polarization microscope (Eclipse LV100pol) equipped with a digital camera (QImaging, MP5) was used to inspect the phase separation and polymerization processes. A retardation filter (optical path difference 530 nm) was inserted at an angle of

45 degrees with respect to the polarizer and analyzer in order to determine the optical birefringence quantitatively.

The nanocomposite samples were analyzed in a dual-beam Focused ion beam-scanning electron microscope (FEI, Nova Nanolab 600, the Netherlands). All scanning electron images were based on the detection of secondary scattered electrons on freshly cut surfaces in the bulk of the samples. The focused Gallium ion beam is used to create nanometer smooth sectioning of the composite at specific sites and under designated orientation. Ion milling of the samples by the focused ion beam was employed to cut out thin sections (approximate size $10 \times 10 \times 0.1 \mu\text{m}$) from the specimen that are suitable to be transferred and observed in a transmission electron microscope. In order to achieve this the sections are first connected to the tip of a sample needle by platinum welds. These were deposited *in situ* by decomposition of organo-platinum gas under irradiation of the focused ion beam. Then the needle was transferred to the vicinity of a copper grid, where it was attached again with platinum welds and released from the needle by ion milling. Finally the lamella is trimmed to the right thickness by ion milling. After this procedure, the grid can be removed from the sample stage of the microscope and transported conveniently to the transmission electron microscope (see [21] for a review on this procedure).

7.3. RESULTS AND DISCUSSION

7.3.1. Phase separation.

Concentrating the dispersion to approximately 11.2 % wt led to a biphasic sample within one day after preparation. There is a large difference between the translucency of the lower and upper phase of this sample. The lower phase was moderately birefringent, in particular the region close to the interface (Figure 7.1A). Flow-induced birefringence was observed in the upper phase of the sample when the cell was gently moved (Figure 7.1B). Increase of the overall particle concentration (to 14.0 % wt) led to an increase of the amount of lower phase, as is expected for isotropic-nematic phase separation. It is evident that we have reached particle concentrations within these samples that would have been prone to form gels that impede the liquid crystal phase separation process, in aqueous solutions.

The structure of the phase separating samples are further inspected by polarizing microscopy. Within hours after homogenization birefringent areas that are reminiscent of nematic tactoids of 6-13 μm are visible in the samples. They appear to have spherical or hemispherical shape and have internal ordering as evidenced by their birefringence. (Figure 7.2). From these micrographs it is clear that the tactoids have director patterns with radial organization as complementary interference colors are aligned parallel and perpendicular to the slow axis of the retardation filter. Therefore, we conclude that the internal ordering is dominated by the anchoring of the particles at the droplet interface.

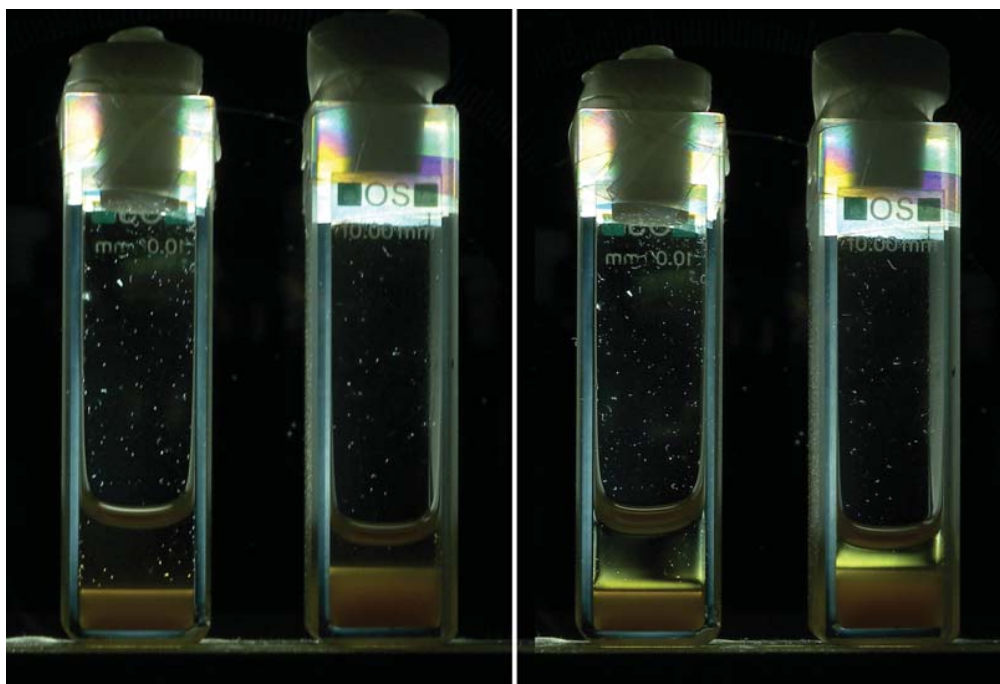


FIGURE 7.1. Phase separated samples of sterically stabilized hectorite particles in toluene as observed in between crossed polarizers, 1 day after preparation. Panel a displays two tubes at different overall concentration with sharp interface in the dispersion. Gentle movement of the tubes induces flow birefringence in the isotropic upper phases (Panel b).

Furthermore, fast moving, birefringent spots (size $< 2 \mu\text{m}$) are visible in the suspension. One day after homogenization the samples were inspected again in the polarizing microscope. Now, an interface has formed. In the upper phase round, birefringent droplets (size $1\text{-}5 \mu\text{m}$) are visible in a completely dark, isotropic background (Figure 7.3A). The lower face appears to be composed of round birefringent droplets (size $3\text{-}9 \mu\text{m}$) although inspection with a larger magnification reveals that these are contained in a weaker birefringent background (Figure 7.3B). In this larger magnification also birefringent patterns of stripes of approximate size $1 \times 11 \mu\text{m}$ are visible.

7.3.2. Polymer dispersion

Dispersions of PIB-grafted hectorite in monomer solution were polymerized by illumination with UV-light. Figure 7.4 shows a polymerized sample that was removed from the sample cell. It has a pale color and turbid appearance, although it is still translucent. This sample was inspected with the scanning electron beam of a FIB-SEM, after sectioning with the focused ion beam. In Figure 7.5, a SEM image of the material is displayed. Bent piles and lamellar stacks of mineral material are visible as well as free mineral laths against a dark background of polymer. However, the mineral appears to be well dispersed throughout the polymer. A TEM lamella from the specimen was

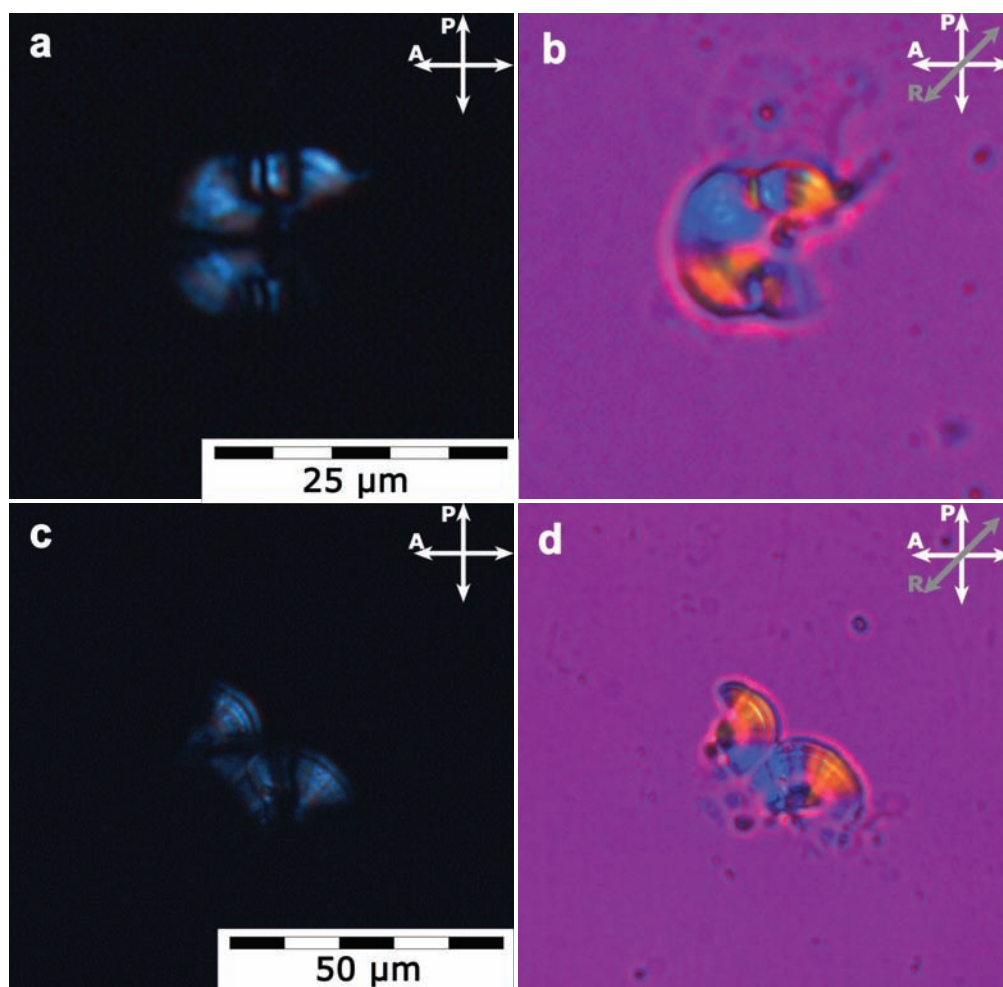


FIGURE 7.2. Nematic droplets are observed in the isotropic upper phase in polarizing light microscopy (Panel a, c). Insertion of a retardation filter (Panel b, d) displays the radial nature of the lath alignment within the tactoids.

prepared by ion milling and was transferred to a copper grid, similarly as described in Chapter 5. Figure 7.6 shows transmission electron micrographs of the hectorite-polymer nanocomposite. These confirm that the hectorite is present both as freely dispersed single-layer particles (of thickness 0.8 - 0.9 nm) as well as small pillars of clay layers and aggregates of many particles. The spacing between the layers in such pillars and aggregates was measured from these micrographs and is equal approximately 0.4 - 0.5 nm. These are the swollen clay pillars as they occur in aqueous solution and that these layers were not covered by the PIB grafting layer, unlike the solitarily dispersed layers, as the polymer brushes would not fit in between the layers. The dimensions of both the single layers as well as the pillars are in agreement with those described in literature, based on atomic force microscope measurements [18] and transmission electron microscopy [19]. We therefore conclude that PIB-grafting can be used to make the hectorite sample organophilic. Furthermore the resulting nanocomposite contains

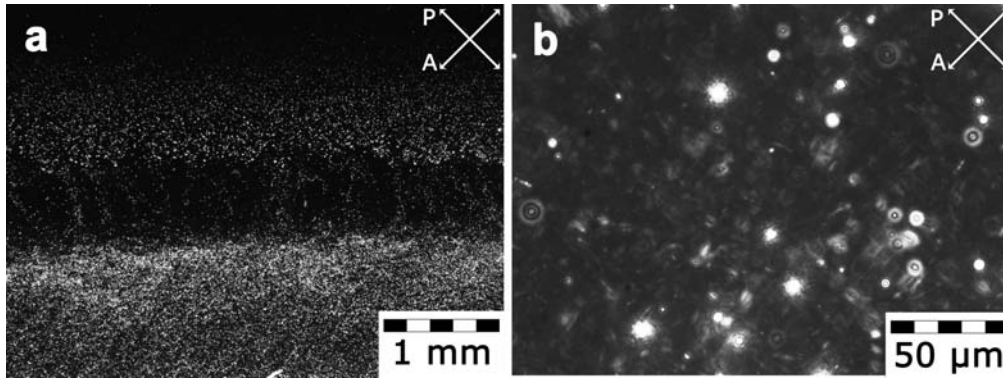


FIGURE 7.3. Isotropic-to-nematic interface in a suspension of sterically stabilized hectorite in toluene (Panel a). Above the coarse interface nematic tactoids are visible in an isotropic background. The lower phase (Panel b) comprises both strongly birefringent spots as well as weak birefringent patterns.

well dispersed hectorite particles. The preparation of nanocomposites in polymer in combination with FIB-SEM sectioning of a TEM lamella enables analysis of the inner structure of pillared clay particles and reveals their pillared structure.

7.4. CONCLUSIONS

Natural hectorite clay particles were sterically stabilized by amino-modified polyisobutylene polymer chains and dispersed in apolar solvents. The polymer-grafted lath-like colloidal particles display nematic tactoid formation and isotropic-nematic liquid crystal phase separation in toluene. The tactoids have radial internal order. The particles were successfully transferred to divinylbenzene monomer solution. Polymer-hectorite nanocomposites were made by *in situ* polymerization of the dispersing phase. These nanocomposites could be sectioned and imaged in a dual beam focused ion beam-scanning electron microscope. From these images it is clear that the particles are well dispersed in the polymer phase and occur both as layered and single sheets. Samples from the specimen were prepared and transferred to a transmission electron microscope (TEM). In this way single- and multi-layered hectorite particles could be resolved in high resolution micrographs.

7.5. ACKNOWLEDGEMENTS

Matthijs de Winter, Arie Verkleij, Kanvaly Sanogo Lacina and Annemieke ten Brinke are acknowledged for their contributions. Laurent Heux, Hans Meeldijk, John Geus and Jeroen van Duijneveldt are acknowledged for discussions.

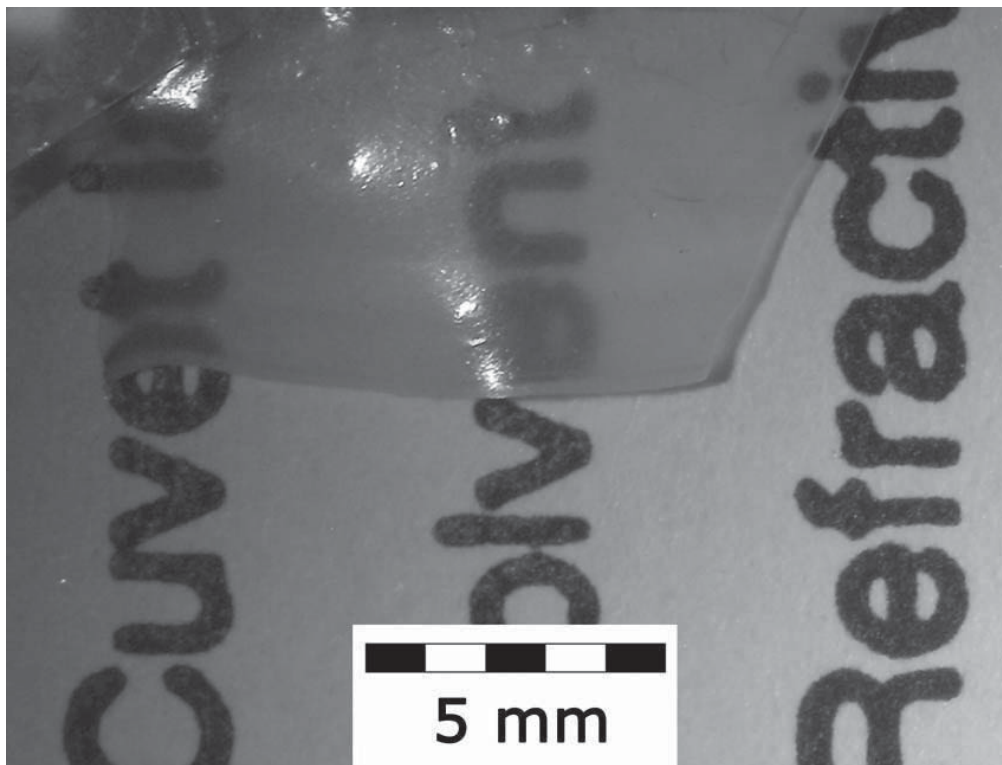


FIGURE 7.4. Sample of a hectorite-polymer nanocomposite. The translucency of the composite is demonstrated by the text behind the sample.

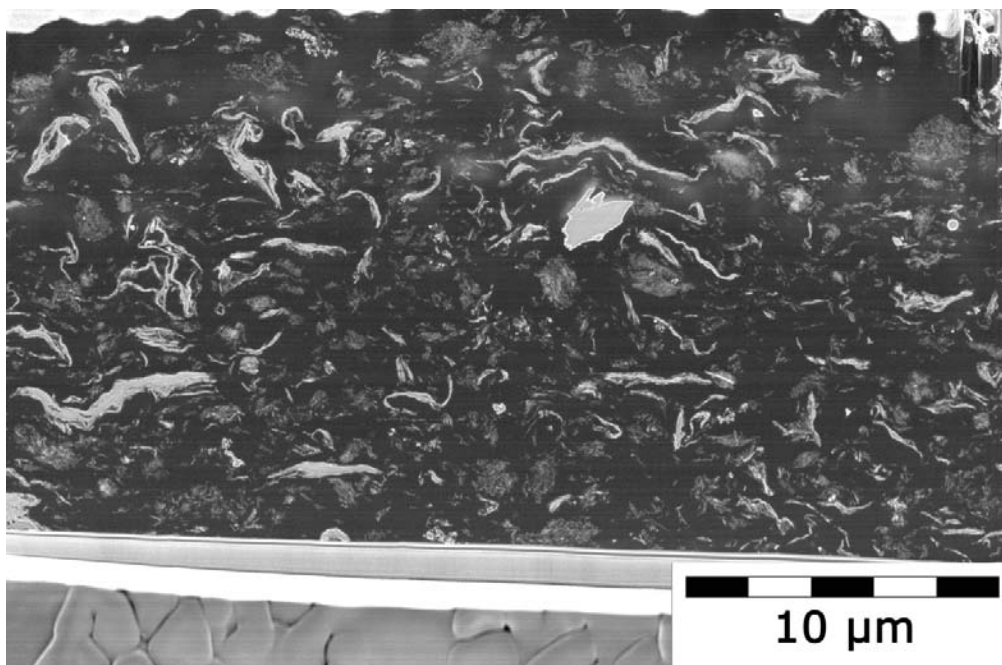


FIGURE 7.5. SEM image of a hectorite-polymer nanocomposite intersect obtained by dual beam FIB-SEM.

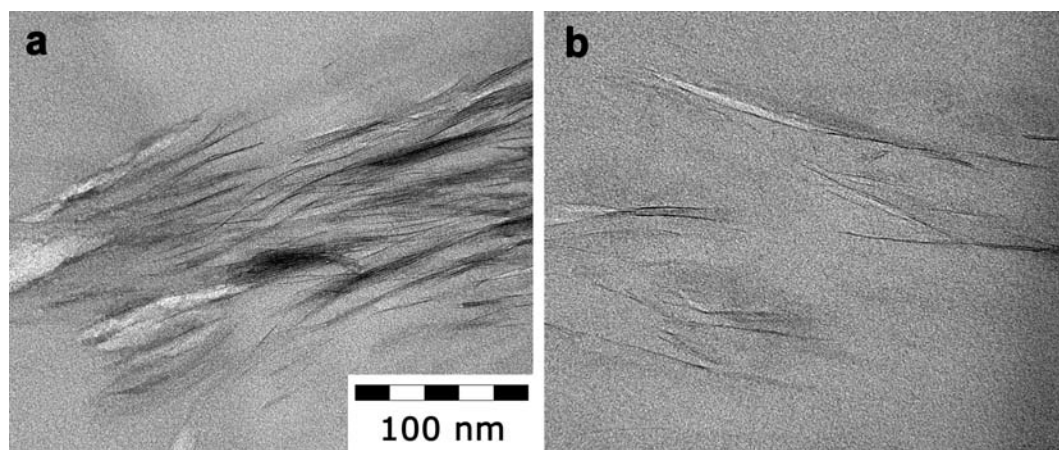


FIGURE 7.6. Transmission electron micrographs of a TEM-lamella of the hectorite-polymer nanocomposite prepared by FIB-SEM. Panel a displays in detail a region with layered sterically stabilized hectorite particles. Panel b displays a region in the sample where single layered sterically stabilized hectorite laths are present.

Bibliography

- [1] C. Pathmamanoharan, *Colloids and Surfaces*, 1988, **34**(1), 81.
- [2] P. A. Buining and H. N. W. Lekkerkerker, *J. Phys. Chem.*, 1993, **97**(44), 11510–11516.
- [3] F. M. van der Kooij and H. N. W. Lekkerkerker, *Journal of Physical Chemistry B*, 1998, **102**(40), 7829–7832.
- [4] Z. X. Zhang and J. S. van Duijneveldt, *Journal of Chemical Physics*, 2006, **124**(15), 154910.
- [5] D. M. E. Thies-Weesie, J. P. de Hoog, M. H. Hernandez Mendiola, A. V. Petukhov, and G. J. Vroege, *Chemistry of Materials*, 2007, **19**(23), 5538–5546.
- [6] M. C. D. Mourad, E. J. Devid, M. M. van Schooneveld, C. Vonk, and H. N. W. Lekkerkerker, *J. Phys. Chem. B*, 2008, **112**(33), 10142–10152.
- [7] P. A. Buining, A. P. Philipse, and H. N. Lekkerkerker, *Langmuir*, 1994, **10**(7), 2106–2114.
- [8] M. C. D. Mourad, J. E. G. J. Wijnhoven, D. D. Van 't Zand, D. Van der Beek, and H. N. W. Lekkerkerker, *Philosophical Transactions of the Royal Society a-Mathematical Physical and Engineering Sciences*, 2006, **364**(1847), 2807–2816.
- [9] M. C. D. Mourad, D. V. Byelov, A. V. Petukhov, and H. N. W. Lekkerkerker, *Journal of Physics: Condensed Matter*, 2008, **20**(49), 494201.
- [10] S. Liu, J. Zhang, N. Wang, W. Liu, C. Zhang, and D. Sun, *Chemistry of Materials*, 2003, **15**, 3240–3241.
- [11] J. Zhang, L. Y. Luan, W. X. Zhu, S. Y. Liu, and D. J. Sun, *Langmuir*, 2007, **23**(10), 5331–5337.
- [12] I. Callaghan and R. Ottewill, *Faraday Discuss.*, 1974, **57**, 110118.
- [13] A. Mourchid, A. Delville, J. Lambard, E. Lécolier, and P. Levitz, *Langmuir*, 1995, **11**, 1942–1950.
- [14] J. C. P. Gabriel, C. Sanchez, and P. Davidson, *J. Phys. Chem.*, 1996, **100**(26), 11139–11143.
- [15] I. Langmuir, *Journal of Chemical Physics*, 1938, **6**, 873–896.
- [16] L. J. Michot, I. Bihannic, S. Maddi, S. S. Funari, C. Baravian, P. Levitz, and P. Davidson, *PNAS*, 2006, **103**(44), 16101–16104.

- [17] L. J. Michot, C. Baravian, I. Bihannic, S. Maddi, C. Moyne, J. e. F. L. Duval, P. Levitz, and P. Davidson, *Langmuir*, 2009, **25**(1), 127–139.
- [18] D. Bosbach, L. Charlet, B. Bickmore, and J. Hochella, Michael F., *American Mineralogist*, 2000, **85**(9), 1209–1216.
- [19] A. J. W. ten Brinke, L. Bailey, H. N. W. Lekkerkerker, and G. C. Maitland, *Soft Matter*, 2007, **3**(9), 1145–1162.
- [20] F. Hussain, M. Hojjati, M. Okamoto, and R. E. Gorga, *Journal of Composite Materials*, 2006, **40**(17), 1511–1575.
- [21] M. L. Richard, *Microscopy Research and Technique*, 2006, **69**(7), 538–549.

Summary

This thesis explores the gelation and liquid crystal phase behavior of colloidal dispersions of platelike particles as well as the use of such dispersions for the generation of nanocomposites.

Part I of this thesis is devoted to the phase behavior of charged colloidal gibbsite (γ -Al(OH)₃).

In **Chapter 2** we report on the sol-gel, sol-glass and liquid crystal phase transitions of positively charged colloidal gibbsite platelets in water over a wide range of particle concentrations (50 g/L - 600 g/L) and salt concentrations (10^{-4} M - 10^{-1} M NaCl). The presence of kinetically-arrested states (both at high and at low salt concentrations) enclosing a sol region is demonstrated. In the sol region -by lowering the salt concentration and/or increasing the gibbsite concentration- the nematic phase gradually transforms from a discotic nematic into a columnar nematic, which has much stronger side-to-side interparticle correlations. Subsequently, the columnar nematic can either be transformed into a hexagonal columnar phase or arrested into a glassy state with columnar nematic structure. The gel found at high salt concentrations shows signatures of a spongelike structure.

In **Chapter 3** we report on the use of charged silica coated gibbsite particles as precursors for ordered silica structures. We demonstrate that the hexagonal columnar liquid crystal phase of these platelets can easily be formed by centrifugation. *In situ* growth of silica from alkoxides can stabilize and fixate the structures, such that the solvent can be removed. In this way, synthetic opals of gibbsite with hexagonal columnar ordering in silica were produced.

Part II of this thesis is devoted to systems of sterically stabilized gibbsite platelets. We introduce a new route to graft particles with polyisobutylene stabilizers in order to make them organophilic.

In **Chapter 4** we show that platelets with an average diameter of 574 nm do form strongly iridescent hexagonal columnar phases in tetralin within hours, while particles of the same size in water do not crystallize at all. Investigation of these hexagonal columnar crystals revealed significant column undulations and bending of the particle

director.

In **Chapter 5** we describe the formation of ordered nanostructures of colloidal gibbsite platelets in bulk polymer. In order to achieve this nematic liquid crystal phases of these platelets were prepared in divinylbenzene (monomer) solution. The solvent was then polymerized to obtain polymer-gibbsite nanocomposites with nematic order. The influence of the average particle size on the degree of orientational ordering in the nanocomposite is discussed.

Systems of other platelike model colloids are discussed in **Part III** of this thesis.

In **Chapter 6** hydrotalcite, a layered double hydroxide of magnesium and aluminium, is investigated. Both systems of charge stabilized hydrotalcite as well as sterically stabilized hydrotalcite are discussed. It is demonstrated that the formation of nematic phases of charged hydrotalcites takes years. Dispersions of sterically stabilized hydrotalcite particles displayed isotropic-to-nematic phase transitions within days. The orientation of these platelets in nematic droplets (tactoids) and at the isotropic-nematic interface are discussed.

Chapter 7 of this thesis reports on systems of sterically stabilized natural hectorite clay particles. In toluene, the polymer-grafted lathlike hectorite particles display tactoid formation and isotropic-to-nematic liquid crystal phase separation. The particles were transferred to divinylbenzene monomer solution and polymer-hectorite nanocomposites were made by *in situ* polymerization of the dispersing phase. In this way the pillared character of the hectorite particles could be demonstrated by high resolution electron microscopy.

Samenvatting voor iedereen

COLLOÏDEN

In de natuur bestaan vloeistoffen zelden uit slechts één component. Meestal zijn er ook opgeloste stoffen, zoals gassen of ionen, of stoffen *in suspensie* (zwevend in de vloeistof), zoals macromoleculen of slecht oplosbare zouten, aanwezig. Wanneer de afmetingen van het materiaal in suspensie tussen de nanometer ($1 \cdot 10^{-9}$ meter) en de micrometer ($1 \cdot 10^{-6}$ meter) zijn, spreken we van *colloïden* of *colloïdale deeltjes* in suspensie en van een *colloïdale suspensie*. Deze colloïden kunnen uit allerlei chemische verbindingen zijn opgebouwd.

Het bijzondere van colloïden is dat ze bij kamertemperatuur -in tegenstelling tot grotere clusters materie- nog flink bewegen onder invloed van de thermische energie (de zogenaamde *Brownse beweging*), zoals ook atomen en kleinere moleculen dat doen. Hierdoor bewegen ze kris kras door de vloeistof. Vergeleken met atomen zijn colloïden echter veel groter en trager en daardoor gemakkelijker te observeren. Bovendien kunnen colloïden in suspensie chemisch aangepast worden, waardoor het mogelijk is de samenstelling en het gedrag in suspensies naar wens te beïnvloeden.

Deeltjes met een hogere dichtheid dan het oplosmiddel zinken naar de bodem van de suspensie, maar vanwege de Brownse beweging is dit proces traag en kunnen colloïden soms jarenlang door het oplosmiddel blijven zweven.

PLAATJES

De colloïdale deeltjes die in dit werk zijn onderzocht, lijken op de deeltjes die voorkomen in natuurlijke klei. Er bestaan veel kleisoorten, die onderling verschillen wat betreft de chemische samenstelling en de vorm van de deeltjes. Wij richten ons in dit werk voornamelijk op synthetische, plaatvormige deeltjes. Door synthetische deeltjes te gebruiken zijn de samenstelling en afmetingen van de deeltjes nauwkeurig te sturen. De mineraalsoorten die zo verkregen worden, komen wel in de natuur voor, maar zijn daar gewoonlijk onderdeel van heterogene mengsels. In deel 1 en 2 van dit proefschrift (hoofdstukken 2 – 5) staat het kleimineraal gibbsiet ($\gamma\text{-Al}(\text{OH})_3$) centraal. Dit wordt geproduceerd vanuit organische, aluminiumhoudende chemische verbindingen in een waterige oplossing. Deze methode levert een zeer zuiver mineraal op, waarvan de groei relatief makkelijk te sturen is. In hoofdstuk 6 wordt beschreven hoe hydrotalciet (mineraal magnesium-aluminium hydroxide) wordt bereid door het tegelijkertijd laten neerslaan

(*coprecipiteren*) van magnesium- en aluminiumionen uit zoutoplossingen in water. De op deze manier verkregen hydrotalcietkristallen kunnen vervolgens aangroeien in warm water onder druk (*herkristalliseren*). Tot slot is er ook gebruik gemaakt van hectoriet, een kleimineraal dat in verschillende landen wordt gewonnen door middel van mijnbouw. De hectoriet waarmee in hoofdstuk 7 is gewerkt komt uit een speciale kleibank, waardoor we onze resultaten kunnen vergelijken met die van andere onderzoekers die met dezelfde natuurlijke kleideeltjes werken.

DEELTJES IN ZOUT WATER

Zout water is een geschikt oplosmiddel om kleiplaatjes in te onderzoeken. Eén van de eigenschappen van kleimineralen is immers dat ze in water ladingen dragen als gevolg van het opsplitsen (*dissociëren*) van chemische groepen aan het oppervlak (bijvoorbeeld hydroxidegroepen) of door vervanging van een ion uit de kristalstructuur door een ion met vergelijkbare afmetingen, maar een andere lading (*isomorfe substitutie*). Deze ladingen zorgen ervoor dat individuele kleideeltjes elkaar afstoten. De wisselwerkingen tussen geladen colloïdale deeltjes in water zijn te variëren met behulp van de hoeveelheid zout in het water. Het zout (NaCl) dissocieert in oplossing namelijk tot de vrije ionen Na^+ en Cl^- die door het water zweven. *Tegenionen* (ionen met een tegengestelde lading ten opzichte van het kleimineraal) worden aangetrokken door de ladingen van het mineraal en blijven in de buurt van het oppervlak zweven waardoor het op afstand lijkt alsof het oppervlak netto minder geladen is. Als gevolg hiervan verandert de afstand en de grootte van de wisselwerkingskrachten tussen de colloïden. Het evenwicht van de attractieve en repulsieve wisselwerkingen tussen colloïdale deeltjes werd meer dan vijftig jaar geleden al theoretisch beschreven door Derjaguin, Landau, Verwey en Overbeek (DLVO). Deze theorie beschrijft dat deeltjes elkaar bij heel weinig zout ($\sim 1 * 10^{-4} \text{M NaCl}$) al op relatief grote afstand beïnvloeden, terwijl de deeltjes elkaar bij middelmatige zoutsterktes ($\sim 1 * 10^{-2} \text{M NaCl}$) eerst dichter moeten naderen voordat zij sterke interacties vertonen (de afscherming door de tegenionen is in dit geval dus efficiënter). Is er (te) veel zout in het oplosmiddel aanwezig ($\sim 1 * 10^{-1} \text{M NaCl}$) dan voldoet de lading niet meer voor het op afstand houden van andere kleideeltjes. Er kunnen dan grote netwerken ontstaan uit vele aan elkaar gekoppelde deeltjes. Deze netwerken worden gels genoemd. Hoewel er in het verleden veel onderzoek is gedaan naar het gedrag van kleideeltjes in water zijn er nog zeer belangrijke openstaande vragen. Met het onderzoek dat beschreven is in hoofdstuk 2 is een bijdrage geleverd aan de kennis van het gedrag van geladen, plaatvormige deeltjes gesuspenseerd in water door gebruik te maken van een zeer zuiver modelsysteem, namelijk synthetisch gibbsiet. Dit modelsysteem werd bestudeerd bij verschillende zoutconcentraties om het effect van de ionconcentratie op de stromingseigenschappen van de suspensie te meten. Met een reometer werd gemeten welke spanningen er nodig zijn om vervorming van de suspensies

te veroorzaken. Bovendien werd in de tijd geanalyseerd hoe een dergelijke vervorming zich ontwikkelt en in welke mate de suspensies zich elastisch gedragen. Om objectief vast te kunnen stellen of suspensies als een vloeistof of als een gel of colloïdaal glas vervormen, werden in hoofdstuk 2 reologische criteria gehanteerd.

DEELTJES MET EEN POLYMEERJAS

Het gedrag van geladen deeltjes in suspensie is zeer gecompliceerd. Er is dan ook relatief veel onbekend over het gedrag van (klei)plaatjes geconcentreerde suspensies. Om de effecten van lading uit te sluiten en aan een eenvoudiger modelsysteem te kunnen werken is in deel 2 en 3 van dit proefschrift (hoofdstukken 4 – 7) gebruik gemaakt van polymeergestabiliseerde systemen. Hiertoe werden polymeerketens op het mineraaloppervlak van de kleiplaatjes aangebracht door middel van een zelfontwikkelde methode die in hoofdstuk 4 wordt beschreven. Deze polymeren bevatten aminogroepen die zich binden aan het mineraaloppervlak en lange polyalkylketens die als haren uitsteken. Dankzij deze haren kunnen plaatjes elkaar niet meer onbeperkt naderen, wat in niet-polaire oplosmiddelen onherroepelijk tot aggregaatvorming zou leiden. De polymeerjas vormt zodoende een brug tussen de polaire groepen op het mineraaloppervlak en het niet-polaire oplosmiddelen maakt het dus mogelijk om de plaatjes in niet-polaire vloeistoffen te suspenderen, zoals toluen (hoofdstukken 5, 6 en 7) of divinylbenzeen (hoofdstukken 5 en 7). Het voordeel van de eerdergenoemde niet-polaire oplosmiddelen is dat zij een hoge brekingsindex hebben. In combinatie met de gesuspendeerde mineraaldeeltjes leidt dit tot weinig verstrooiing (een lage *turbiditeit*) waardoor veel informatie kan worden verkregen uit experimenten met een polarisatiemicroscoop. Vergeleken met de melkwitte waterige suspensies uit hoofdstuk 2, 3 en 6 zijn de niet-polaire suspensies uit hoofdstukken 4 – 7 zo goed als transparant.

Veel voor de industrie interessante organische polymeren zijn niet-polair. Toch is er een wens om kleimineralen te kunnen verwerken in deze polymeren om zo hybride materialen te kunnen produceren, die betere materiaaleigenschappen hebben dan conventionele polymeren. Het aanbrengen van een polymeerjas, zoals hier beschreven, kan dit mogelijk maken (zie de paragraaf *Materialen met nanometerschaalordering*).

GEOMETRIE EN STRUCTUUR

Behalve de wijze waarop deeltjes op afstand interactie met elkaar hebben, zijn ook de concentratie en de deeltjesvorm van invloed op de structuur en eigenschappen van suspensies. Als het voor ieder deeltje beschikbare volume klein wordt, kunnen ze *kristalliseren*: de plaatjes rangschikken zich dan regelmatig om het volume dat beschikbaar is efficiënt met elkaar te delen. Dicht opeengepakte deeltjes verliezen weliswaar hun vrijheid van oriëntatie maar beschikken in ruil daarvoor individueel over een bescheiden

ruimte in het kristal waarin ze zich vrijer kunnen bewegen dan mogelijk zou zijn in een niet-opgelijnde, wanordelijke toestand. De overgang naar een meer geordende toestand is dus te begrijpen aan de hand van de entropie van het systeem.

Bijzonder aan de manier waarop plaatvormige deeltjes zich rangschikken is dat zij niet direct de kristalfase bereiken, maar eerst meerdere stadia van toenemende ordening (*vloeibare kristallen*) doorlopen.

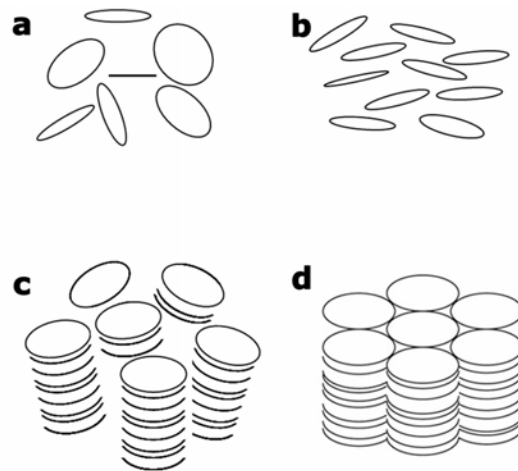
Onder vloeibare kristallen worden geordende structuren gerekend die slechts ten dele gekristalliseerd zijn en dus tussen de (wanordelijke) vloeistoffase en de (drie-dimensionaal geordende) kristalfase in moeten worden geplaatst. Bij de simpelste verschijningsvorm van een vloeibaar kristalfase, de nematische fase, zijn de plaatjes slechts opgelijnd (Figuur 1 b). Ook de in twee dimensies gekristalliseerde *hexagonaal columnaire fase* (Figuur 1 d), waarin stapels van plaatjes zich op een hexagonaal rooster ordenen, komt voor in de systemen die in dit onderzoek bestudeerd zijn (hoofdstuk 2, 3 en 4). Het onderzoek beschreven in hoofdstuk 2 van dit proefschrift heeft voor het eerst aangetoond dat de kristallisatie van de nematische naar de hexagonaal columnaire fase verloopt via stapelvorming van de gibbsietdeeltjes. In dit tussenstadium, de *columnair nematische fase*, zijn de plaatjes opgelijnd en vormen ze stapels die lokaal weliswaar in hoge mate zesvormig omringd worden door naburige stapels plaatjes, maar nog niet op een kristalrooster lijken te liggen (Figuur 1 c).

Bij hoge deeltjesconcentraties vormen de plaatjes in colloïdale suspensies behalve vloeibare kristallen echter ook colloïdale glasfasen. Hierin zitten de deeltjes zo dicht op elkaar dat ze door ruimtegebrek geen kans krijgen om zich opnieuw te rangschikken en daarom in een metastabiele, wanordelijke toestand gevangen blijven zitten. Het onderzoek in hoofdstuk 2 gaat in op de structuren die de deeltjes in een glasachtig georganiseerde toestand vormen en beschrijft hoe over jaren uitgespreid de herverdeling van plaatjes toch kan plaatsvinden, geholpen door de zwaartekracht.

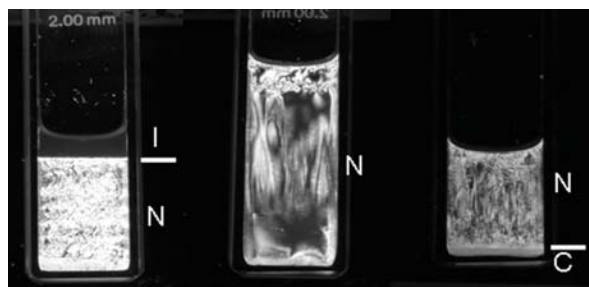
ORDENING IN BEELD

Een relatief eenvoudige manier om de ordening van colloïdale plaatjes in suspensie te bestuderen is door gebruik te maken van gekruiste polarisatoren. Dat zijn lichtfilters, vergelijkbaar met polariserende glazen uit een zonnebril, die het licht langs één polarisatierichting uitdoven. Als gevolg daarvan laten twee gekruiste polarisatoren helemaal geen licht door. Een suspensie van opgelijnde colloïdale plaatjes is in staat om de polarisatierichting van licht te veranderen. Wanneer een buisje met een dergelijke suspensie tussen gekruiste polarisatoren wordt gehouden kan licht toch door de gekruiste polarisatoren worden doorgelaten (Figuur 2).

Uit de resulterende kleuren en de textuur van de suspensie kan worden opgemaakt wat voor structuur en ordening van de plaatjes aanwezig is. In combinatie met een lichtmicroscop kan de plaatjesoriëntatie op kleine schaal worden geanalyseerd, terwijl de



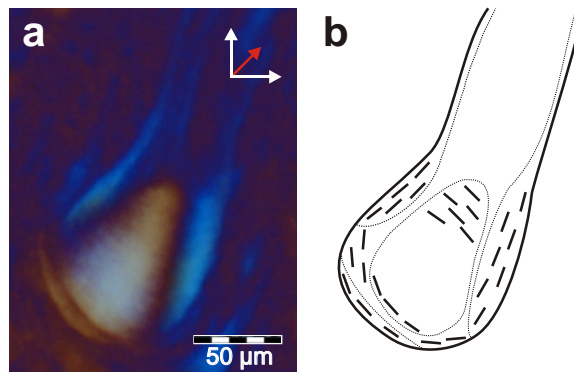
Figuur 1. Schematische weergave van de verschillende fasen van plaatvormige colloïden in volgorde van oplopende orde: (a) isotrope fase, (b) de nematische fase, (c) de columnair nematische fase en (d) de hexagonaal columnaire fase



Figuur 2. Buizen met polymeergestabiliseerde gibbsietsuspensies die vloeibare kristallen vormen, laten licht door tussen gekruiste polarisatoren. In de foto zijn suspensies te zien bij verschillende gibbsietconcentraties. De verschillende fasen zijn aangeduid naast de monsters: isotrope fase (I), nematische fase (N) en hexagonaal columnaire fase (C).

kleiplaatjes zelf nog te klein zijn om waar te nemen. Deze techniek werd toegepast voor alle in dit proefschrift beschreven systemen. Zo kon worden bepaald dat hydrotalcietplaatjes zich oplijnen in de buurt van (isotroop-nemaat) grensvlakken (hoofdstuk 6). Ook kon voor dit systeem de plaatjesorientatie in een druppel vloeibaar kristal (*tactoid*) worden bepaald (Figuur 3). In hoofdstuk 5 wordt met behulp van polarisatiemicroscopie aangetoond dat de kolommen van de hexagonaal columnaire fase van gibbsietplaatjes grote golfvormige verstoringen vertonen.

Een andere techniek om onzichtbare structuren te ontrafelen zijn verstrooiingsexperimenten. Geordende suspensies verstrooien licht en röntgenstraling anders dan ongeordende suspensies. In het geval van de hexagonaal columnaire fase wordt licht soms heel regelmatig verstrooid en zijn iriserende delen zichtbaar in de suspensie, zoals ook



Figuur 3. Een tactoïd in een suspensie van polymeergestabiliseerde hydro-talcietplaatjes in toluen. In (a) is een polarisatiemicroscopiebeeld te zien. In (b) laat een cartoon zien hoe de deeltjes in de druppel georiënteerd zijn, zoals opgemaakt kon worden uit het kleurenspeel in (a).



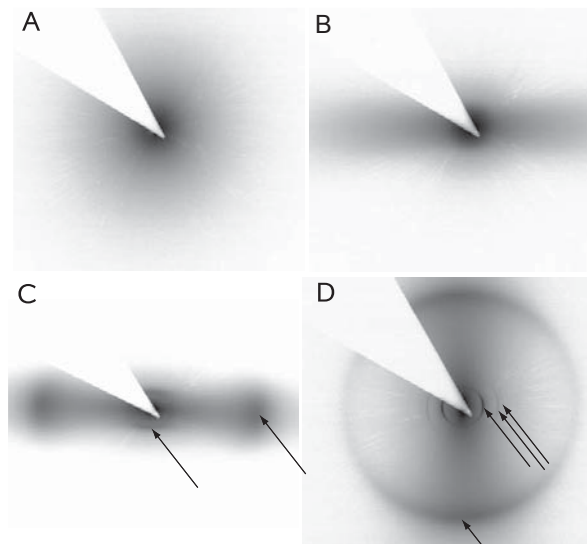
$$n \lambda = 2 d \sin \theta$$

Figuur 4. In de hierboven afgebeelde gibbsietsuspensie is de iridisatie van de hexagonaal columnaire fase onderin te zien. De wet van Bragg beschrijft de relatie tussen ordening en iridisatie van straling. In deze natuurwet is d de repeterende afstand in het monster, λ de versterkte golflengte (de iridiserende kleur) en θ de hoek tussen de verstrooiende regelmatig geordende vlakken en de inkomende (licht)bundel. n is een geheel getal en stelt de orde van de reflectie voor ($n = 1$ levert de sterkste verstrooiing).

bij parelmoer in schelpen. De colloïdale plaatjes zijn in deze gedeelten van de suspensie zo regelmatig gerangschikt, dat de verstrooiing van sommige golflengtes van licht onder een bepaalde hoek versterkt wordt, terwijl bij diezelfde hoek licht met andere golflengtes juist afgezwakt worden. De wet van Bragg relateert de kleur van het licht en de verstrooiingshoek aan de periodieke afstanden in het monster (Figuur 4).

Röntgenstraling heeft een veel kortere golflengte dan zichtbaar licht en kan ook verstrooid worden volgens de wet van Bragg. In kleine-hoek-röntgenverstrooiingsexperimenten kunnen de afstanden tussen de plaatjes in gibbsietsuspensies nauwkeuriger worden gemeten dan met licht. Bovendien zijn ook structuren met lagere orde (zoals nematische structuren) meetbaar. Deze techniek wordt in hoofdstuk 2 toegepast om de verschillende ordeningen van gibbsietplaatjes in zout water te bepalen (Figuur 5). In

hoofdstuk 4 wordt de techniek gebruikt om een gedetailleerd beeld te krijgen van de ordening in de hexagonaal columnaire fase van polymeergestabiliseerde gibbsietplaatjes. Een indirectere manier om de ordening van kleiplaatjes in beeld te brengen is door een druppel suspensie zeer snel te bevriezen in vloeibaar stikstof en vervolgens te bekijken met behulp van elektronenmicroscopie. Hierbij werd ook gebruik gemaakt van een gefocuseerd ionenkanon, waarmee de bevroren druppels open werden gesneden. Zo werden de gel- en glasfase van gibbsietplaatjes in water in beeld gebracht (hoofdstuk 2), als aanvulling op de resultaten uit de röntgenverstrooiingsexperimenten. Ook de materialen uit hoofdstuk 5 en 7 werden met behulp van elektronenmicroscopie en het ionenkanon in beeld gebracht. Aangezien deze monsters door polymerisatie niet meer vloeibaar waren, hoefden ze niet eerst bevroren te worden.



Figuur 5. Röntgenverstrooiingspatronen van gibbsietsuspensies met (a) isotrope, (b) nematische, (c) nematisch columnaire en (d) hexagonaal columnaire ordening. Bragg reflecties in de patronen zijn aangegeven met een pijl.

MATERIALEN MET NANOMETERSCHAALORDENING

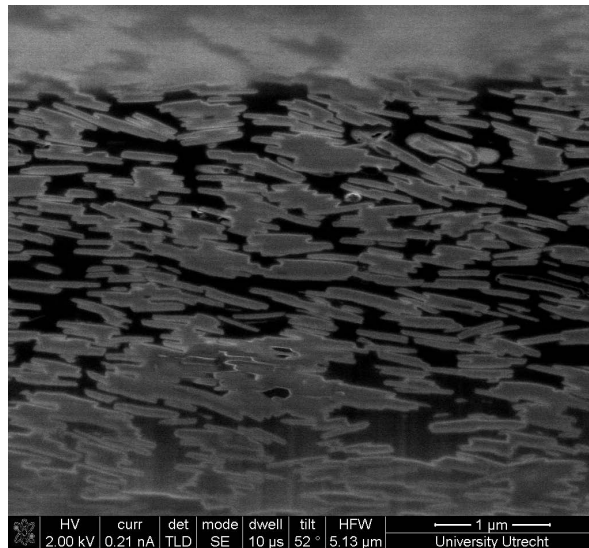
Botweefsel, tandglazuur en parelmoer zijn voorbeelden van natuurlijke materialen die bestaan uit minerale plaatjes die zijn omgeven door organisch polymeer. Dit soort hybride materialen hebben bijzondere materiaalkundige eigenschappen omdat ze de hardheid van mineralen combineren met de vervormbaarheid van polymeren.

Colloïdale suspensies van minerale plaatjes kunnen als uitgangsmateriaal dienen voor zulke hybride materialen. Synthetische gibbsietdeeltjes (hoofdstuk 5) en natuurlijke hectorietkleideeltjes (hoofdstuk 7) werden in hoge volumefracties in het polymeer polyvinylbenzeen ingesloten. Om dit te bewerkstelligen werden de molekulen van het oorspronkelijke oplosmiddel van de colloïdale suspensies, divinylbenzeen, aangezet tot

polymerisatie. De resulterende hybride materialen zijn relatief transparant en kleurloos. Bovendien zijn de plaatjes in staat zich te ordenen voordat het polymerisatieproces van start gaat, waardoor ze een hoge mate van ordening hebben in het uiteindelijke hybride materiaal (Figuur 6).

Zulke hybride materialen hebben naar verwachting een zeer hoge duurzaamheid vergeleken met klassieke polymeermaterialen, door een sterk absorptievermogen van UV-licht en een verlaagde doorlaatbaarheid voor vloeistoffen als gevolg van de hoge mate van ordening van de plaatjes.

Naast mineraal-in-polymer werd ook een hybride materiaal gemaakt van mineraal-in-mineraal (hoofdstuk 3). In een suspensie van colloïdale gibbsietplaatjes werd vanuit een oplossing silica aangebracht op het gibbsiet. Zo kon een hybride materiaal van hexagonaal columnair geordend gibbsiet in silica worden verkregen. Een dergelijk materiaal is interessant, omdat het als een uitgangsmateriaal kan dienen voor nieuwe katalysatoren waarmee chemische reacties kunnen worden versneld.



Figuur 6. Elektronenmicroscopie aan een gibbsiet-polymer hybride materiaal toont het zijaanzicht van de nematisch geordende gibbsietplaatjes in het polymeer.

List of publications

This thesis is based on the following publications:

- M. C. D. Mourad, A. A. Verhoeff, D. V. Byelov, A. V. Petukhov and H. N. W. Lekkerkerker *Devitrification of the Glassy State in Suspensions of Charged Platelets* accepted for publication in J. Phys.: Condens. Matter (Chapter 2)
- M. C. D. Mourad, D. V. Byelov, A. V. Petukhov, D. A. M. de Winter, A. J. Verkleij, and H. N. W. Lekkerkerker *Sol-Gel Transitions and Liquid Crystal Phase Transitions in Concentrated Aqueous Suspensions of Colloidal Gibbsite Platelets* J. Phys. Chem. B **113** (2009) 11604. (Chapter 2)
- M. C. D. Mourad, D. V. Byelov, A. V. Petukhov, H. N. W. Lekkerkerker *Structure of the repulsive gel/glass in suspensions of charged colloidal platelets* J. Phys.: Condens. Matter **20** (2008) 494201 (Chapter 2)
- M. C. D. Mourad, E. J. Devid, M. M. van Schooneveld, C. Vonk and H. N. W. Lekkerkerker, *Formation of nematic liquid crystals of sterically stabilized layered double hydroxide platelets* J. Phys. Chem. B **112** (2008) 10142 (Chapter 6)
- M. C. D. Mourad, E. Groeneveld, P. J. de Lange, C. Vonk, D. van der Beek, and H. N. W. Lekkerkerker *Columnar liquid crystals of gibbsite platelets as templates for the generation of ordered silica structures* J. Mater. Chem. **18** (2008) 3004 (Chapter 3)
- M. C. D. Mourad, J. E. G. J. Wijnhoven, D. D. van 't Zand, D. van der Beek and H. N. W. Lekkerkerker *Gelation versus Liquid Crystal Phase Transitions in Suspensions of Plate like Particles* Phil. Trans. R. Soc. A **364** (2006) 2807-2816 (Chapter 2)

Other papers by the author:

- R. P. A. Dullens, V. W. A. de Villeneuve, M. C. D. Mourad, A. V. Petukhov and W. K. Kegel, *Confocal microscopy of geometrically frustrated hard sphere crystals* Eur. Phys. J. Appl. Phys. **44**, 21-28 (2008)
- S. Roy, M. C. D. Mourad and M. T. Rijneveld-Ockers, *Synthesis and characterization of large surface hexagonal polyoxometalate platelets* Langmuir **23** (2007) 399-401
- R. P. A. Dullens, M. C. D. Mourad, D. G. A. L. Aarts, J. P. Hoogenboom and W. K. Kegel *Shape-Induced frustration of hexagonal order in polyhedral colloids* Phys. Rev. Lett **96** (2006) 028304-1-4

Curriculum Vitae

Maurice Mourad was born in Leiden, the Netherlands, on February 9, 1982. In 2000 he graduated at the ‘Stedelijk Gymnasium Leiden’ (Grammar School), with exams in Dutch, English, German, Latin and in mathematics, physics, chemistry, biology and economy. The same year he started studying Chemistry at Utrecht University. In 2005 he obtained his ‘doctoraal’(MSc) degree with a major in the Chemistry of Condensed Matter group at Utrecht University with Peter Vergeer and Andries Meijerink. Other undergraduate research included projects at the Physical and Colloid Chemistry group at Utrecht University (with Roel Dullens and Willem Kegel) and the Physical Chemistry group at Lund University (with Emma Sparr and Håkan Wennerström).

In May 2005 he started his research at the ‘van ‘t Hoff Laboratory for Physical and Colloid Chemistry’ under supervision of Henk Lekkerkerker. The project was funded by ‘The Netherlands Organisation for Scientific Research’ (NWO) under the title ‘Self-organized Nanostructures: From Colloidal Liquid Crystals to Optical, Magnetic and Macroporous Materials’. During his research he participated in several specialist courses: Soft Condensed Matter (Utrecht University, 2005), Han-sur-Lesse Winter school on Macroscopic Physical Chemistry (Stichting Fysische Chemie Nederland, 2006 and 2007), Colloids in External Fields (SFB-TR6, 2006) and the International School of Liquid Crystals (Italian Liquid Crystal Society, 2007). In turn, he taught (physical) chemistry to grammar school and university students. Results from his research were presented at national and international conferences and published in scientific journals.

In 2009 his PhD-thesis was published. It contains fundamental scientific insight on the behavior of anisotropic colloidal particles in suspension as well as results on nanostructured hybrid materials that were synthesized from these suspensions.

Acknowledgement

Tot slot wil ik graag iedereen bedanken die heeft bijgedragen aan het totstandkomen van dit proefschrift. Allereerst Henk Lekkerkerker, bedankt voor de enthousiaste dagelijkse begeleiding van dit onderzoek. Gert Jan Vroege en Andrei Petukhov, bedankt voor de inwijding in de röntgenverstrooiing en dat jullie copromotor willen zijn.

In het laboratorium en bij de analyse van resultaten heb ik geprofiteerd van de goede samenwerking met Chantal Vonk, Annemieke ten Brinke, David van der Beek, Judith Wijnhoven en Dima Byelov. Job Thijssen en Laurent Heux, bedankt voor de discussies.

Esther Groeneveld, Peter de Lange, Matti van Schooneveld en Edwin Devid hebben een grote bijdrage geleverd aan het onderzoek. Jullie projecten vormden bovendien de basis van hoofdstukken 3 en 6 en twee publicaties. Bedankt voor jullie tijd en inzet.

Het uitvoeren van metingen werd mogelijk gemaakt door een enthousiaste groep mensen, die mij hun tijd en apparatuur ter beschikking stelden. Hans Meeldijk, Matthijs de Winter, Arie Verkleij en Chris Schneijdenberg dank ik voor de goede samenwerking en ondersteuning bij de elektronenmicroscopie. Bonny Kuipers, Emile Bakelaar, Dominique Thies-Weesie en Kanvaly Sanogo Lacina, bedankt voor de goede hulp op het laboratorium. John Geus en Marjan Versluijs-Helder dank ik voor de metingen en discussies over resultaten van microscopie en diffractie. Wim Bras en het DUBBLE-team dank ik voor het faciliteren van de verstrooiingsmetingen aan het ESRF in Grenoble.

Bij de uitvoering en verslaglegging van experimenten werd ik goed geholpen door Hans Heeze, Jan den Boesterd en Ingrid van Rooijen.

Mijn kamergenoten Stefano Sacanna, Lia Verhoeff, Laura Rossi en Julius de Folter dank ik voor de hulp, gezelligheid en afleiding. Behalve bovengenoemden zijn er veel groeps- en vakgenoten bij scheikunde en natuurkunde die ervoor zorgen dat het bijzonder aangenaam is om in deze omgeving te werken. Met name wil ik Daniela, Volkert, Maria, Bob, Esther, Sandra, Willem, Alan, Ben, Mieke, Marina, Albert, Jan, Cees, Didi, Peter, Esther, Michiel, Laura, Teun, Eduardo, Jos, Niels, Alfons, Marjolein, René, Elif en Sandra noemen.

De afgelopen jaren heb ik veel beleefd met een groep mensen die mij uitsluitend buiten de werkomgeving zagen. Ik bedank familie en vrienden, de roeiers, zondagavond-bierdrinkers, fietsers, vakantiegangers en schaatsers voor alle etentjes, concerten, uitstapjes, vakanties en meer. In het bijzonder wil ik Hanna, Marije, Jesse, Joris, Maike en mijn paranimfen Rick en Ernst Jan noemen.

Mijn broer Daniël, bedankt voor de vele discussies, vakanties en post-conferentietrips.

Mijn zus Selma, veel succes komende weken met het afronden van je eigen proefschrift.

Mijn ouders, bedankt voor jullie aanmoediging om vooral door te leren en geen genoegen te nemen met half werk. Bovendien waardeer ik zeer dat jullie bij mij de interesse hebben gewekt om me te verdiepen in zoveel andere dingen dan scheikunde.

Froukje, bedankt voor je liefde, afleiding en gezelschap.